Fundamental processes and applications of chemical reaction induced by plasma at gas-liquid interface

HAYASHI Yui

Contents

Chapter 1

Introduction

1.1 Introduction

In the past few decades, plasma technologies have been actively studied for application in various fields. Today, it become important technology for electronic industry [1] and material synthesis [2, 3]. Plasmas are classified into thermal and non-thermal plasmas depending on electron temperature T_e and ion temperature T_h. Thermal plasmas are in thermal equilibrium between electrons and ion ($T_e \simeq T_h$). They enable chemical reactions in high-temperature, and suitable for metal nanoparticles synthesis [4–6] and waste treatment [7,8]. On the other hand, non-thermal plasmas show different temperature between electrons and ions. Ions have much lower temperature than electrons ($T_e \gg T_h$) due to mass difference of them. Non-thermal plasmas exhibit non-liner and high capacity plasma without heating. They have the advantage of nanomaterials and nanostructure creation, which cannot realize by thermal equilibrium and liner processes, such as manufacturing of large scale integration (LSI) [9, 10]. T_e and T_h are strongly influenced on pressure condition. Figure 1.1 shows typical values of T_e and T_h as a function of

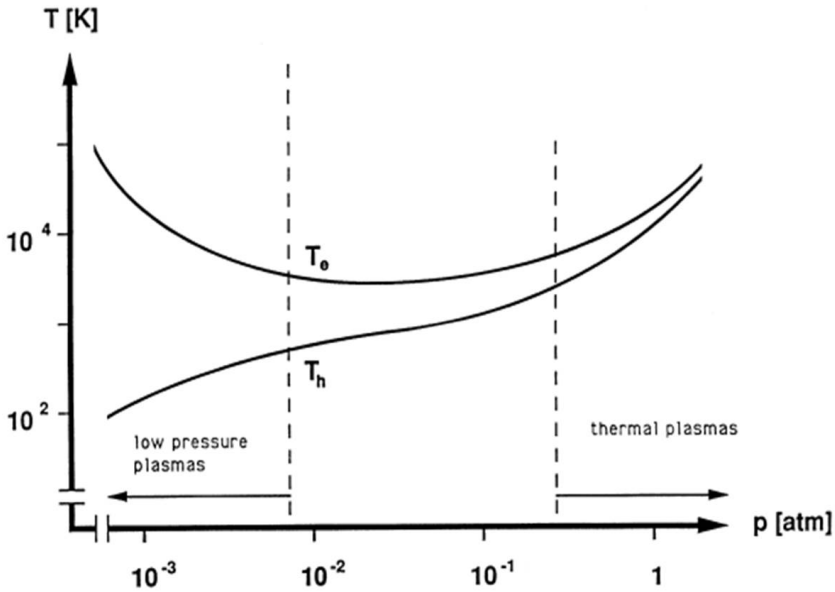

Figure 1.1 Typical values of T_e and T_h as a function of pressure [11]

pressure [11]. At high pressure condition, T_h is close to T_e because the frequency of collision between electrons and ions is high. Namely, plasmas are easy to reach thermal equilibrium at high pressure such as atmospheric pressure. Non-thermal plasmas are produced in low pressure condition typically. Thus, vacuum vessel and exhaust apparatus are required, resulted in rise in manufacturing costs in many cases. Recently, many researchers have studied on non-thermal plasmas at atmospheric pressure because they can perform high-speed and continuous processing without vacuum exhaust devices. Now, non-thermal plasmas can generate at atmospheric pressure by using various plasma sources such as plasma jet (APPJ) [12, 13], pulsed discharge [14], and dielectric barrier discharge (DBD) [15]. They prevent a transition to thermal plasmas by devising electrode structures and power sources, leading to non-thermal plasma generation.

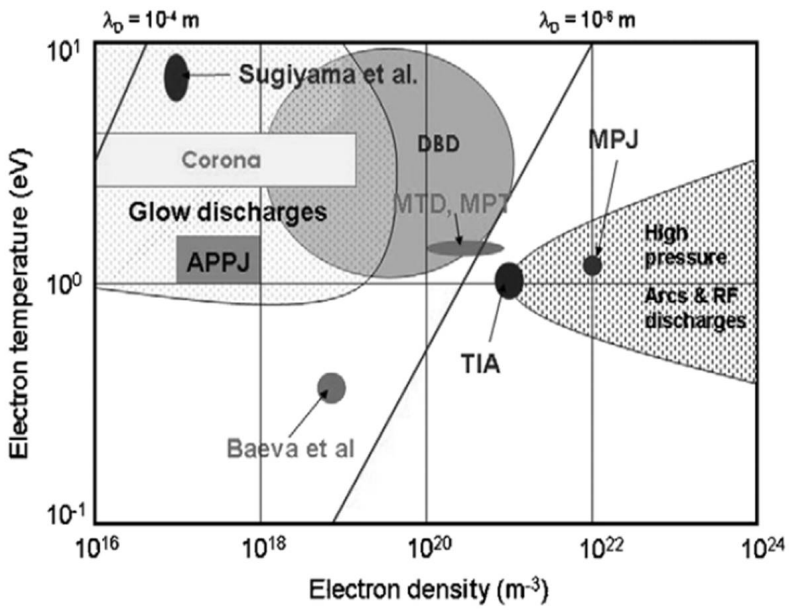

Figure 1.2 Classification of atmospheric plasma [16]

Figure 1.2 shows classification of atmospheric pressure plasma sources by electron temperature and density [16]. Thermal or non-thermal plasmas are defined by Debye length λ_D, which is determined by electron temperature T_e and density n_e as shown in Eq.(1.1).

$$\lambda_D = \sqrt{\frac{\varepsilon_0 k_b T_e}{n_e e^2}} \tag{1.1}$$

where ε_0 is electric constant; k_b is Boltzmann constant; e is elementary charge. The λ_D of non-thermal atmospheric plasmas is in the range of 10^{-4} to 10^{-6} m. The APPJ exhibits characteristics like glow discharge, which is high impedance. The characteristics of pulsed discharge and DBD are between glow and arc discharge. By using these plasma sources,

non-thermal plasmas are easy to form even at atmospheric pressure, and applied not only to material synthesis but also wide fields. For example, non-thermal plasmas are valid for surface modification [17, 18] and decontamination of biological media [19, 20] because it is possible to avoid thermal damages to samples by plasma irradiation.

1.2 Electric discharge in the presence of water

Plasma-chemical processes performed gas-phase reactions or reactions at plasma-solid interface mainly in previous works. Studies on plasma for liquid were conducted as glow-discharge electrolysis under vacuum condition [21–23]. They confirmed production of some active species by non-thermal plasmas for liquid, but these researches were hardly carried out because there was no advantage of plasmas for liquid at low pressure condition compared with conventional methods for active species production. However, plasmas for liquid have been attracting attention in recent years, because they can be generated at atmospheric pressure by technological progress. Non-thermal plasmas for liquid at atmospheric pressure are convenient for application to biomedicine and environmental cleaning, since the samples of these applications often utilized water as a medium. Non-thermal plasmas for liquid can induce chemical reactions without heating only by setting electrodes and applying power. Additionally, catalyst and chemical agent are unnecessary for chemical reactions on this process. Therefore, plasmas for biomedical and environmental applications have been actively researched in the past 15 years [24–28]. What is more, unique materials, which could not be realized by other methods, were produced by plasma with liquid under atmospheric pressure reportedly [29–32].

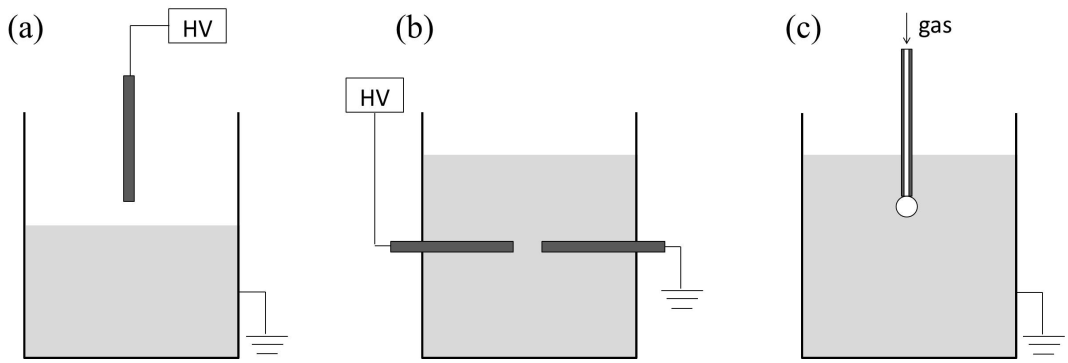

Figure 1.3 Three type of discharge methods; (a) on liquid surface, (b) discharge directly in liquid, and (c) inside bubble in liquid

The way of generating non-thermal plasmas for liquid was divided into two types of discharge; discharge on liquid surface [33–35] and discharge directly in water [36–39], as shown in Figure 1.3. In case of the discharge on liquid surface, the liquid behaves as an electrode (Fig.1.3 (a)). Discharge plasmas are generated from the metal electrode suspended in gas phase to the liquid surface on a typical configuration. In contrast, discharge plasmas directly in liquid are generated pin-to-pin, pin-to-plate, or plate-to-plate in liquid by using pulsed power in most cases (Fig.1.3 (b)). It requires high voltage and short gap length because breakdown voltage in liquid phase is higher than that in gas phase [41]. In some cases, discharge plasmas are generated inside bubbles in liquid [42–45], as shown in Fig.1.3 (c). The principles of these plasmas are the same as that of discharges on liquid surface, but active species generated by the plasmas are enclosed inside the bubble, leading to high efficiency of chemical reactions.

However, contact area between plasma and liquid of these discharge methods is small. In order to enlarge contact area between plasma and liquid, some discharge methods were

proposed recently. Takeuchi *et al.* located some pin electrodes in gas phase upon aqueous solution, and realized large area of plasmas from pin electrodes to aqueous solution [35]. Ishijima *et al.* generated microwave bubble plasmas in water using multiple slots [44], and Shirafuji *et al.* generated three-dimensionally integrated micro-solution plasmas using porous media [45]. They enabled discharge plasmas to generate in multiple bubbles at the same time.

Discharge plasmas in the presence of water are generated active species derived from water in any case, and mostly induce oxidation-reduction reactions in water. In fact, emission of OH radicals and production of hydrogen peroxide were confirmed when discharge plasmas were generated in contact with water [46–48]. These oxidation species were supposed to induce chemical and biological effects in water [49, 50]. Moreover, reduction reactions also occur at plasma-liquid interface, and applied for nanomaterials synthesis [51–53]. Although there are a lot of studies on fundamental mechanisms and application of discharge plasma in the presence of water, chemical reactions induced by discharge plasmas and transport mechanisms of active species in water are still uncertain.

1.3 Motivation and purpose of the present work

This work focused on discharge plasma at gas-aqueous solution interface. In order to utilize it for chemical process, understandings of not only detailed chemical reactions by discharge plasmas but transport mechanisms of active species of active species are essential, moreover high efficient processes are required. Now, the effects of pulsed discharge plasmas over aqueous solution were investigated in *Chapter 2*. Especially, spatial

distributions of solution properties under plasma irradiation were observed *in situ* by using chemical methods. It is certainly helpful to design a reactor for efficient process. Based on the results of *Chapter 2*, new plasma processes using gas-liquid two phase flow were developed in *Chapter 3*.

Meanwhile, the discharge plasmas inside bubbles improved the reactive efficiency of plasmas at aqueous solution interface reportedly. However, bubbles from nozzle have high rising speed, resulted in unstable discharge plasmas. Therefore, fine bubbles, which have slow rising speed, introduced in water, and discharge plasma were generated in water with fine bubbles in *Chapter 4*. The effects of fine bubbles on characteristics of discharge plasmas and generation of reactive species were examined.

What is more, discharge plasmas were generated at pressurized gas-aqueous solution interface in *Chapter 5*, although they were generated under atmospheric pressure until *Chapter 4*. Pressure condition exerts great impacts on plasma properties. Thus, a discharge under pressurized gas has a possibility of new materials synthesis. The present work performed pulsed discharge generated at pressurized gas/amino acid solution interface, and investigated the characteristics of the plasmas and the application for synthesis of water-dispersible carbon nanomaterials.

Reference

[1] P K Chu, S Qin, C Chan, N W Cheung and L A Larsoni (1996) Plasma immersion ion implantation-a fledgling technique for semiconductor processing *Mater. Sci. Eng.* **R17** 207-280.

[2] F E Kruis, H Fissana and A Peled (1998) Synthesis of nanoparticles in the gas phase for electronic, optical and magnetic applications-a review *J. Aersol. Sci.* **29** 5/6: 511-535.

[3] M A Lieberman and A J Lichtenberg (2005) Principles of plasma discharges and materials processing 2nd edition *Wiley*.

[4] L Tong and R G Reddy (2005) Synthesis of titanium carbide nano-powders by thermal plasma *Scripta Materialia* **52** 1253-1258.

[5] M Nirmala and A Anukaliani (2011) Characterization of undoped and Co doped ZnO nanoparticles synthesized by DC thermal plasma method *Physica B* **406** 911-915.

[6] M Keidar, A Shashurin, J Li, O Volotskova, M Kundrapu and T S Zhuang (2011) Arc plasma synthesis of carbon nanostructures: where is the frontier? *J. Phys. D: Appl. Phys.* **44** 174006.

[7] H Sekiguchi, T Honda and A Kanzawa (1992) Thermal plasma decomposition of chlorofluorocarbons *Plasma Chem. Plasma Proces.* **13** 3: 463-478.

[8] E Gomez, D A Rani, C R Cheeseman, D Deegan, M Wise and A R Boccaccini (2009) Thermal plasma technology for the treatment of wastes: A critical review *J. Hazardous Mater.* **161** 614-626.

[9] W Kern and G L Schnable (1979) Low-pressure chemical vapor deposition for very large scale integration processing-a review *IEEE Trans. Electron Devices* **26** 4: 647-657.

[10] R Agostino, P Favia, C Oehr and M R Wertheimer (2005) Low-temperature plasma processing of materials: past, present, and future *Plasma Process. Polym.* **2** 7-15.

[11] M Y A Mollah, R Schemmach, J Pastscheider, S Promrek and D L Coocke (2000) Plasma chemistry as a tool for green chemistry, environmental analysis and waste management *J. Hazardous Mater.* **B79** 301-320.

[12] A Sarani, A Y Nikiforov and C Leys (2010) Atmospheric pressure plasma jet in Ar and Ar/H_2O mixtures: optical emission spectroscopy and temperature measurements *Phys. Plasmas* **17** 063504.

[13] A Tani, Y Ono, S Fukui, S Ikawa and K Kitano (2012) Free radicals induced in aqueous solution by non-contact atmospheric-pressure cold pressure *Appl. Phys. Lett.* **100** 254103.

[14] H Akiyama, T Sakugawa, T Namihira (2007) Industrial applications of pulsed power technology *IEEE Trans. Dielectrics Electrical Insulation* **14** 5: 1051-1064.

[15] U Kogelschatz (2003) Dielectric-barrier discharge: their history, discharge physics, and industrial application *Plasma Chem. Plasma Process.* **23** 1: 1-46.

[16] C Tendero, C Tixier, P Tristant, J Demaison and P Leprince (2006) Atmospheric pressure plasmas: a review *Spectrochimica Acta B* **61** 2-30.

[17] Z Fang, Y Qiu and E Kuffel (2004) Formation of hydrophobic coating on glass surface using atmospheric pressure non-thermal plasma in ambient air *J. Phys. D: Appl. Phys.* **37** 2261-2266.

[18] T Desmet, R Morent, N D Geyter, C Leys, E Schacht and P Dubruel (2009) Nonthermal plasma technology as a versatile strategy for polymeric biomaterials surface modification: a review *Biomacromolecules* **10** 9: 2351-2378.

[19] M Laroussi (2002) Nonthermal decontamination of biological media by atmospheric-pressure plasmas: review, analysis, and prospects *IEEE Trans. Plasma Sci.* **30** 4: 1409-1415.

[20] M Nagatsu, Y Zhao, I Motrescu, R Mizutani (2012) Sterilization method for medical container using microwave-excited volume-wave plasma *Plasma Process. Polym.* **9** 590-596.

[21] A Hickling and J K Linacre (1954) Glow-discharge electrolysis. part.II the anodic oxidation of ferrous sulphate *J. Chem. Soc.* 711-720.

[22] A Hickling and M D Ingram (1964) Glow-discharge electrolysis *J. Electronal. Chem.* **8** 65-81.

[23] Y Kanzaki, M Hirabe and O Matsumoto (1986) Glow discharge electrolysis of aqueous sulfuric acid solution in various atmosphere *J. Electrochem. Soc.* **133** 11: 2267-2270.

[24] S Ikawa, K Kitano and S Hamaguci (2010) Effects of pH on bacterial inactivation in aqueous solutions due to low-temperature atmospheric pressure plasma application *Plasma Process. Polym.* **7** 33-42.

[25] H Tanaka, M Mizuno, K Ishikawa *et al.* (2015) Plasma with high electron density and plasma-activated medium for cancer treatment *Clinical Plasma Medicine* **3** 2: 72-76.

[26] Y Hayashi, Wahyudiono, S Macmudah, H Kanda, N Takada, K Sasaki and M Goto (2013) Removal of water pollutants by pulsed discharge plasma and observation of its optical emission intensity at atmospheric pressure *Jpn. J. Appl. Phys.* **52** 11NE02-1-6.

[27] Y Hayashi, Wahyudiono, S Macmudah, N Takada, H Kanda, K Sasaki and M Goto (2014) Decomposition of methyl orange using pulsed discharge plasma at atmospheric pressure: effect of different electrode *Jpn. J. Appl. Phys.* **53** 010212-1-8.

[28] D Gumuchian, S Cavadias, X Duten, M Tatoulian, P D Costa and S Ognier (2014) Organic pollutants oxidation by needle/plate plasma discharge: on the influence of the gas nature *Chem. Eng. Process. Process Intensification* **82** 185-192.

[29] N Saito, J Hieda and O Takai (2009) Synthesis process of gold nanoparticles in solution plasma *Thin Solid Films* **518** 912-917.

[30] N Shirai, S Uchida and F Tochikubo (2014) Synthesis of metal nanoparticles by dual plasma electrolysis using atmospheric dc glow discharge in contact with liquid *Jpn. J. Appl. Phys.* **53** 046202-1-5.

[31] Z Abdullaeva, E Omurzak, C Iwamoto, H S Ganapathy, S Sulaimankulova, C Liliang and T Mashimo (2012) Onion-like carbon-encapsulated Co, Ni, and Fe magnetic nanoparticles with low cytotoxicity synthesized by a pulsed plasma in a liquid *Carbon* **518** 1776-1785.

[32] Q Chen, T Kitamura, K Saito, K Haruta, Y Yamano, T Ishikawa, H Shirai (2008) Microplasma discharge in ethanol solution: Characterization and its application to the synthesis of carbon microstructure *Thin Solid Films* **516** 4435-4440.

[33] P Bruggeman, J L Walsh, D C Schram, C Leys and M G Kong (2009) Time dependent optical emission spectroscopy of sub-microsecond pulsed plasmas in air with water cathode *Plasma Source Sci. Technol.* **18** 045023-1-5.

[34] P Rumbac, D M Bartels, R M Sankaran and D B Go (2015) The effect of air on solvated electron chemistry at a plasma/liquid interface *J. Phys. D: Appl. Phys.* **49** 424001-1-8.

[35] N Takeuchi, M Ando and K Yasuoka (2015) Investigation of the loss mechanisms of hydroxyl radicals in the decomposition of organic compounds using plasma generated over water *Jpn. J. Appl. Phys.* **54** 116201-1-8.

[36] A K Sharma, B R Locke, P Arce and W C Finney (1993) A preliminary study of pulsed streamer corona discharge for the degradation of phenol in aqueous solutions *Hazardous Waste Hazardous Mater.* **10** 2: 209-215.

[37] I Marinov, S Starikovskaia and A Rousseau (2014) Dynamics of plasma evolution in a nanosecond underwater discharge *J. Phys. D: Appl. Phys.* **47** 224017-1-10.

[38] W F L M Hoeben, E M Veldhuizen, W R Rutgers and G M W Kroesen (1999) Gas phase corona discharges for oxidation of phenol in an aqueous solution *J. Phys. D: Appl. Phys.* **32** 2: L133-137.

[39] P Zhao and S Roy (2014) A modified resistance equation for modeling underwater spark discharge with salinity and high pressure condition *J. Appl. Phys.* **115** 173301-1-9.

[40] R P Joshi, J F Kolb, S Xiao and K H Schoenbach (2009) Aspects of plasma in water: streamer physics and application *Plasma Process. Polym.* **6** 763-777.

[41] K Y Shih and B R Locke (2010) Chemical and physical characteristics of pulsed electrical discharge within gas bubbles in aqueous solution *Plasma Chem. Plasma Process.* **30** 1-20.

[42] W T Shin, A Mirmiran, S Yiacoumi and C Tsouris (1999) Ozonation using microbubbles formed by electric fields *Separarion Purification Tech.* **15** 271-282.

[43] H Homma, H Katayama and K Yasuoka (2008) Pulsed dielectric barrier discharge of argon gas ingas-liquid two-phase flow *IEEE Trans. Plasma Sci.* **36** 4: 1344-1345.

[44] T Ishijima, H Sugiura, R Saito, H Toyoda and H Sugai (2010) Efficient production of microwave bubble plasma in water for plasma processing in liquid *Plasma Sources Sci. Technol.* **19** 015010-1-5.

[45] T Shirafuji, J Ueda, A Nakamura, S P Cho, N Saito, O Takai (2013) Gold nanoparticle synthesis using three-demensionally integrated micro-solution plasmas *Jpn. J. Appl. Phys.* **52** 126202-1-5.

[46] P Sunka, V Babicky, M Clupek, P Lukes, M Simek, J Schmidt and M Cernak (1999) Generation of chemically active species by electrical discharges in water *Plasma Source Sci. Technol.* **8** 258-265.

[47] B Sun, M Sato and J S Clements (1997) Optical study of active species produced by a pulsed streamer corona discharge in water *J. Electrostatics* **39** 189-202.

[48] T Takamatsu, K Uehara, Y Sasaki, H Miyaara, Y Matsumura, A Iwasawa, N Ito, T Azuma, M Kohno and A Okino (2014) Investigation of reactive species using various gas plasmas *RSC Adv.* **4** 39901-39905.

[49] P Lukes, E Dolezalova, I Sisrova and M Clupek (2014) Aqueous-phase chemistry and bactericidal effects from an air discharge plasma in contact with water: evidence for the formation of peroxynitrite through a pseudo-second-order post-discharge reaction of H_2O_2 and HNO_2 *Plasma Source Sci. Technol.* **23** 015019-1-15.

[50] B J J Zheng, S Q M Wu, Q Zhang, Z Yan, Q Xue (2014) Review on electrical discharge plasma technology for wastewater *Chem. Eng. J.* **236** 348-368.

[51] J Zou, Y Zhang and C Liu (2006) Reduction of supported noble-metal ions using glow discharge plasma *Langmuir* **22** 11388-11394.

[52] X Liang, Z Wang and C Liu (2010) Size-controlled of colloidal gold nanoparticles at room temperature under the influence of glow discharge *Nanoscale Res. Lett.* **5** 124-129.

[53] G Saito and T Akiyama (2006) Nanomaterial synthesis using plasma generation in liquid *J Nanomaterials* **123696** 1-21.

Chapter 2

Characterizations of aqueous solution under irradiation of pulsed discharge plasma

2.1 Introduction

Recently, a large number of papers were published about application using discharge plasmas on water surface, particularly in biological and environmental applications. Plasma-water interactions are significant to understand reaction mechanisms by discharge plasmas on water surface. When discharge plasmas are generated from a metal pin electrode in gas phase to water surface, light emissions including UV light are usually observed between the electrode and water surface due to excitation, ionization, and dissociation of gas and water molecules. Optical emission spectra of plasmas inform not only excited species but also characteristics of the plasma. Many researchers observed optical emission spectra of plasmas on water surface, and determined excited species,

plasma temperature, and electron density [1, 2]. In case of discharge plasmas over water surface, active species derived from H_2O are also observed by optical emission of discharge plasma [3, 4].

Chemical reactions by discharge plasmas are supposed to occur at irradiation position and its surrounding when chemical reactive species irradiated on water surface. It leads to induction of chemical reactions. In case of water cathode, energetic positive ions generated by electrical discharge are irradiated on water surface. When these ions have chemical reactivity, reactions occur at plasma-water interface presumably. Even in case inert ion species were irradiated, water molecules (H_2O) are dissociated by charge transfer at gas/liquid interface, and generated oxidation species derived from H_2O such as OH radical and hydrogen peroxide (H_2O_2) [5, 6]. On the other hand, in water anode case, electrons are irradiated to water surface, and part of them dissolved into water. Some electrons convert into hydrated electrons in water, which have strong reduction power.

Focused on inside water under plasma irradiation, OH radicals were detected on the water via terephthalic acid [6, 7]. H_2O_2 and HNO_2 were also generated in water reportedly by discharge plasmas on water surface experimentally and computationally [8–10]. However, it is difficult to detect and identify active species in water directly during plasma irradiation in general. Therefore, detailed reactions and transport of reaction species by the discharge plasmas on water surface and in water have not been clarified yet, although some reaction mechanisms were proposed [11, 12]. Nevertheless, characterizations of aqueous solution under plasma irradiation are essential to utilize it for chemical processing. Thus, properties of pulsed discharge plasma and aqueous solution under plasma irradiation from a macro-viewpoint were examined in this work. Discharge plasmas are accompanied by an electric current resulted in difficulties in direct measurement of solution properties.

Therefore, chemical methods were used for observation of active species and pH value in aqueous solution in present work. They enable to observe spatial distributions of solution properties *in situ* during plasma irradiation. These results may be helpful for efficient reactor design of discharge plasma in contact with water.

There are many studies on discharge plasmas at gas-liquid interface. Researchers conducted the experiments by using individual power sources and reactors, and indicated most efficient condition for reactions on each reactor [13]. Malik compared major type of reactors and conditions of discharge plasmas over water as reported by different research groups [14], and concluded that the energy yield by discharge plasmas over water follows the orders: pulsed DC > continuous DC or AC power, and plasma-water interface > thin film > deep layer. However, the effects of reactor shapes on reaction induced by discharge plasmas are not clear in actuality because the above order was estimated from various experimental conditions by different research groups.

2.2 Experimental setup

Pulsed discharge plasmas were generated from a pin copper electrode to aqueous solution surface. Experiment setup is shown in Figure 2.1. A copper cylindrical electrode with a diameter of 1.00 mm was placed at a distance of 3 mm from the solution surface under atmospheric air. Except the end surface, the outside of the electrode was covered with polyether ether ketone, which exhibits good insulation. The reactor was 50 mm in height, 100 mm in width, and 10 mm in side depth, unless otherwise noted. The side of reactor consists of acrylic resin, which has low permittivity. The bottom is copper sheet, which is

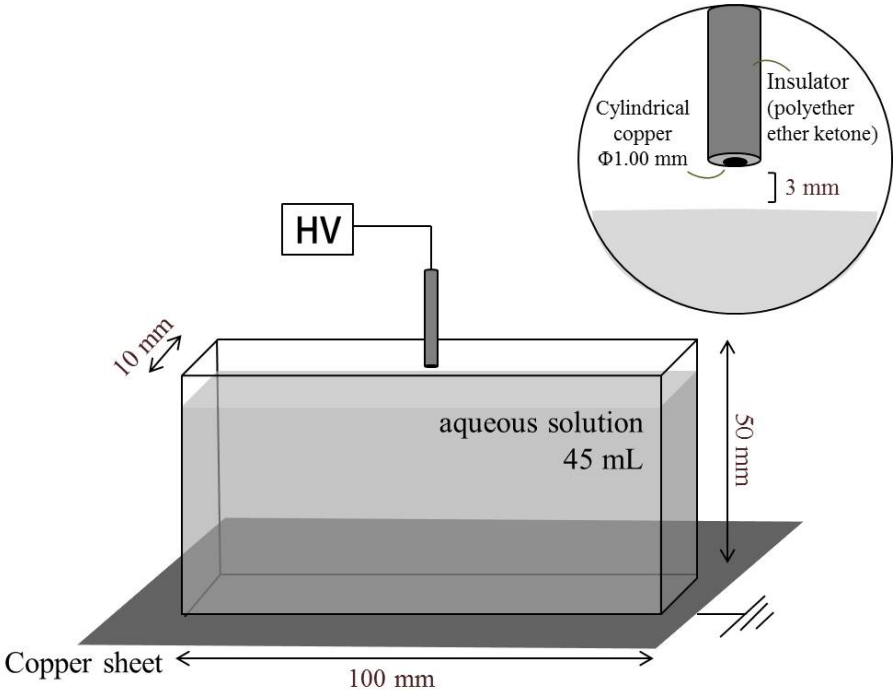

Figure 2.1 Experimental setup of pulsed discharge over solution surface

grounded. The reactor filled with an aqueous solution of 45 mL. In this case, the aqueous solution behaved as the electrode, and the discharge plasmas were irradiated between the metal electrode and solution surface. In section 2.7, the discharge plasmas were generated at N_2, O_2, and Ar atmosphere by using a improved electrode. The closed reactor, which made of stainless steel, was also utilized in order to avoid influences by reactive gases (N_2 and O_2) in atmosphere.

Pulsed voltages were applied to the copper electrode at a frequency of 10 kHz by a pulsed power supply (TE-HVP1510K300NP, Tamaoki Electronics Co. Ltd.). In this work, three types of input power were applied: (a) bipolar pulse, (b) positive pulse, and (c) negative pulse as shown in Figure 2.2. Pulsed voltages were operated by an ON/OFF

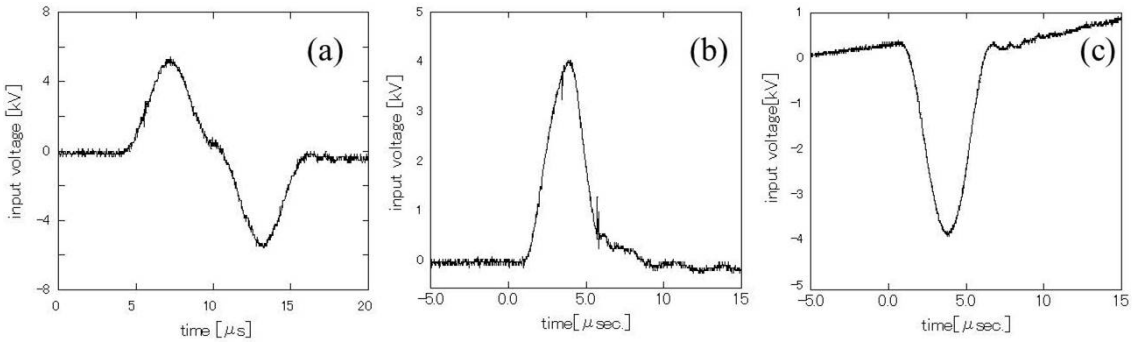

Figure 2.2 Input voltage wavelengths: (a) bipolar pulse, (b) positive pulse, and (c) negative pulse

control (AFG-2005, Goodwill Instrument Co. Ltd.) at a frequency of 20 Hz and duty ratio of 10% to avoid erosion of the metal electrode. Thus, 50 pulses were applied in duration of 5 mseconds prior to a pulse-free interval of 45 mseconds; this operation was performed repeatedly.

2.3 Effects of solution conductivity

2.3.1 Method

When discharge plasmas generated over solution surface, aqueous solution is considered as a dielectric substance [15]. Accordingly, conductivity of aqueous solution is an important factor for plasma properties. The effects of solution conductivity on plasma properties and solution temperature were examined when bipolar pulses at ±4 kV discharge over

NaCl solution, whose conductivity was in a range of 2.5 μS/cm to 10 mS/cm. It is well known that conductivity is proportional to concentration of a solute in a dilute solution by Kohlraush's low. For example, NaCl solution at 1 mS/cm is equal to 0.05 wt%. The experiments were conducted by using a batch type reactor, which filled with 10 mL of NaCl solution and purged by argon gas.

2.3.2 Effects on plasma emissions

ICCD images of bipolar pulsed discharges over NaCl solution depending on solution conductivity were shown in Figure 2.3. In case of discharge over low conductivity solution, the plasma emission was observed in a wide area between a copper electrode and solution

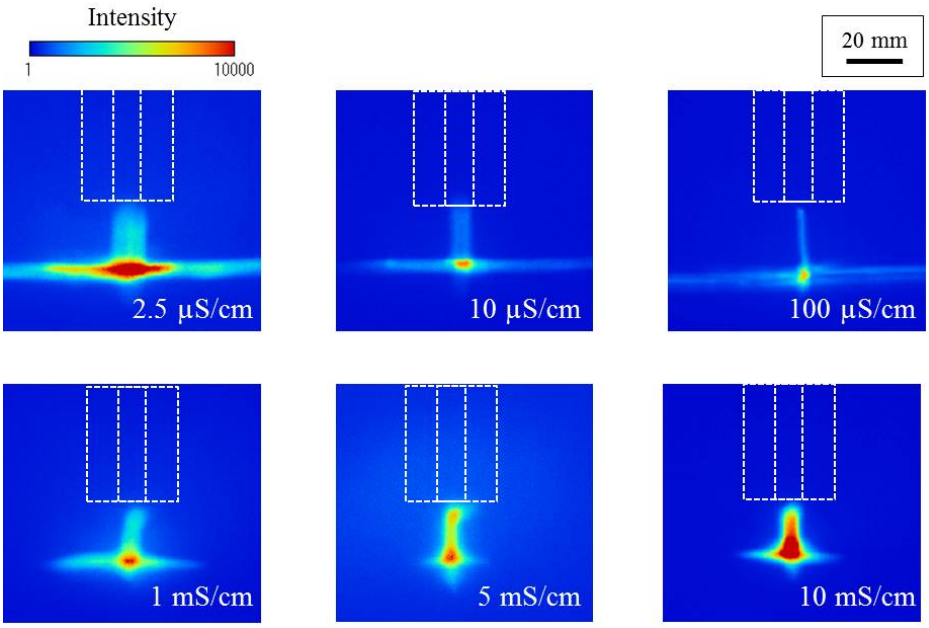

Figure 2.3 ICCD images of bipolar pulsed discharges over NaCl solution depending on solution conductivity

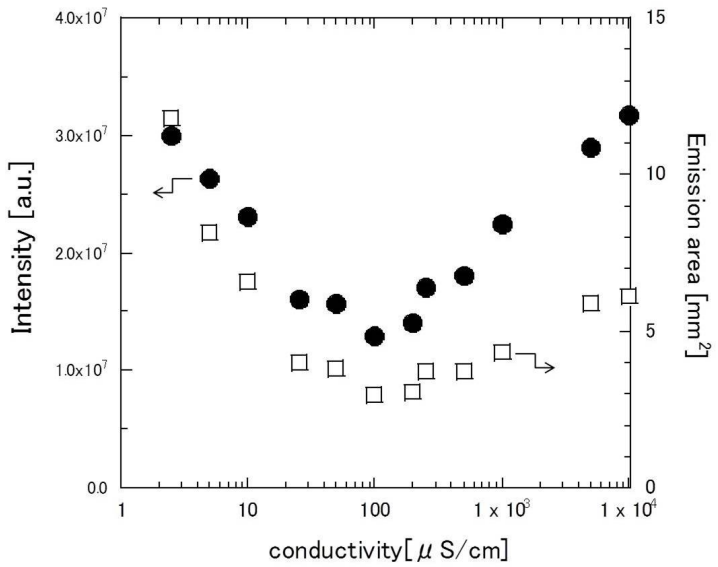

Figure 2.4 The effects of solution conductivity on emission intensity and area of discharge plasma over NaCl solution

surface. Especially, intense emission was observed at solution surface directly under the electrode. Emission region was narrow and weak emission exhibited with increasing solution conductivity. However, in case of high conductivity solution over 100 μS/cm, emission is more intense with increasing solution conductivity. The emission spread in the horizontal direction on the solution surface was suppressed by using NaCl solution over 1 mS/cm. Fig.2.4 shows the effects of solution conductivity on emission intensity and emission area of discharge plasma over NaCl solution. Discharges over the solution at very low conductivity or above certain conductivity exhibited high emission intensity and large emission area, but both of them reached the minimum value at 100 μS/cm.

Figure 2.5 shows the effects of solution conductivity on emission intensity of Ar (810 nm), Hα (656 nm), and OH (310 nm) lines. Emission intensity of Ar line increased

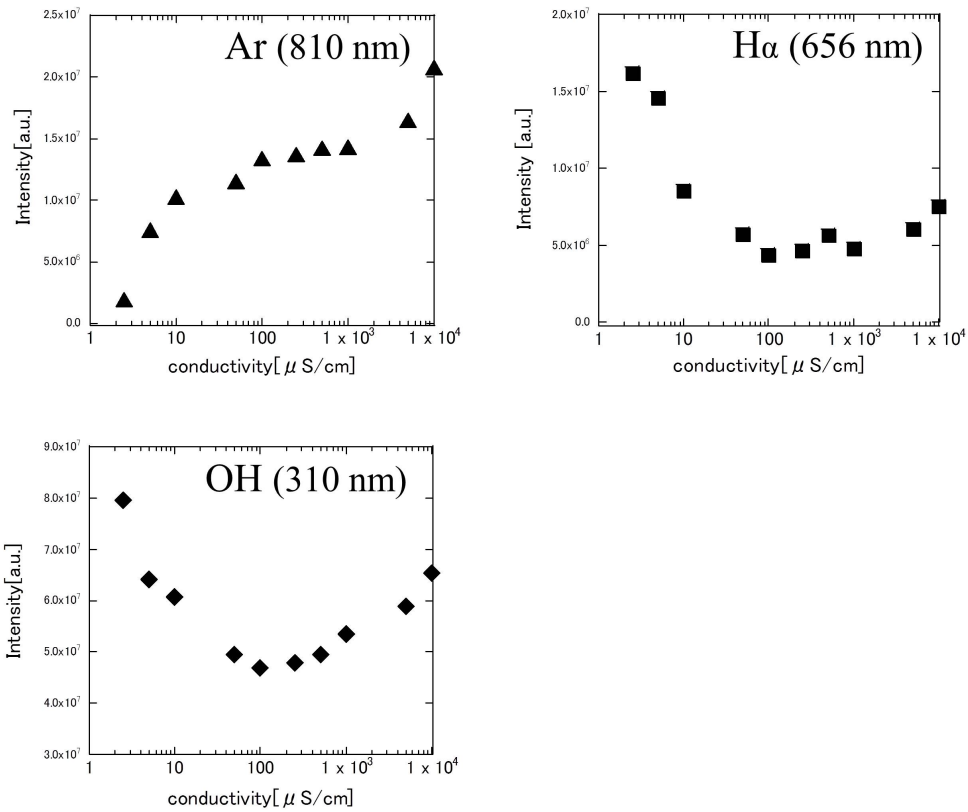

Figure 2.5 The effects of solution conductivity on emission intensity of Ar (810 nm), Hα (656 nm), and OH (310 nm) lines

with increasing solution conductivity, but that of Hα and OH lines had a minimum value at 100 μS/cm. Intensity of each line cannot be compared simply because of the difference in transmittance of each filter, but it was obvious that Hα and OH radical were contributed to the minimum value of emission intensity as shown in Fig.2.4. Their emissions derived from dissociation of H_2O molecules certainly. The conductivity of the solution was great impact on aqueous solution, resulted in influences on plasma properties.

2.3.3 Effects on solution temperature

When discharge plasmas are irradiated over water surface, a temperature of aqueous solution rises in most case. Figure 2.6 shows increasing ratio of the solution temperature by bipolar pulsed discharge at 15 minutes depending on conductivity. The experiments were conducted at 19.0±0.1^{o}C. The low conductivity solution was easy to rise temperature of the solution. Generally, the main cause of temperature rise by discharge plasmas was supposed to be Joule heating. When an electric current I flows for a certain time t in aqueous solution, whose conductivity is Λ, Joule heating Q can be expressed as follow.

$$Q = \frac{I^2}{\Lambda}\, t \tag{2.1}$$

Namely, the increase in temperature by Joule heating determines a ratio of conductivity to a square of electric current. Fig.2.7 shows maximum current of the pulsed discharge depending on solution conductivity by bipolar pulsed discharge over NaCl solution. In general, high conductivity solution is flowed much more current than low conductivity solution. The current values of discharge over low conductivity solution shows almost no difference, but they increased sharply over at 100 μS/cm. When large electric current flowed by discharge plasmas at high conductivity solution above 100 μS/cm, the variation in temperature became small. Therefore, solution conductivity rather than electric current influenced on Joule heating in the solution under plasma irradiation in case of low conductivity solution. Besides, conductivity also influenced on emission intensities of Hα and OH radical. When discharge plasmas were generated over high conductivity solution, electrical current rather than solution conductivity influenced on the increase

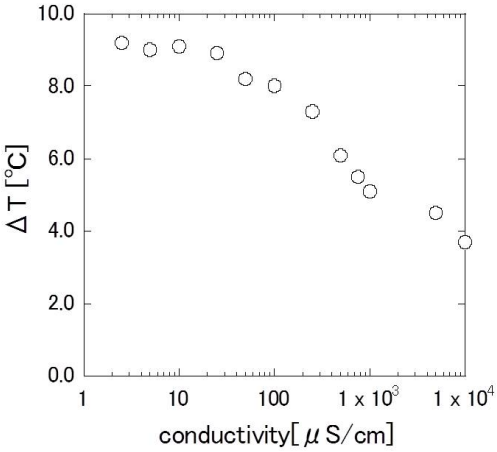

Figure 2.6 Increasing ratios of the solution temperature by bipolar pulsed discharges at 15 minutes depending on conductivity

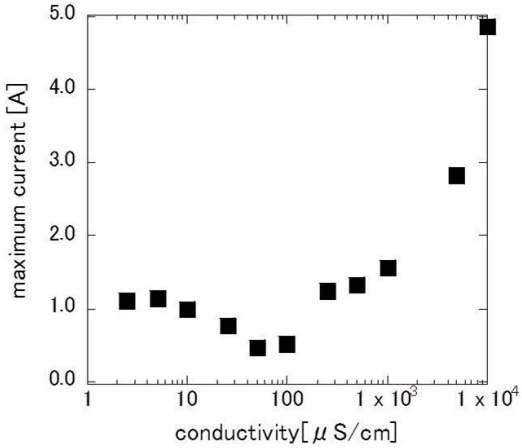

Figure 2.7 Maximum current depending on solution conductivity by bipolar pulsed discharges over NaCl solution

in temperature. It is thought that the solution was considered as an insulator in case of the discharge for low conductivity solution, resulted in intense emission and temperature rise during the discharge.

2.4 Generation of active species

2.4.1 Active species over water surface

2.4.1.1 Optical emission specta

Discharge plasmas were generated over NaCl solution at 100 μS/cm (46.6 mg/L) by pulsed discharges at $\pm$4 kV/+4 kV/$-$4 kV respectively. Optical emission spectra of plasma

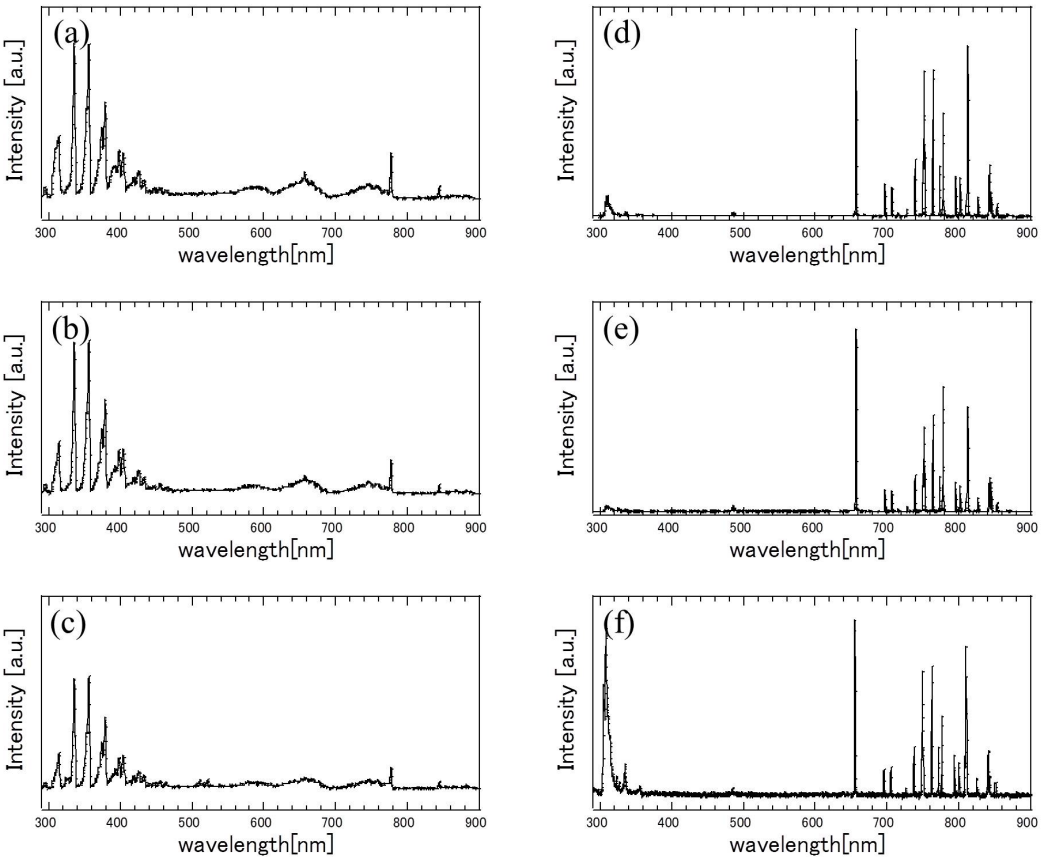

Figure 2.8 Optical emission spectra of discharge plasma over NaCl solution under atmospheric air (a-c) and argon (d-f) by bipolar (a,d), positive (b,d), and negative (c,f) pulses

emissions were observed by using a high-resolution spectrometer (HR2000CG, Ocean Optics Inc.). Figure 2.8 shows optical emission spectra of (a) bipolar, (b) positive, and (c) negative pulsed discharges at atmospheric air. The emissions of N_2 were dominant in either case: N_2 first (550-800 nm) and second (300-400 nm) positive bands. Because N_2 is easy to transition compared to other species, emissions of N_2 2nd positive ($C^2\Pi_u$-$B^3\Pi_g$) and 1st positive ($B^3\Pi_g$-$A^3\Sigma_u^+$) bands are often dominant emissions in the plasmas at

air [16]. The sharp emission lines of O atoms (777 and 845 nm) were also observed in the spectra. They derived from O_2 molecules in air presumably. However, some researchers confirmed emission species from dissociation of water when discharge plasmas were generated at gas-liquid interface [5, 8, 17]. In order to identify other species in discharge plasmas especially from aqueous solution, optical emission spectra were also observed in atmospheric argon as shown in Fig.2.8 (d)-(f). Some Ar lines were detected in 700-850 nm. Besides, Hα (656 nm), O (777 nm), and OH (310 nm) lines derived from water molecules were emitted obviously. They were supposed to be generated near the water surface, thus reactive species derived from water molecule had great impacts on aqueous solution because they have high reactivity.

2.4.1.2 Spatial distribution of each emission species

Spatial distribution of each emission species were observed by using intensified charge coupled device (ICCD) camera (PI-MAX512RB-FG-44, Prinston Instruments Inc.) with interface filter of each spectral line. The gate width of ICCD camera was 15 μseconds, namely images displayed emission intensity while one pulsed voltage was applied. The preceding section mentioned that the emission of N_2 bands were dominant in spectra. This section focused on emission species derived from water molecules, thus the experiments were conducted in closed reactor purged argon gas (Ar).

Figure 2.9 shows ICCD images of all spectra, Ar (810 nm), Hα (656 nm), and OH radical (310 nm) by bipolar, positive, and negative pulsed discharges. Plasma emissions were generated from the electrode toward the solution surfaces. Furthermore, they were also generated along the solution surfaces. Intense emissions were observed on solution

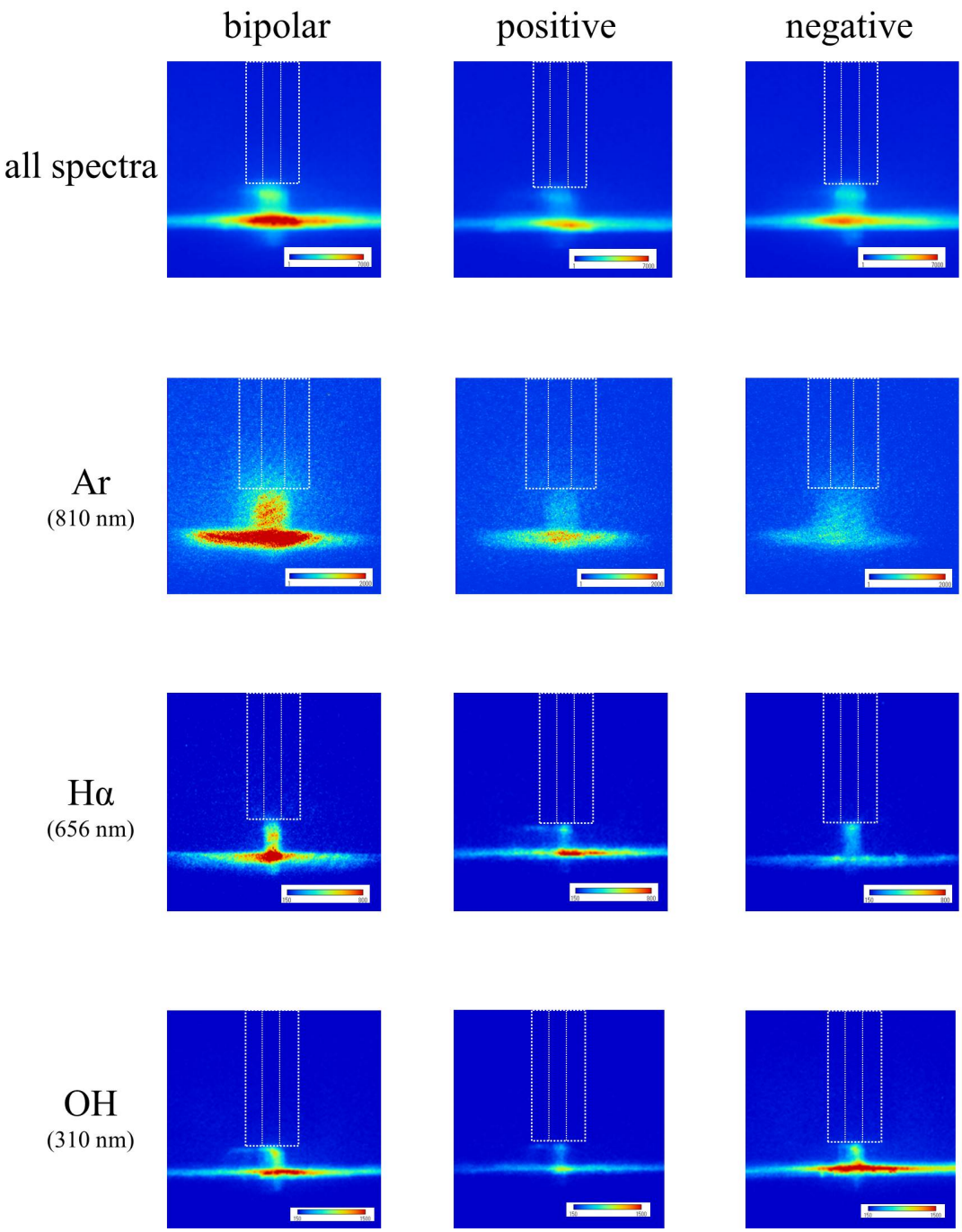

Figure 2.9 ICCD images of all spectra, Ar (810 nm), Hα (656 nm), and OH radical (310 nm) by bipolar, positive, and negative pulsed discharges

surface under the electrode. The emission of Ar was observed at relatively wide region. Positive pulses induced more intense emission of Hα and Ar than negative pulses, but OH radical was easy to obtain by negative pulses. Kang *et al.* researched the effects of voltage polarity on the wavelength-resoluted ICCD images [18], although they used nozzle electrode, in which helium gas flowed during the discharge. The similar effects of voltage polarity on ICCD images were observed in their study: helium (atmospheric gas) was emitted by positive discharges between a metal electrode and aqueous solution, but sodium contained in aqueous solution was emitted by negative discharges near the solution surface. Additionally, generation of OH radicals at gas-liquid interface by the discharge was also observed by Sasaki *et al.* by using laser-induced fluorescence [19]. Impact of electrons by negative pulse is less powerful than that of ions [6]. Additionally, OH radicals are formed easily by excitation energy transfer from Ar metastable atom (Penning ionization) [16]. Energy of electron impact by negative pulses was sufficient for formation of OH radical, but that by positive pulses was supposed to be excess energy for OH radical formation. It led to dissociation of OH radicals, and generated H and O atoms, resulted in the increase in emission of Hα. ICCD images by bipolar pulses were similar to the sum of positive and negative pulses.

2.4.2 Active species in water

2.4.2.1 Method

Reactive oxidation species in aqueous solution were measured by iodometric method using potassium iodide (KI). Iodine ions (I^-) are oxidized easily because of low oxidation-reduction potential, and convert into iodine molecules (I_2) as shown in Eq.(2.2).

$$2I^- \longrightarrow I_2 + 2e^- \qquad E^0 = -0.535\ V \tag{2.2}$$

When oxidation species generated by the discharge in water, I^- ions are oxidized and produce I_2 molecules, which can detected by iodo-starch reaction. By using this method, concentration, distribution, and transportation of reactive oxidation species in water can be observed during plasma irradiation.

In present work, discharge voltages at +4 kV and −4 kV were applied to the electrode, and discharge plasmas were generated over 100 mmol/L KI solution including starch at 0.35 wt%.

2.4.2.2 Reactive oxidation species in water under plasma irradiation

Figure 2.10 shows distribution of reactive oxidation species as a function of treatment time by positive pulsed discharges at +4 kV. After beginning of the discharge, reactive oxidation species were produced at plasma-solution interface, and transported toward the bottom of the reactor. However, they did not flow toward the bottom after few seconds, and accumulated near water surface directly under the electrode. Then, they flowed toward the side walls of the reactor. As the flow reached the side walls, it turned and formed a layer approximately 10 mm of reacted solution region on the upper part of the reactor. Even with increasing treatment time over 300 seconds, thickness of the layer did not change, and reacted solution just diffused to the lower part of the reactor. Fig.2.11 shows enlarged images of the solution applied positive pulses after beginning of the discharge. The reacted solution flowed toward the bottom until 4 seconds, but swirled around the solution surface nearby plasma irradiation position. It was due to the effect of ionic wind. When positive

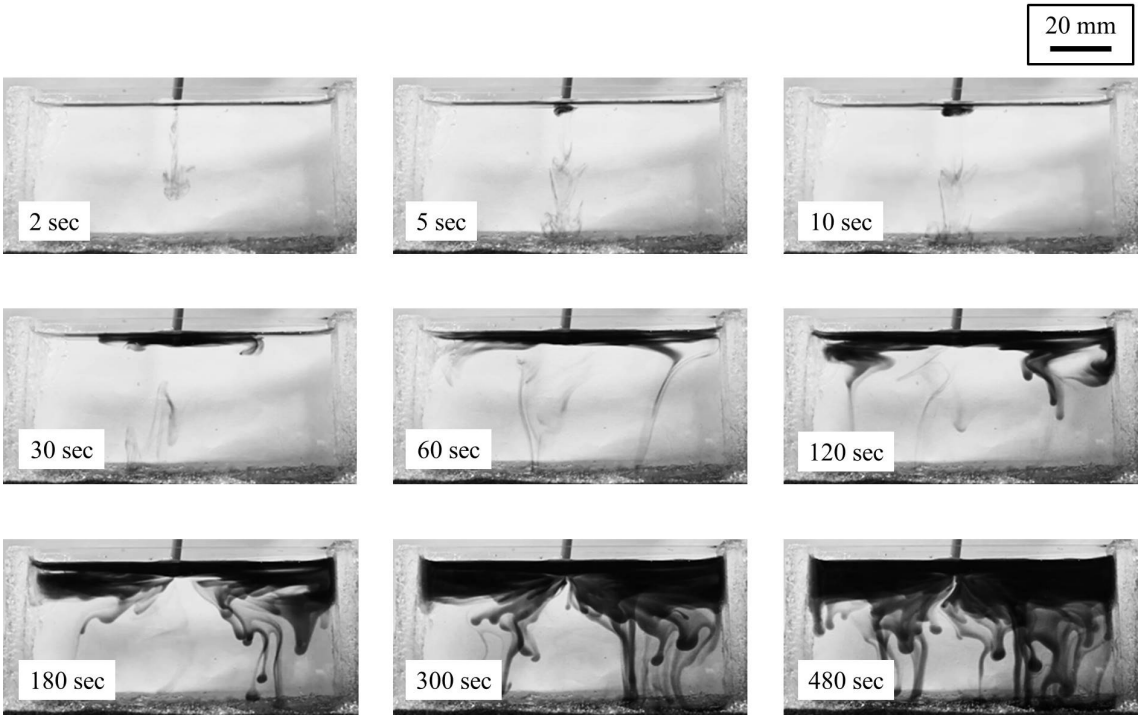

Figure 2.10 Distributions of reactive oxidation species as a function of treatment time by positive pulsed discharge at +4 kV

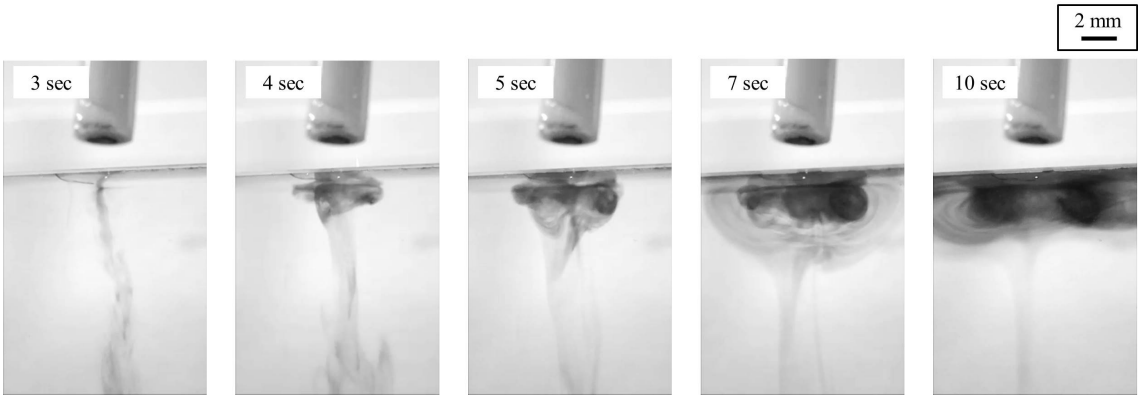

Figure 2.11 Enlarged images of the solution applied positive pulses after beginning of the discharge

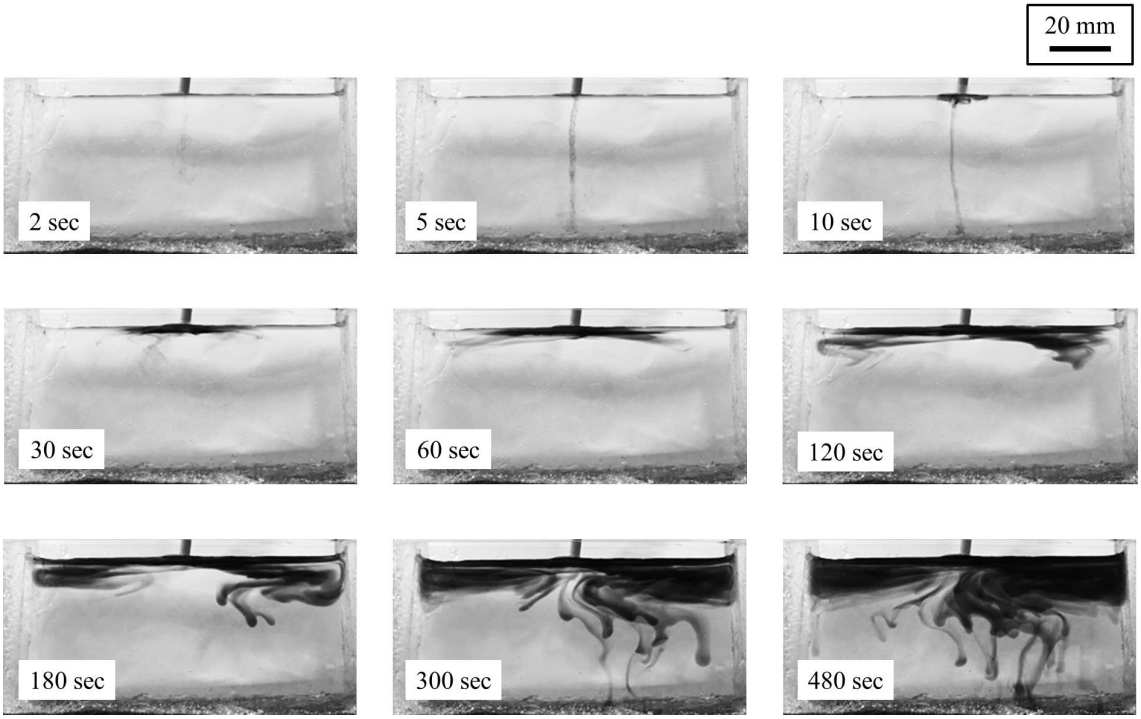

Figure 2.12 Distributions of reactive oxidation species as a function of treatment time by negative pulsed discharges at −4 kV

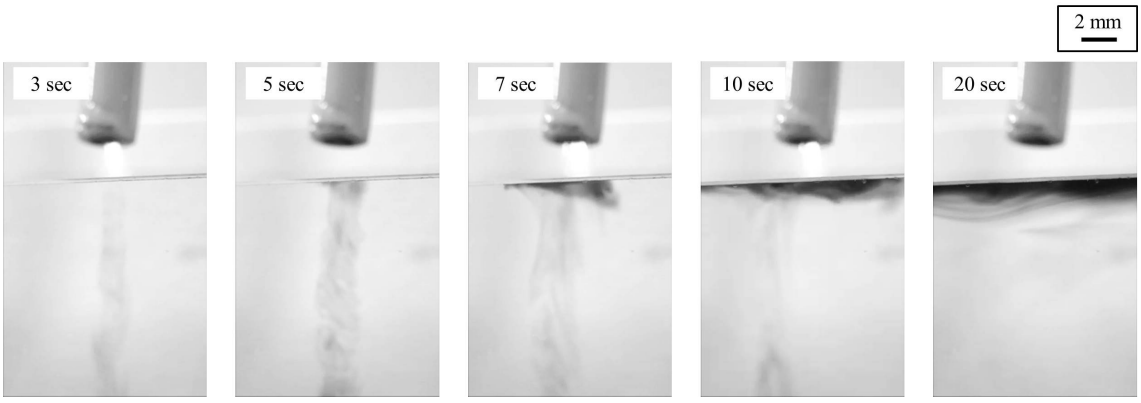

Figure 2.13 Enlarged images of the solution applied negative pulses after beginning of the discharge

discharges are generated over water surface, the ionic wind progressed outward along the air-solution interface [20]. It leads to clockwise and counterclockwise flows of the solution [7, 21]. It took about 5 seconds until the influence of ionic wind on solution flow. Therefore, the flow of reacted solution toward the bottom of the reactor was the influence on discharge plasma purely. In contrast, the effect of ionic wind was superiority after 4 seconds. The thickness of reacted solution after 10 seconds was about 2 mm. It progressed to the side walls while keeping the thickness of the layer.

In case of water cathode, a little amount of OH radical is generated by the discharge (see preceding section), but impacts of positive ions on water surface were presumably efficient for generation of oxidation species. However, it is thought that not only OH radicals but also superoxide (O_2^-) and hydrogen peroxide (H_2O_2) [6], which have long-life time compared with OH radical, were produced by positive discharges, and affected on aqueous solution. Nevertheless, these oxidation species reached directly 2 mm from the solution surface in the deepest by positive pulsed discharges.

On the other hand, Figures 2.12 and 2.13 show images of KI solution applied negative pulsed discharges at -4 kV. Negative pulsed discharges were hard to form ionic wind, leading to suppression of reacted solution flow. The progress in flow of reacted solution by negative pulses is similar to positive pulses, and reacted region after 10 seconds was also 10 mm in the depth. Overall, an amount of reactive oxidation species by negative pulses were smaller than positive pulses according to color of the solution after discharges. The thickness of reacted solution after beginning of negative discharge as shown in Fig.2.13 was about 1 mm, which was thinner than positive case. Negative pulsed discharges generated a lot of OH radicals at solution surface (see preceding section). OH radical has strong oxidizability, but the life time of OH radical is very short compared with

other oxidation species. Accordingly, reactive oxidation species were generated only at plasma-solution interface, and flowed in the upper part of the reactor.

2.5 Oxidation-reduction reactions

2.5.1 Oxidation reactions

2.5.1.1 Materials

Oxidation reactions induced by pulsed discharge plasmas were examined by using three model materials: (a) coomassie brilliant blue R-250 (CBB, Wako Chemical Co.), (b) congo red (CR, Sigma Chemical Co.), and (c) acid orange 7 (AO7, Aldrich Chemical Co.). The structure of each material is indicated in Figure 2.14. They dissolved in purified water at 10 mg/L, and pulsed discharge plasmas at $+10$ kV and -10 kV were generated over

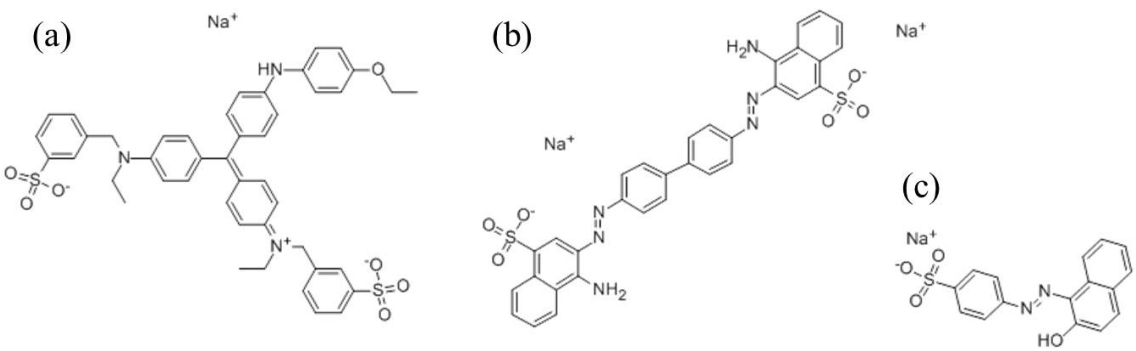

Figure 2.14 Structures of (a) coomassie brilliant blue R-250, (b) congo red, and (c) acid orange 7

solution surface. The conductivity of CBB, CR, and AO7 solution were 3.1, 11.6, and 8.1 μS/cm respectively. I observed oxidation reactions of model compounds in aqueous solution by positive and negative pulses. Concentrations of CBB after treatment of the discharge were measured by UV-Vis spectrophotometer (V-550, Jasco Co.).

2.5.1.2 Oxidation reactions

Figures 2.15 and 2.16 show images of (a) coomassie brilliant blue (CBB), (b) congo red (CR), and acid orange 7 (AO7) solution under irradiation of positive and negative pulsed discharges as a function of treatment time. All materials were decomposed by oxidation reaction induced by positive and negative pulsed discharge. In case of CBB and CR solutions, compounds in water oxidized from the upper part of the reactor, as a layer of reacted solution was clearly visible. The thickness of the layer was 10 mm, corresponded to existence region of active oxygen species (see preceding section). In positive pulses case, reacted solution remained this region until 40 minutes, but began to diffuse throughout the reactor after 10 minutes. Consequently, the concentrations of compounds were uniform in the whole of the reactor after 60 minutes. In all cases, oxidation reactions were occurred through the similar progress. In contrast, negative pulses took much time to form the layer of reacted solution, and concentrations of compounds were ununiformed in the reactor after 60 minutes of the discharge. Red color of the solution after negative discharges for AO7 was supposed to be caused by degradation products. CBB and AO7 were oxidized easily by positive pulses, although negative pulses were more efficient to decompose CR than positive pulses. It is believed that high oxidation potential was required in order to decomposed CR. Negative discharges generated more OH radicals, which had

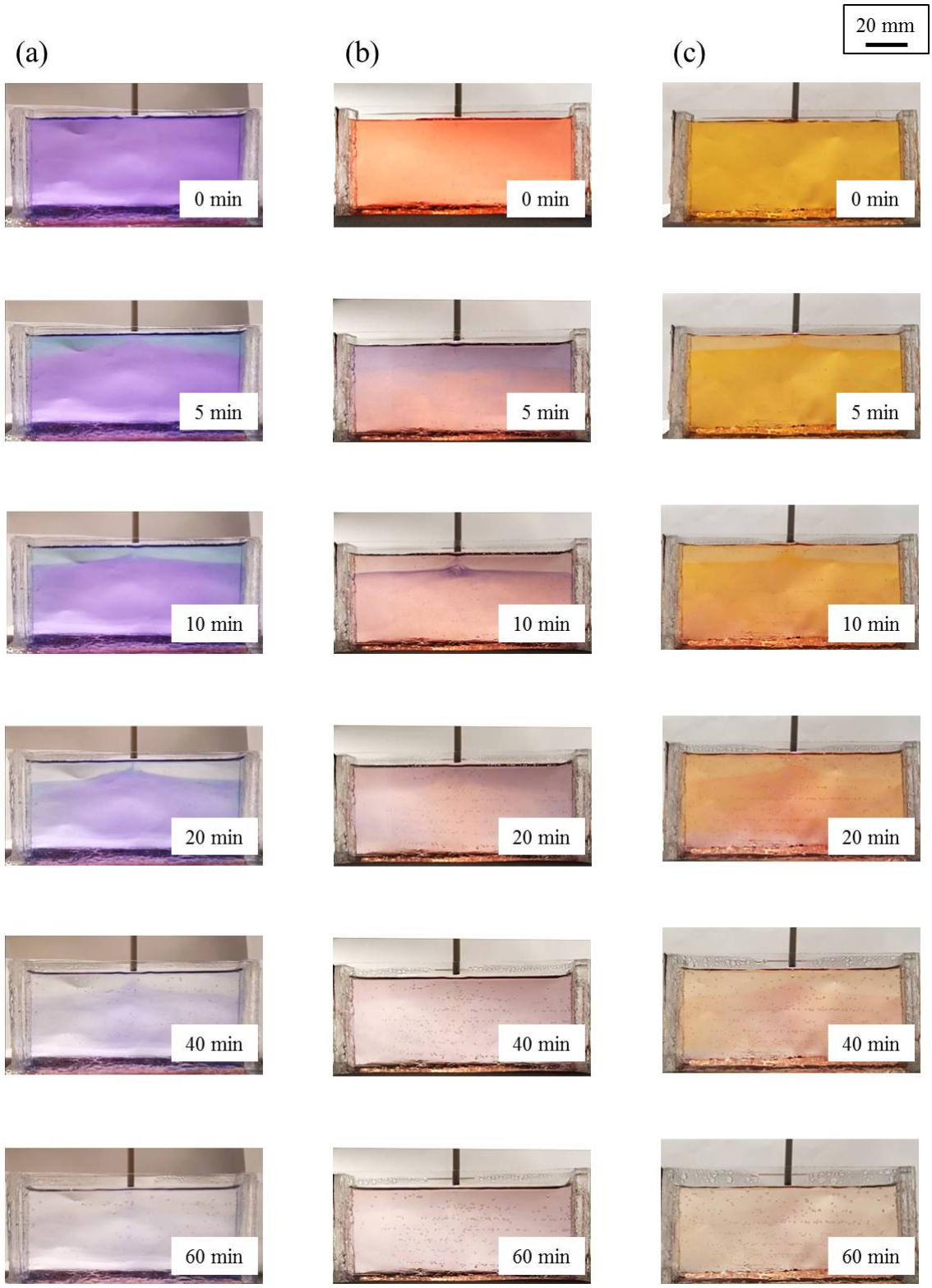

Figure 2.15 Images of (a) CBB, (b) CR, and AO7 solution under irradiation of positive pulsed discharges as a function of treatment time

Figure 2.16 Images of (a) CBB, (b) CR, and AO7 solution under irradiation of negative pulsed discharges as a function of treatment time

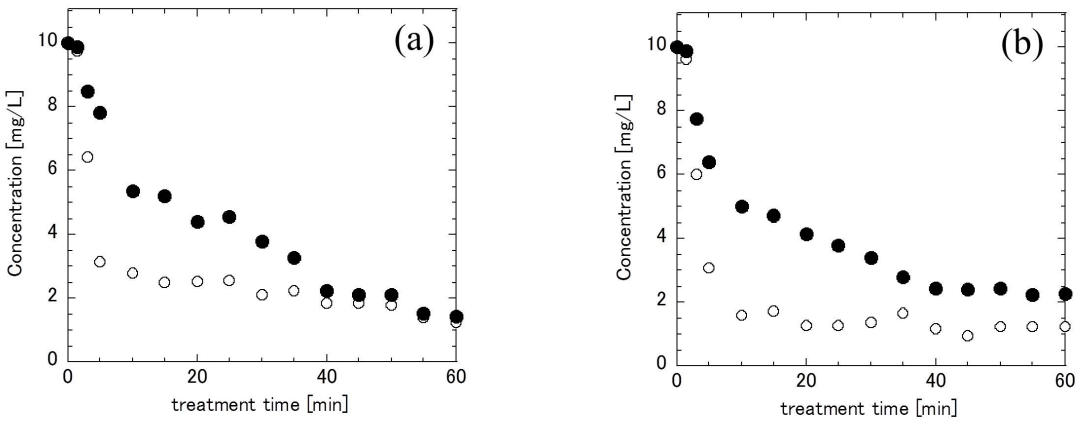

Figure 2.17 Concentrations of CBB at surface of the solution (○) and total concentration in the reactor (●) after (a) positive and (b) negative pulsed discharge

high oxidation potential (2.80 V) [22], leading to CR decomposition. However, CR was difficult to be decomposed by oxidation species with low oxidation potential such as H_2O_2 (1.70 V) and HO_2^- (1.78 V). Therefore, the compounds, which could be decomposed easily, were oxidized by positive pulsed discharges effectively. However, decomposing persistent compounds were effectively oxidized by negative pulsed discharges.

Figure 2.17 shows concentrations of CBB at surface of the solution and total concentration in the reactor after positive and negative pulsed discharges. CBB at surface of the solution decomposed immediately after beginning of the discharges in both cases. Concentration of CBB at solution surface degraded rapidly by positive pulses until 5 minutes, and decreased gradually after that. Negative pulses also induced the decrease in CBB concentration at the solution surface. Concentration of CBB at solution surface saturated after 10 minutes of negative discharge. Focused on total CBB concentrations in the reactor, they decreased suddenly after beginning of the discharge due to decomposition

Table 2.1 Reaction rates of CBB decomposition by positive and negative pulsed discharge

	Reaction rate [nmol·L^{-1}·s^{-1}]	
time	positive pulses	negative pulses
0-10 min	9.1	11.0
10-40 min	1.5	1.6
40-60 min	0.9	0.2

of CBB nearby solution surface, but they decreased gradually as time went by. At this time, the region of reacted solution became wider because of diffusion according to Fig.2.15 and 2.16. After 60 minutes of positive pulsed discharges, total CBB concentration reached that at solution surface, but did not reached by negative pulsed discharges.

Table 2.1 indicates reaction rate of CBB decomposition by positive and negative pulsed discharges. The reaction rate of negative pulses was higher than that of positive pulses at the beginning of the discharge. After 10 minutes, they are similar to each other. Positive pulses oxidized CBB by degree after 40 minutes, although negative pulses hardly induced the reaction. Eventually, positive pulses were more efficient for oxidation reactions at 60 minutes in case of decomposition of CBB in the solution.

2.5.2 Reduction reactions

2.5.2.1 Materials

Reduction reactions induced by pulsed discharge plasma were examined by material synthesis from metal ions in water. Some researchers reported that nanomaterials synthesized from metal ions in water by discharge plasma at gas-liquid interface [23, 24].

In present work, 0.2 mM tetrachloroauric acid ($HAuCl_4$, Wako Chemical. Co.) and 0.1 mM silver nitrate ($AgNO_3$, Wako Chemical. Co.) were utilized for gold and silver particles syntheses. The half equations and oxidation-reduction potential of $AuCl_4^-$ and Ag^+ ions indicates in Eqs.(2.3) and (2.4).

$$AuCl_4^- + 3e^- \longrightarrow Au + 4Cl^- \qquad E^0 = +1.00\ V \tag{2.3}$$

$$Ag^+ + e^- \longrightarrow Ag \qquad E^0 = +0.80\ V \tag{2.4}$$

Pulsed discharge at $+10$ kV and -10 kV, which controlled by on/off control at 20 % of duty ratio, were generated over $HAuCl_4$ and $AgNO_3$ solution, and observed Au and Ag metal particles production.

2.5.2.2 Reduction reactions

Au particle was not formed from $HAuCl_4$ by neither positive nor negative pulses even by long-time discharge. Ag particle was not also synthesized by positive pulsed discharges. However, negative pulsed discharges synthesized Ag particles slightly as shown in

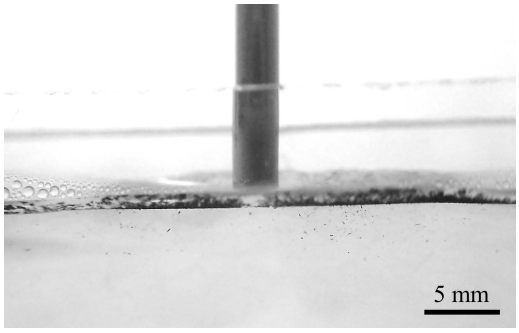

Figure 2.18 The Ag particles synthesized by negative pulsed discharge

Figure 2.18. Ag particles were generated only at plasma irradiation area (plasma-solution interface). Because redox potential of Ag^+ ion is lower than $AuCl_4^-$ ion, redox power of pulsed discharge plasma was supposed to lack for Au particle synthesis, but reach for Ag particle synthesis. It is thought that a main cause of reduction reactions by discharge plasma at air-water interface is hydrated electrons. In case of positive discharge, hydrated electrons generated only when high energy ions are collide with water surface [6]. Positive pulses of my experiments were hard to generate high energy ion probably, thus reductions reactions did not occur by positive pulsed discharge. On the other hand, negative discharge produced a little amount of hydrated electron. It led to production of Ag particles.

2.6 Spatial pH distribution

2.6.1 Material

The pH value of aqueous solution gives a great influence on chemical reactions. It also affects plasma properties because conductivity of aqueous solution is changed depending

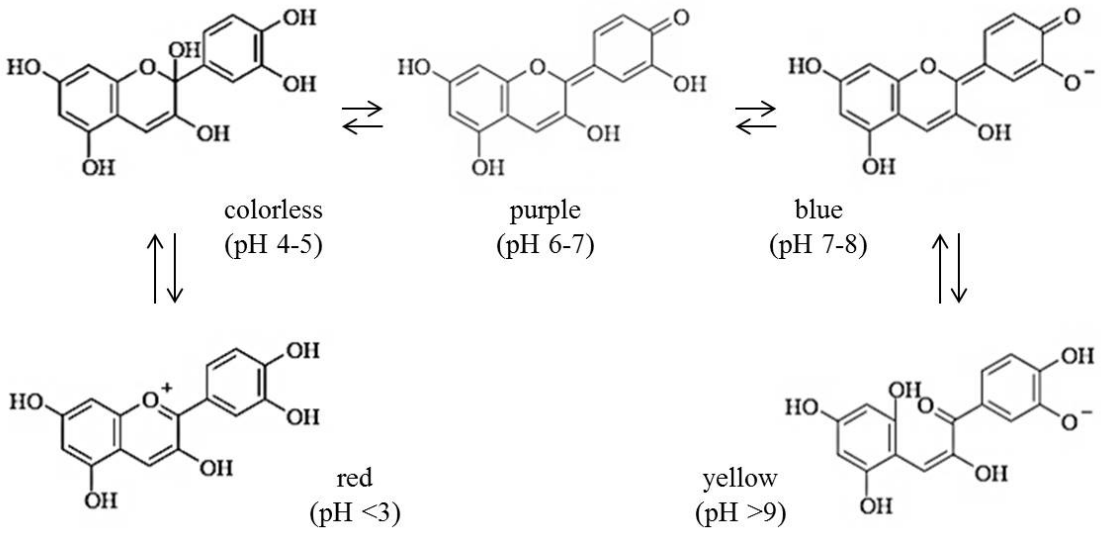

Figure 2.19 Structures of cyanidin (one of the anthocyanins) depending on pH value

on pH value [25, 26]. When discharge plasmas irradiate over aqueous solution surface, oxidation reactions are induce in aqueous solution mainly, leading to a decrease in pH value of the solution. The solution has spatial distribution of pH value in a reactor presumably during plasma irradiation. Nevertheless, a direct measurement of pH values cannot conduct during the discharge because of electric current. In addition, the correction is required in case of direct measurement because the pH value changes depending on a solution temperature. The solution temperature increases by discharge plasmas (see section 2.3). Thus, the direct measurement is unsuitable, but the chemical method is valid for pH observation in water under plasma irradiation. Tochikubo *et al.* utilized bromothymol blue (BTB) for pH indicator during discharge over aqueous solution surface reportedly [6]. There are a lot of pH indicators, but the indicators ranges of them are narrow, and we only get the information whether pH value of the solution increase or

decrease in general. This work used anthocyanins as pH indicator, which has wide indicator range. Anthocyanins are plant pigment including flower, vegetable, and so on. They form a variety of structures as pH changes as shown in Figure 2.19. By using anthocyanins for pH indicator, slight changes of pH value can be detected visually.

2.6.2 Method

Positive and negative pulses at $+4$ kV and -4 kV discharged over anthocyanins solution and observed spatial pH distribution of the solution under plasma irradiation. Anthocyanins powder was prepared to extract from violet cabbage by hot water, refine, and freeze-dry. Some kind of anthocyanins included in this anthocyanins powder, thus concentration of all anthocyanins determined as cyanidin-3-glucoside chloride by UV-Vis spectrometer. The experiments were conducted by using 0.3 mmol/L anthocyanins solution. The anthocyanins solution was controlled at pH 8.0 before the discharge in order to observe pH changes of the solution clearly. The conductivity of the solution was 750 μS/cm. The images of the solution under plasma irradiation were analyzed by image analysis (Igor Pro 6, WaveMetrics Inc.), and determined the pH value of the solution.

2.6.3 Spatial pH distribution induced by pulsed discharge

Figure 2.20 shows images of anthocyanins solution under plasma irradiation by positive pulses as a function of treatment time. Although the decrease in pH value was caused by oxidation reactions of anthocyanins, there was no effect on pH measurement owing to

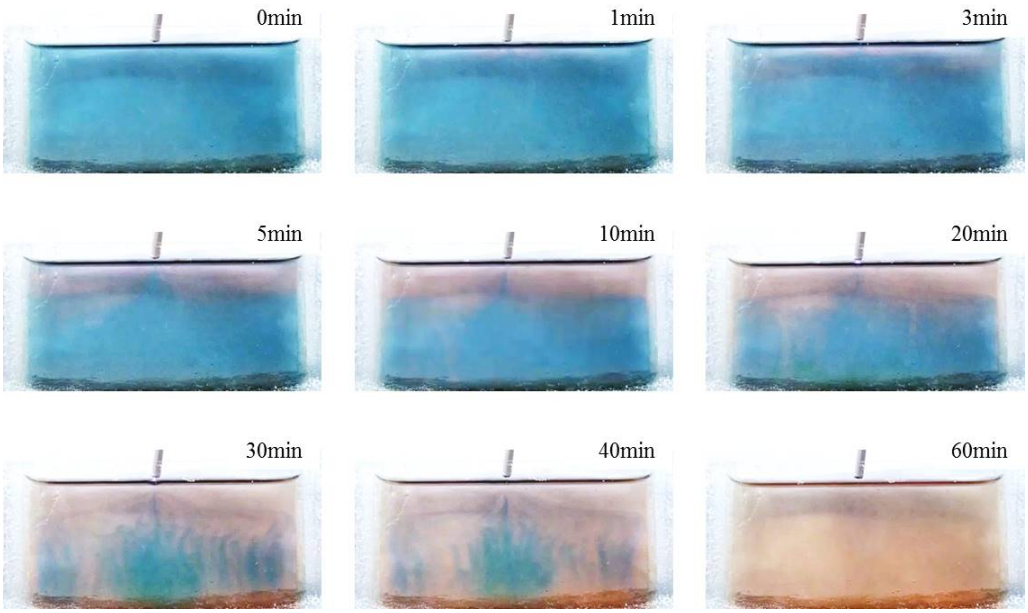

Figure 2.20 The images of anthocyanins solution under plasma irradiation by positive pulses as a function of treatment time

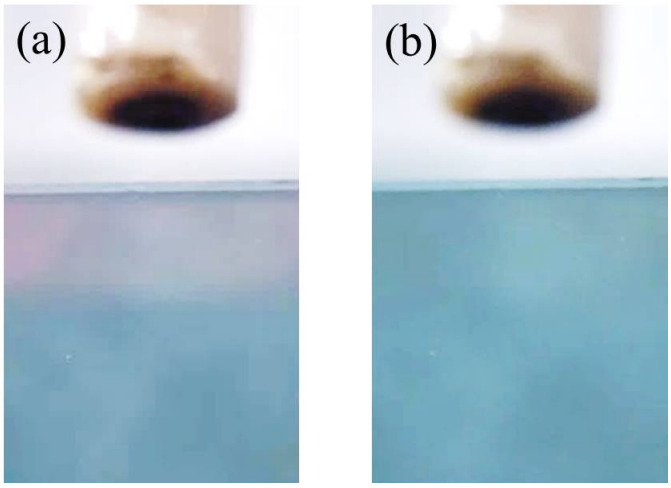

Figure 2.21 The enlarged images of anthocyanins solution after 1 minute of positive and negative pulsed discharges

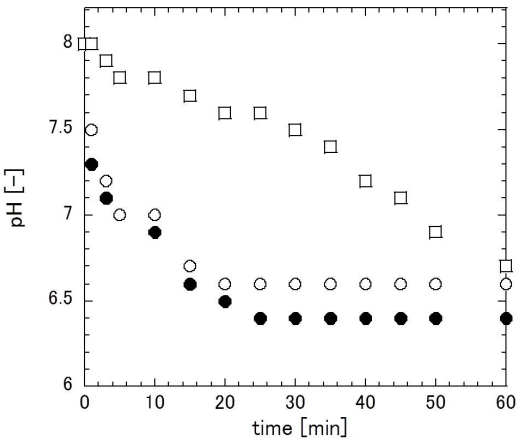

Figure 2.22 The averages of pH values at the outermost surface layer (●, 2mm in depth from solution surface), the upper surface layer (○, 10 mm in depth from solution surface), and the lower area (□, the solution area except upper surface layer) by positive pulsed discharges

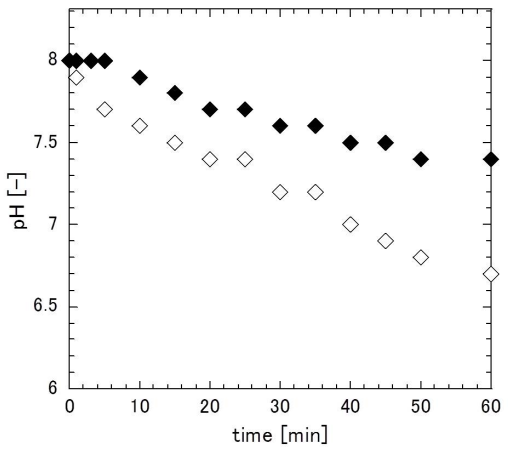

Figure 2.23 Comparison of pH changes by positive (◇) and negative (◆) pulses during plasma irradiation

low decomposition of anthocyanins. Positive pulsed discharges induced the decrease in pH value at the solution surface primarily, but the pH values of the solution are steady until 5 minutes in case of negative pulsed discharges. Fig.2.21 shows the enlarged images of anthocyanins solution after 1 minute of positive and negative pulsed discharges. The region of 2 mm from solution surface changed the pH values from pH 8.0 to 7.0 by positive pulsed discharge. It coincided with the existing region of reactive oxidation species shown in Fig.2.11 (see section 2.4). Low pH region after 5, 10, and 20 minutes of positive pulsed discharges in Fig.2.20 is similar to reacted region of CBB in Fig.2.15 (see preceding section). Therefore, the pH distribution by positive pulses in the reactor depended on oxidation reactions.

Figure 2.22 shows the averages of pH values at the outermost surface layer (2 mm

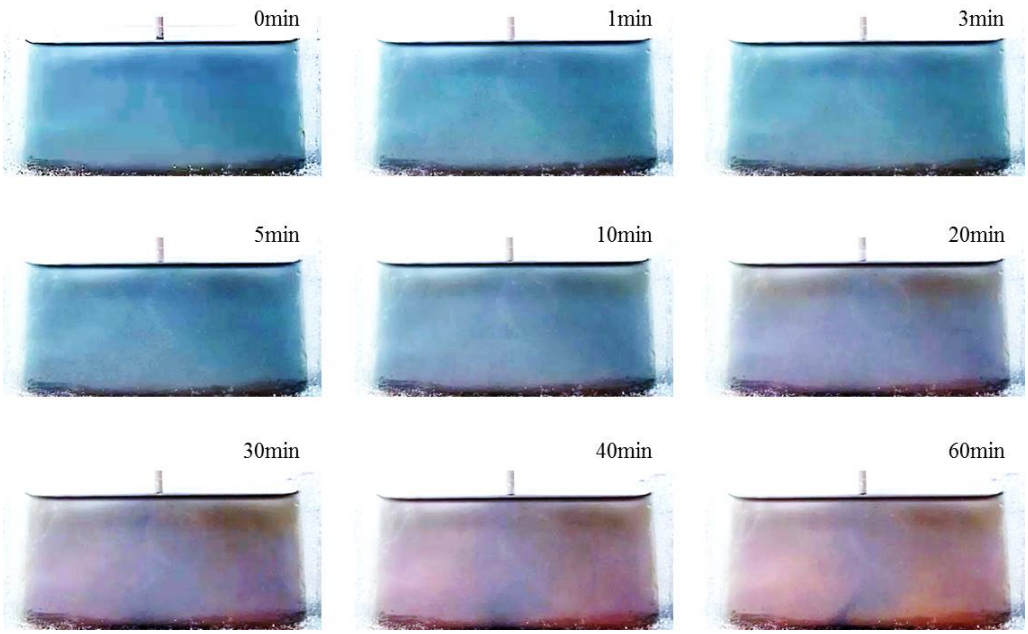

Figure 2.24 The images of anthocyanins solution under plasma irradiation by negative pulses as a function of treatment time

in depth from solution surface), the upper surface layer (10 mm in depth from solution surface), and the lower area (the solution area except upper surface layer) by positive pulsed discharges. The pH values of the outmost and upper layer did not decrease immediately after discharge beginning unlike the decomposition of CBB as shown in Fig.2.17 (see preceding section). It took 20 minutes to decrease the pH value at the outmost and upper layer, and the pH values at the outmost and upper layer were saturated after 20 minutes. In contrast, the pH values at the lower area decreased monotonously.

Figure 2.24 shows images of anthocyanins solution under plasma irradiation by negative pulses as a function of treatment time. In case of negative discharges, the pH values decrease gradually as a whole. Fig.2.23 shows comparison of pH changes by

positive and negative pulses during plasma irradiation. Negative pulses were harder to decrease in pH value than positive pulses. Negative pulses induced oxidation and reduction reactions. These reactions occurred only at solution surface, but their impacts were small not so much as the change in solution pH, leading to slow speed of pH changes by negative discharges.

2.7 Effects of gas atmosphere

2.7.1 Experimental setup

In previous sections, the discharge plasmas were basically generated in atmospheric air. Air contains nitrogen (N_2), oxygen (O_2) molecules, and so on. In order to identify which molecules is effective for chemical reactions induced by pulsed discharge, discharge plasmas were generated at varying conditions of atmospheric gases by using improved electrode as shown in Figure 2.25. The cylinder copper electrode at ϕ 1.00 mm was put into glass tube, whose inner diameter is 3.9 mm. N_2, O_2, and argon (Ar) gases flowed in glass tube at 150 mL/min, and introduced gas-rich conditions were created between the electrode and solution surface. Additionally, dry air, which included N_2 at 75.5%, O_2 at 23.2%, and Ar at 1.3% , was also introduced and produced discharge plasma as reference data. The electrode protruded from glass tube at 1 mm. The gap length between the copper electrode and solution surface was 3 mm. Optical emission spectra of discharge plasma were observed in order to identify species of discharge plasmas, and the influences on oxidation reaction induced by discharge plasmas were examined.

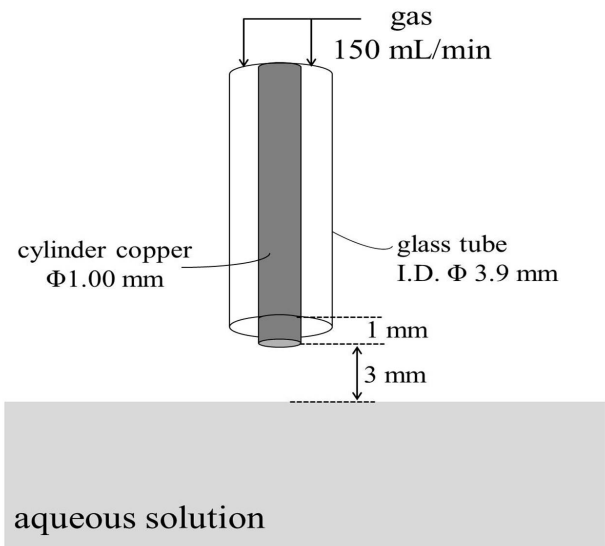

Figure 2.25 The improved electrode of pulsed discharge at varying conditions of atmospheric gases

2.7.2 Optical emission spectra

Optical emission spectra of the plasma emissions were observed during positive and negative pulsed discharges under N_2, O_2, and Ar atmosphere as shown in Figure 2.26. The emission of plasma under atmospheric air was similar to that under N_2 gas. In addition, emissions of oxygen atoms at 777 and 845 nm were also observed in the spectrum of atmospheric air. The positive discharges under N_2, O_2, and Ar atmosphere exhibited Hα line at 656 nm. It also observed in the spectra of negative discharge under Ar atmosphere. In case of the discharge at O_2 gas, emissions of O atoms (777 and 845 nm) were dominant

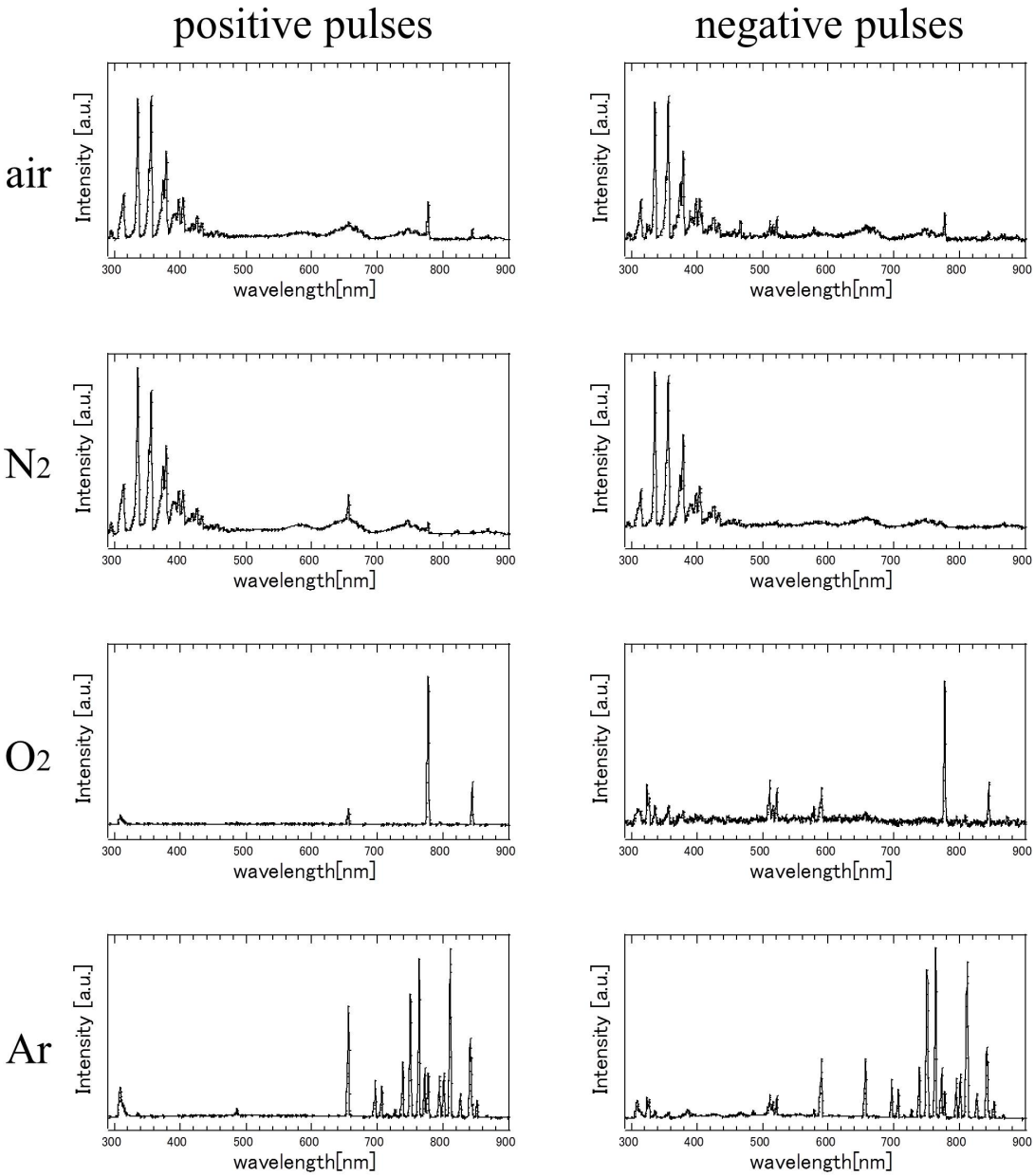

Figure 2.26 Optical emission spectra of positive and negative pulsed discharges at air, N_2, O_2, and Ar atmospheres

of the discharge. The discharge under Ar atmosphere also emitted O atoms derived from water molecules. The emission of OH radicals (310 nm) was detected when discharge plasmas were generated under O_2 and Ar gas. Additionally, negative pulsed discharges usually emitted Na line (589 nm), which included in aqueous solution. In case large current flows in aqueous solution as a cathode, slight emission of solute were measured near the water surface [27]. Although the current waveforms of the discharges could not measure, impulse current by negative pulsed discharges assumed to be high, leading to Na emissions in Fig.2.26.

2.7.3 Oxidation reactions

The effects of gas atmosphere on oxidation reactions were examined by CBB decomposition. Figure 2.27 shows CBB concentrations after 30 minutes of positive and negative pulsed discharges at air, N_2, O_2, and Ar atmosphere. CBB was decomposed from 10 mg/L by all conditions. Negative discharges decomposed CBB in water a little more than positive discharges in either case. The discharge at atmospheric air was the most efficient of the four gases. However, oxidation reactions did not depend on atmospheric gas particularly. Therefore, oxidation reactions induced by discharge plasma were caused by not only specific species but some species. According to the results of the discharge at air, it is implied that mixed gas generated more oxidation species by the discharge, and enhanced reactivity of pulsed discharge plasma.

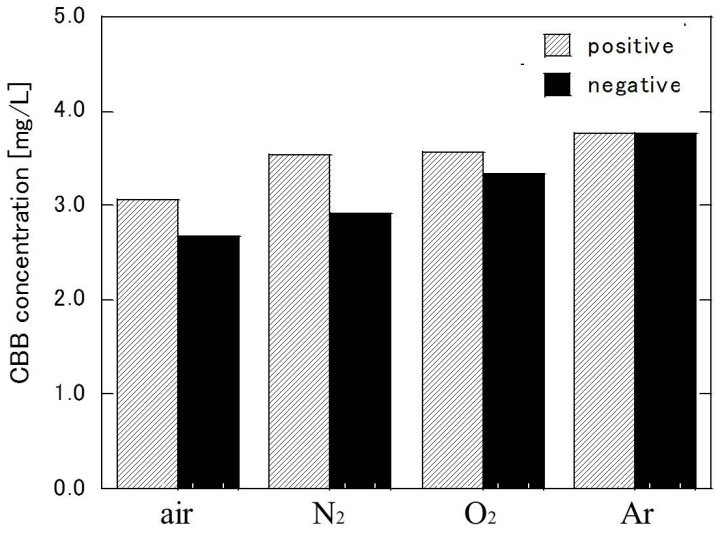

Figure 2.27 CBB concentrations after 30 minutes discharge by using air, N_2, O_2, and Ar atmospheres

2.8 Effects of reactor shapes

2.8.1 Method

The experiments were conducted by using three type of reactors, which have different shapes with the same volume as shown in Figure 2.28. The effects of reactor shapes on the reactions induced by discharge plasmas were investigated. Discharge plasmas were generated over KI solution and CBB solution at +4 kV/−4 kV and +10 kV/−10 kV respectively in order to observed generations of active oxidation species and oxidation reaction (cf. sections 2.4 and 2.5).

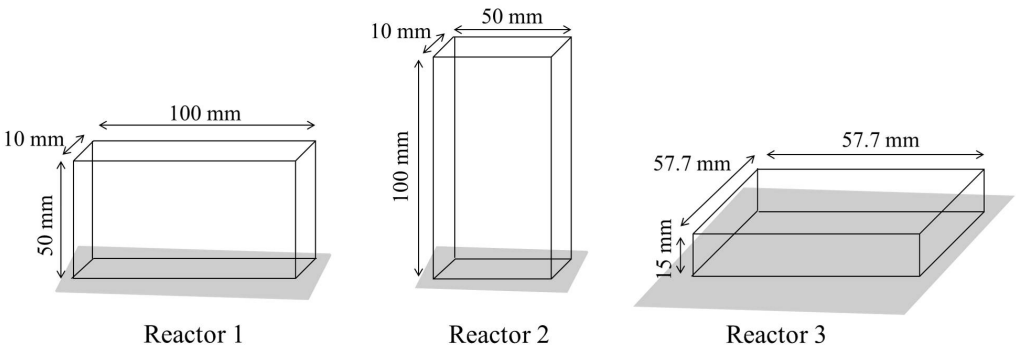

Figure 2.28 Three types of reactors of discharge plasma over aqueous solution

2.8.2 Active species generation and oxidation reaction using tall reactor

Spatial distributions of active oxidation species in tall reactor (reactor 2) were observed by generating discharge plasmas over KI solution surface. Figure 2.29 shows KI solutions after 3 minutes of (a) positive and (b) negative pulsed discharges. The layers of reacted solution were observed clearly in both cases. The thicknesses of the layers by using reactor 2 were approximately 10 mm, which were similar to that by wide reactor (reactor 1) as shown in Figs.2.10 and 2.12 (see section 2.4). Fig.2.30 shows CBB solutions after the treatments of 5 minutes by (a) positive and (b) negative pulsed discharges. Reacted layers of CBB solution were also similar to Fig.2.29. Therefore, the existence depth of oxidized solution by the discharge did not depend on height and width of the reactor.

The concentrations of CBB at surface layer and total in the reactor 2 after treatments of positive and negative pulsed discharges as a function of treatment time were shown in Figure 2.31. Compared to reactor 1 as shown in section 2.5, the times until saturated

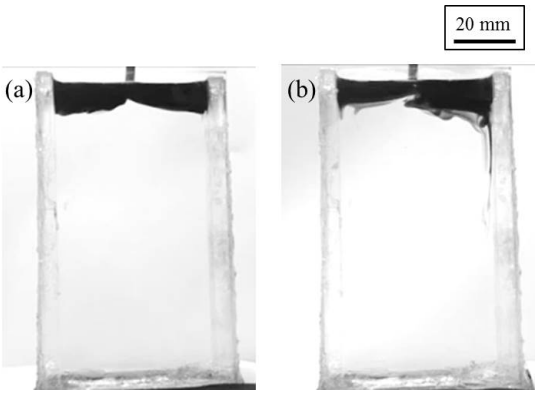

Figure 2.29 KI solutions after 3 minutes of (a) positive and (b) negative pulsed discharges

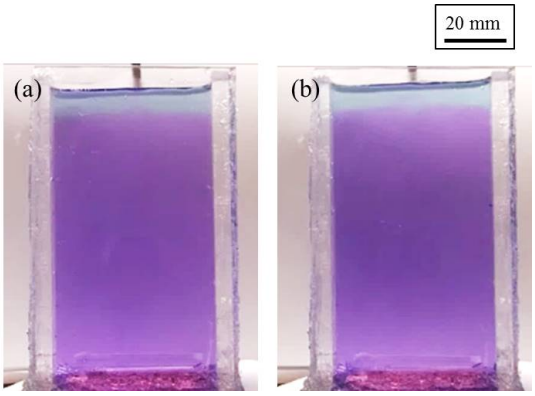

Figure 2.30 CBB solutions after treatments of 5 minutes by (a) positive and (b) negative pulsed discharges

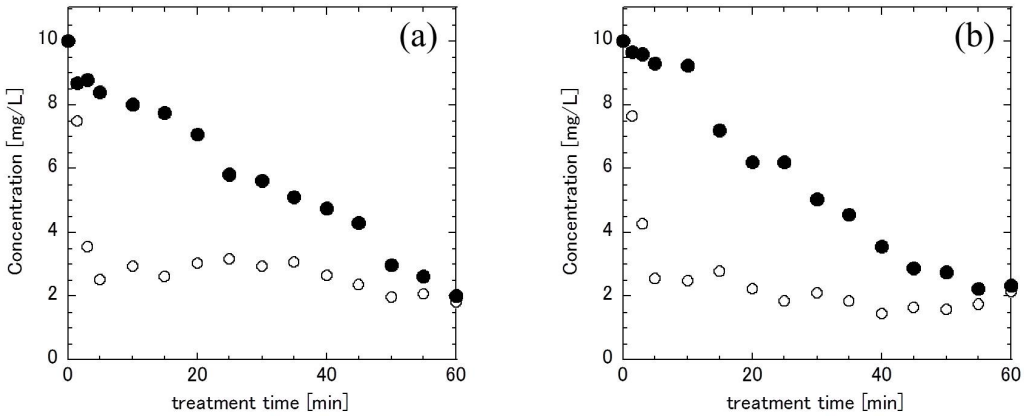

Figure 2.31 The concentrations of CBB at surface layer (○) and total in the reactor 2 (●) after treatments of (a) positive and (b) negative discharges as a function of treatment time

of CBB concentration at surface layer were fast by using reactor 2 because the volume of surface layer in reactor 2 was smaller than reactor 1. The changes in total CBB concentration in reactor 2 hardly depended on discharge polarity.

2.8.3 Effects of reactor shapes on oxidation reactions

Comparisons of CBB concentration by positive and negative pulsed discharges by using different shapes of the reactors were shown in Figure 2.32. The CBB concentrations after 60 minutes of the discharge did not depend on reactor shapes, but the progress in CBB decomposition was different until the discharge at 60 minutes. The progress of oxidation reactions by the discharge using wide reactor (reactor 1) was mentioned previously in section 2.5. CBB in water was oxidized by the discharge monotonously by using tall reactor (reactor 2). On the other hand, the discharge using thin reactor (reactor 3) oxidized CBB in water immediately in the beginning, and then the concentration of CBB was degraded gradually.

Consequently, the thin reactor was efficient for fast treatment of oxidation reaction induced by pulsed discharge, because reacted solution reached only in the depth of 10

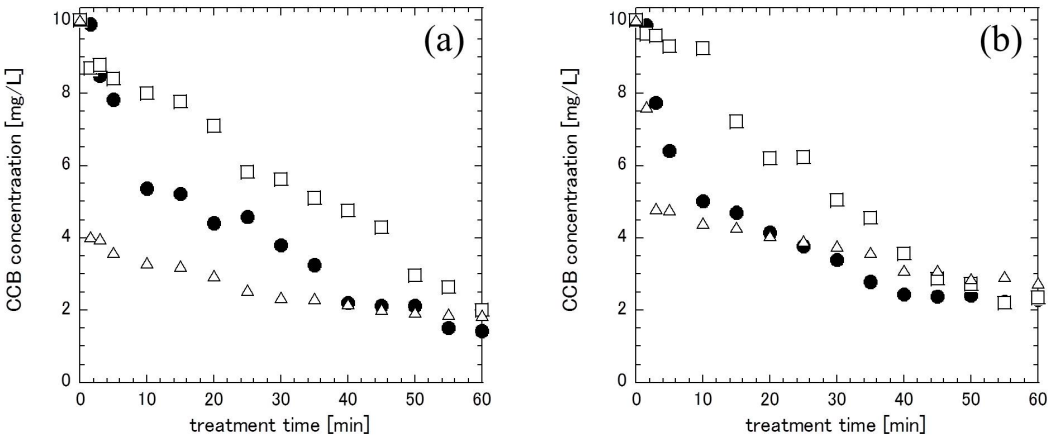

Figure 2.32 Comparisons of CBB concentration by (a) positive and (b) negative discharges by using reactor 1 (●), reactor 2 (□), and reactor 3 (△)

mm from solution surface. Therefore, in case an efficient batch-reactor is designed, the depth of the reactor should configure less than 10 mm. Otherwise, an efficient process is supposed to be possible by controlling a flow of reacted solution in the reactor. If you design a continuous reactor, it is to be desired that the depth of solution in the reactor is less than 2 mm, which is the region of acts on aqueous solution directly by active species generated by discharge plasmas.

2.9 Conclusions

The pulsed discharge plasmas were generated over aqueous solution surface, and investigated the effects of the discharge on characteristics of discharge plasmas and aqueous solution. Reactive species were generated by the discharge between the metal electrode in gas phase and aqueous solution surface especially near the solution surface, and affected on aqueous solution. In case of the discharge under atmospheric air, the emissions of N_2 were dominant of optical emission spectra, but Hα and OH from dissociation of H_2O molecules were also generated at plasma-solution interface. Conductivity of the solution related to production of active species. Reactive oxidation species, which were formed by the discharge in water, induced oxidation reactions in water. Oxidation reactions were caused by not only particular species but various species. In case of positive pulsed discharges, reactive oxidation species reached and acted directly 2 mm from the solution surface in the deepest. In contrast, negative discharge plasmas affected 1 mm from the solution in the deepest. When the compounds in aqueous solution

were decomposed easily, positive pulsed discharges were efficient for oxidation reactions. However, decomposing persistent compounds were effectively oxidized by negative pulsed discharges.

The layer of reacted solution was formed during plasma irradiation in the depth of 10 mm from solution surface by using any reactor due to convection flow of reacted solution. Therefore, the depth of the reactor should configure less than 10 mm if an efficient batch-reactor is design. Otherwise, an efficient process is supposed to be possible by controlling a flow of reacted solution in a reactor.

Reference

[1] P Bruggeman, E Ribezl, A Maslani, J Degroote, A Malesevic, R Rego, J Vierendeels and C Leys (2008) Characteristics of atmospheric pressure air discharges with a liquid cathode and a metal anode *Plasma Sources Sci. Technol.* **17** 1-11.

[2] Q Chen, K Saito, Y Takemura and H Shirai (2008) Physcochemistry of the plasma-electrolyte solution interface *Thin Solid Films* **516** 6688-6693.

[3] P Rumbach, D M Bartels, R M Sankaran and D B Go (2015) The effect of air on solvated electron chemistry at a plasma/liquid interface *J. Phys. D: Appl. Phys.* **48** 424001-1-22.

[4] Y Itikawa and N Mason (2005) Cross sections for electron collisions with water molecules *J. Phys. Chem. Ref. Data* **34** 1: 1-22.

[5] Q Chen, T Kaneko and R Hatakeyama (2012) Reduction in gold nanoparticle synthesis using gas-liquid interfacial discharge plasmas *Appl. Phys. Exp.* **5** 086201-1-3.

[6] F Tochikubo, Y Shimokawa, N Shirai and S Uchida (2014) Chemical reactions in liquid induced by atmospheric-pressure dc glow discharge in contact with water *Jpn. J. Appl. Phys.* **53** 126201-1-8.

[7] S Kanazawa, H Kawano, S Watanabe, T Furuki, S Akamine, R Ichiki, T Ohkubo, M Kocik and J. Mizeraczyk (2011) Observation of OH radicals produced by pulsed dischrges on the surface of a liquid *Plasma Source Sci. Technol.* **20** 034010-1-8.

[8] S M Thagard, K Takashima and A Mizuno (2009) Chemistry of the positive and negative electrical discharges formed in liquid water and above a gas-liquid surface *Plasma Chem. Plasma Process.* **29** 455-473.

[9] P Lukes, E Dolezalova, I Sisrova and M Clupek (2014) Aqueous-phase chemistry and bactericidal effects from an air discharge plasma in contact with water: evidence for the formation of peroxynitrite through a pseudo-second-order post-discharge reaction of H_2O_2 and HNO_2 *Plasma Source Sci. Technol.* **23** 015019-1-15.

[10] W Tian and M J Kushner (2014) Atmospheric pressure dielectric barrier discharges interacting with liquid covered tissue *J. Phys. D: Appl. Phys.* **47** 165201-1-21.

[11] T Cserfalvi and P Mezei (1996) Operating mechanism of the electrolyte cathode atmospheric glow discharge *Fresenius J. Anal. Chem.* **355** 813-819.

[12] T Takamatsu, K Uehara, Y Sasaki, H Miyahara, Y Matsumura, A Iwasawa, N Ito, T Azuma, M Kohno and A Okino (2014) Investigation of reactive species using various gas plasmas *RSC Advances* **4** 39901-39905.

[13] B R Locke and K Y Shih (2011) Review of the methods to form hydrogen peroxide in electrical discharge plasma with liquid water *Plasma Source Sci. Technol.* **20** 034006-1-15.

[14] M A Malik (2010) Water purification by plasmas: which reactors are most energy efficient? *Plasma Chem. Plasma Process.* **30** 21-31.

[15] T Shirafuji, A Nakamura and F Tochikubo (2014) Numerical simulation of electric double layer in contact with dielectric barrier discharge: effects of ion transport parameterin liquid *Jpn. J Appl. Phys.* **53** 03DG04-1-6.

[16] P J Bruggeman, N Sadeghi, D C Schram and V Lines (2014) Gas temperature determination from rotational lines in non-equilibrium plasmas: a review *Plasma Source Sci. Technol.* **23** 023001-1-32.

[17] M Adamson, A Padmanabhan, G J Godfrey and S J Rehse (2007) Laser-induced breakdown spectroscopy at a water/gas interface: a study of bath gas-dependent molecular species *Spectrochimica Acta Part B* **62** 1348-1360.

[18] W S Kang, M Hur and Y H Song (2015) Effect of voltage polarity on the plasma-liquid interactions *Appl. Phys. Lett.* **107** 094101-1-4.

[19] K Sasaki, H Ishigame and S Nishiyama (2015) Density distributions of OH, Na, water vapor, and water mist in atmospheric-pressure dc helium glow plasmas in contact with NaCl solution *Eur. Phys. J. Appl. Phys.* **71** 20807-1-6.

[20] H Kawamoto and S Umezu (2005) Electrohydrodynamic deformation of water surface in a metal pin to water plate corona discharge system *J. Phys. D: Appl. Phys.* **38** 887-894.

[21] R Ohyama, K Inoue and J S Chang (2007) Schlieren optical visualization for transient EHD induced flow in a straified dielectric liquid under gas-phase ac corona discharges *J. Phys. D: Appl. Phys.* **40** 573-578.

[22] M A Malik, A Gaffar and S A Malik (2001) Water purification by electric discharges *Plasma Source Sci. Technol.* **10** 82-91.

[23] D Mariotti, J Patel, V Svrcek and P Maguire (2012) Plasma-liquid interactions at atmospheric pressure for nanomaterials synthesis and surface engineering *Plasma Process. Polym.* **9** 1074-1085.

[24] Q Chen, J Li and Y Li (2015) A review of plasma-liquid interactions for nanomaterial synthesis *J. Phys. D: Appl. Phys* **48** 424005-1-26.

[25] T Cserfalvi, P Meizei and P Apai (1993) Emission studies on a glow discharge in atmospheric pressure air using water as a cathode *J. Phys. D: Appl. Phys.* **26** 2184-2188.

[26] T Cserfalvi and P Meizei (1994) Dierect solution analysis by glow discharge: electrolyte-cathode discharge spectrometry *J. Anal. Atomic Spectrometry* **9** 345-349.

[27] N Shirai, M Nakazawa, S Ibuka and S Ishii (2009) Atmospheric DC glow microplasmas using miniature gas flow and electrolyte cathode *Jpn. J Appl. Phys.* **48** 036002-1-6.

Chapter 3

Development of plasma process using gas-liquid two phase flow

3.1 Introduction

Multiphase flow is the flow of a mixture with two or more phase such as gas-liquid, liquid-liquid, and gas-liquid-solid. Focused on gas-liquid two-phase flow, several patterns of flows can make by controlling superficial velocities of liquid and gas, which are defined volume flow rate per unit cross-sectional area [13–15]. When superficial velocity of gas U_{GS} is sufficiently low, bubbly flow is observed as shown in Fig.3.1(a). With increasing U_{GS}, cylindrical bubbles are arranged in the flow, named slug flow (Fig.3.1(b)). In contrast, annular flow like Fig.3.1(c) is formed when superficial velocity of liquid U_{LS} is sufficiently low. We can enhance mixing rates and control mass and heat transfers by using these flows [16], thus they were widely applied to chemical reactions [17], materials synthesis [18,19], crystallization [20], and analytical method [21, 22]. I developed two plasma processes

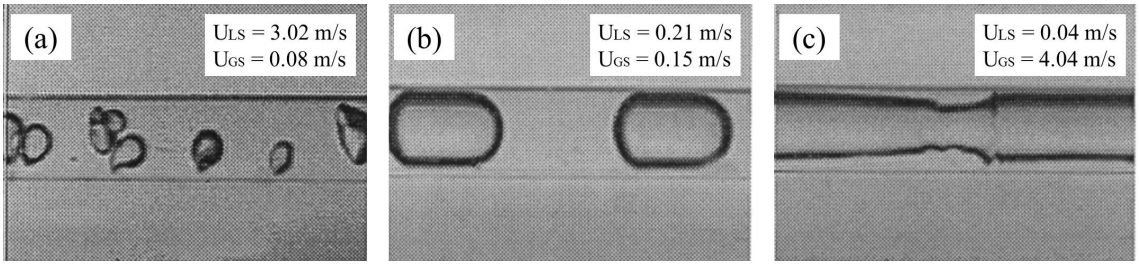

Figure 3.1 Patterns of gas-liquid two-phase flow [15]

using gas-liquid slug flow and wet walls based on the results of *Chapter 2*, and examined the characteristics of the plasmas and their relativities.

One is the discharge in gas-liquid slug flow. Over the past few years, electric discharge inside bubbles in water have been received attention, and many types of discharge methods in water using bubbles were proposed [1–4]. It leads to reduction in input power and high reaction efficiency. When the discharge plasma generated inside a floating bubble in water, the displace current of the bubble need to be larger than the conduction current of water [5]. However, water exhibits high conductivity in most cases because of solutes. Thus, it is difficult to generate discharge plasma in floating bubbles. Instead, it can be generated inside the bubbles in contact with a substance, which linked to an electrode. In a typical case, the plasma is generated only inside the bubble, which attached incidentally to the electrodes or dielectric substance connected to the electrode [9–12]. However, in previous methods, the bubbles float one after another in the reactor because of buoyancy, resulted in instability of discharge plasma and low efficiency. Some researchers have studied recently the discharge method to keep bubbles attaching to the electrode [6–8], but the bubble did not control sufficiently even in these methods.

I arranged controlled gas bubbles in the capillary as shown in Fig.3.2. If the discharge

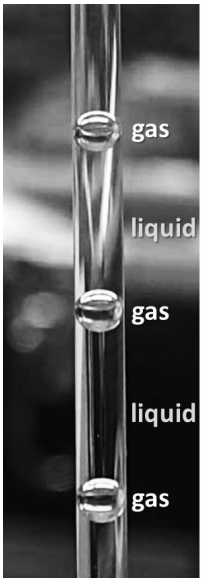

Figure 3.2 The image of controlled gas bubbles arranged in the capillary

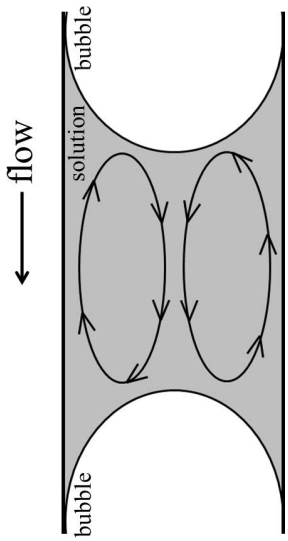

Figure 3.3 The convection flow in the solution in gas-liquid slug flow

plasmas are generated at controlled bubbles in the slug flow, stable discharge method in continuous process is feasible because bubbles attach inner wall of the tube constantly. In addition, liquid phase of the slug flow is circulated by shearing force, shown in Fig.3.3 [23, 24]. In case the reactions by discharge plasma occur at gas-liquid interface, reacted solution flows in a direction away from a bubble surface, and unreacted solution is fed the bubble surface. Thereby, high reaction efficiency is expected by using this process. The other method in the current work is discharge plasma over wet wall (like annular flow). It is found that active species, produced by discharge plasma over solution surface, reach directly at 2 mm in the depth at the deepest according to *Chapter 2*. Conversely, a high efficiency is accomplished when discharge plasmas were irradiated over solution layer of 2 mm or less. In present work, I tried to generate creeping discharge on wet wall.

3.2 Discharge in gas-liquid slug flow

3.2.1 Experimental setup

The discharge plasmas were generated in gas-liquid slug flow. The schematic of experimental setup was shown in Figure 3.4. The gas-liquid slug flow was formed in glass capillary tube with an inner diameter of 2.0 mm. The interval of bubbles was adjusted by changing flow rate of gases. Aqueous solution and gas were mixed at the upper part of capillary at 1.5 mL/min and less than 0.5 mL/min respectively controlled by plunger pump (LC-10AD, Shimadzu Co.) and flow meter (RK-1250, Kofloc Instruments Inc.). In this case, liquid and gas flowed in the same direction toward the bottom. Air, argon (Ar), helium (He), oxygen (O_2), and nitrogen (N_2) gases were introduced feed gases of slug flow. Aqueous solution was dissolved sodium chloride (NaCl) to control conductivity at 500 μS/cm of the solution in order to unify the conductive current in water. The pulsed bipolar voltages at $\pm$10.0 kV were applied repetitively at 10 kHz to the copper sheet wrapped around the exterior of glass tube by a pulse power supply (TE-HVP1510K300-NP, Tamaoki Electronics Co. Ltd.). The discharge voltages were monitored using an oscilloscope (TDS2024C, Tektronix Inc.) with a high voltage (EP-50K, Nissin Pulse Electronics Co. Ltd.). Two types of cathodes were utilized for the experiments: (a) water cathode and (b) copper cathode as shown in Fig.3.4. In case of water cathode, the copper electrode set 25 mm apart from water surface. The glass tube was submerged in water at 10 mm. The saucer including the solution was grounded. On the other hand, a copper sheet, which was grounded, was rolled up in a position 25 mm apart from the upper copper sheet in case of copper cathode.

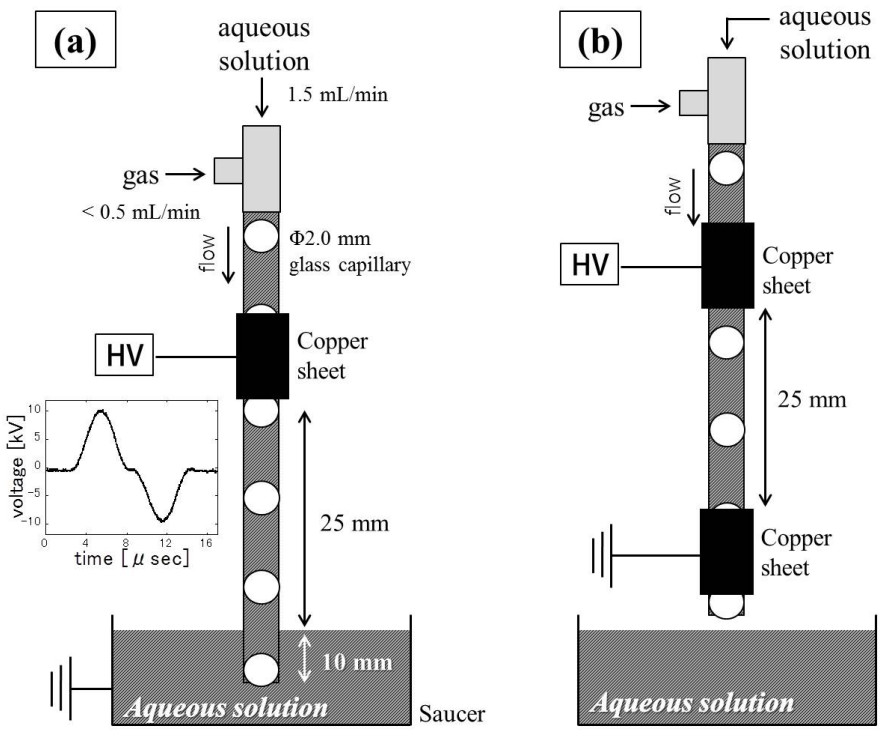

Figure 3.4 The schematic of experimental setup

3.2.2 Characteristics of discharge plasma

The appearances of discharge plasmas in gas-liquid slug flow using Ar gas were shown in Figure 3.5. Discharge plasmas were generated inside bubbles continuously while bubbles flowed between the electrodes by using either cathode. In case of water cathode as shown in Fig.3.5 (a), the bubble in the capillary, which immersed in water cathode, also had plasma emission.

In order to observe plasma emission inside bubbles, the ICCD image was photographed

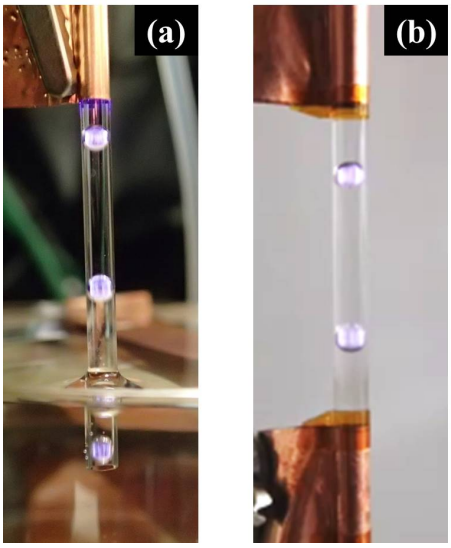

Figure 3.5 The appearances of discharge plasmas in gas-liquid slug flow using Ar gas

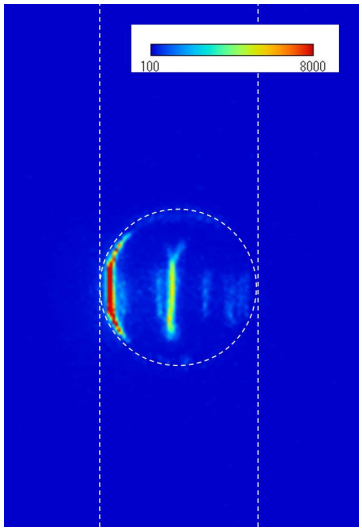

Figure 3.6 The ICCD image during a pulse of plasma irradiation in gas-liquid slug flow using Ar gas

during a pulse of the discharge through 20 μseconds of gate width. Fig.3.6 shows the ICCD image during a pulse of plasma irradiation in gas-liquid slug flow using Ar gas. The white dotted lines indicate a bubble surface and inner walls of the glass tube. The liner emissions were formed along the bubble surface. It was due to large gradient in dielectric constant, which enhances electric field [25].

It is believed that the mechanism of plasma generation in my process is similar to the methods by Bruggeman *et al.* [26–29], although they created a bubble by heating. The highest electric field was created at the edge of a bubble near the capillary wall by the discharge, leading to initiation of discharge plasma along the bubble surface. These discharge method required high conductivity of the solution in order to form the plasmas because the solution behaved as dielectric substance. In fact, also by my method, the

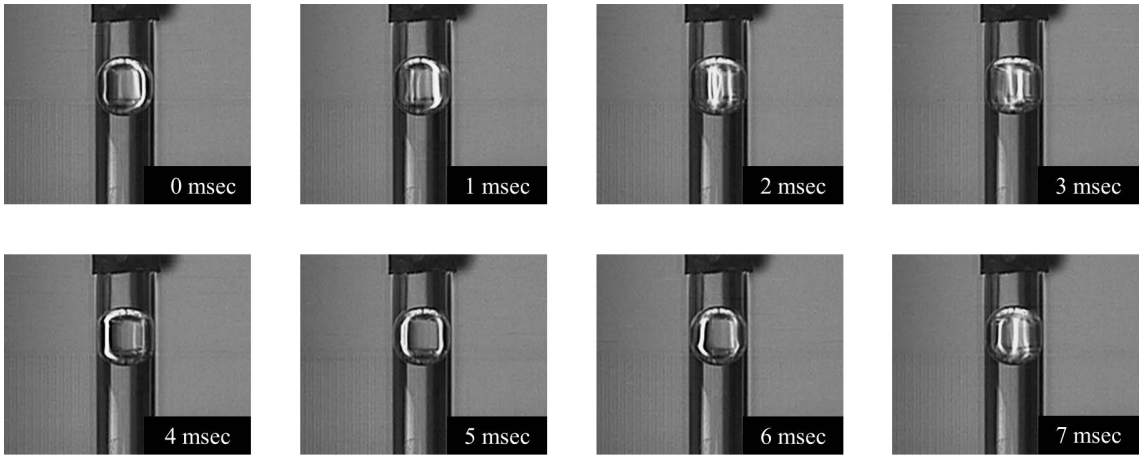

Figure 3.7 The images of discharge plasma in gas-liquid slug flow obtained by high speed camera

discharge plasma did not generate inside bubbles of gas-liquid slug flow in case a low conductivity solution such as distilled water was utilized for liquid phase. Thus, the mechanism of propagation of discharge plasma in slug flow was same as the experiments by Bruggeman.

In addition, the total number of bubbles between electrodes is considered to be gap length of discharge plasma in my method. When many bubbles existed between the electrodes, namely gap length was long, high input voltage was supposed to be required to generate discharge plasma inside bubbles. After this section, the intervals of bubbles of gas-liquid slug flow were set at 13 mm. In this condition, two or three bubbles exist between the electrodes. The superficial velocities of gas U_{GS} and liquid U_{LS} were 0.85 and 8.0 mm/s respectively.

Moreover, the appearance of plasma emission in slug flow observed by using high speed camera (GX-8, Nac Image Tech. Inc.). The images obtained by high speed

camera were shown in Figure 3.7. Discharge plasmas were generated with rotation while a bubble fallen. The temperature at bubble surface was supposed to be increased momentarily by plasma irradiation. It assumed to be the main cause of plasma rotation inside bubbles. Additionally, convection of gas in slug flow also contributed to plasma rotation presumably.

3.2.3 Generation of active species

3.2.3.1 Active species over water surface

Optical emission spectra of plasma emission inside bubbles in slug flow were observed to identify the active species generated by discharge plasma. Figure 3.8 shows optical emission spectra of plasma emission in slug flow by using Ar, He, O_2, and N_2 as introduced gases. Emission lines derived from respective feed gas were detected by all spectra. Especially, O atom (777 nm) and N_2 second positive system (300-400 nm) were supposed to have reactivity for aqueous solution. Besides, the emissions derived from water molecule such as Hα (656 nm) and OH (310 nm) lines were detected clearly, but the emission of Na (589 nm) was hardly observed. In case of N_2 gas introduction, the emission of OH radical was not clear because of overlap with N_2 second positive system, but OH radicals were emitted certainly [30].

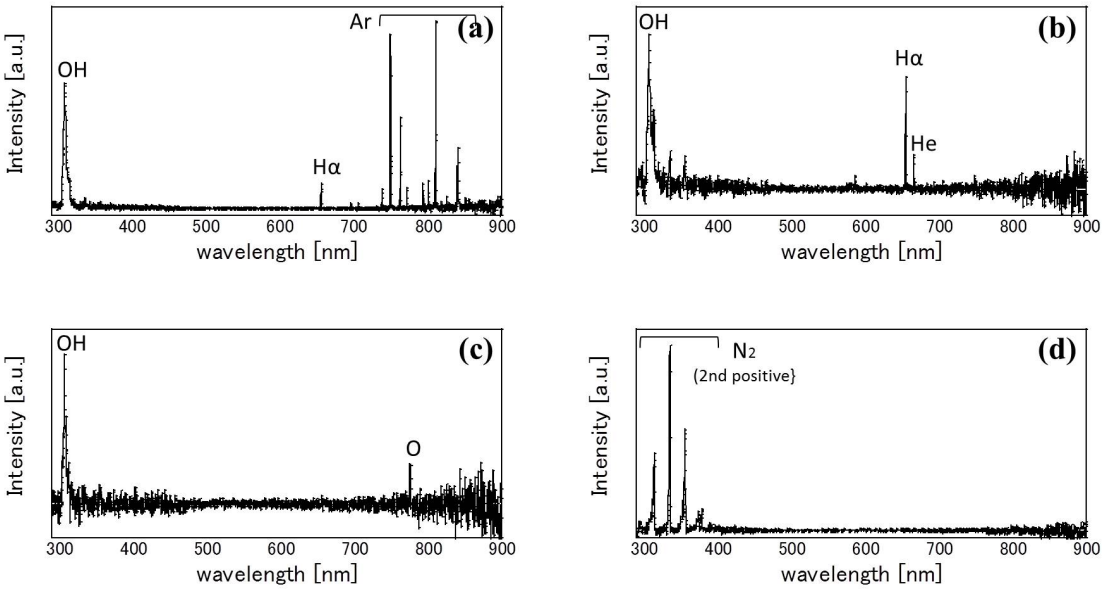

Figure 3.8 Optical emission spectra of plasma emission inside bubbles in slug flow by using (a) Ar, (b) He, (c) O_2, and (d) N_2 as feed gases

3.2.3.2 Active oxidation species in water

Reactive oxygen species were generated in gas-liquid slug flow by bipolar pulsed discharges at ±6.8 kV, and observed by using 100 mM KI solution (see section 2.4.2). Figure 3.9 shows the images of KI solution in slug flow during plasma irradiation. Reactive oxygen species were generated near the bubble surface, and flowed to the downstream. According to the enlarged image as shown in Fig.3.9 (b), reactive oxygen species also flowed up near the walls. Therefore, reacted solution was circulated by convection flow of slug flow.

The amount of total reactive oxidation species were determined by a titration of KI

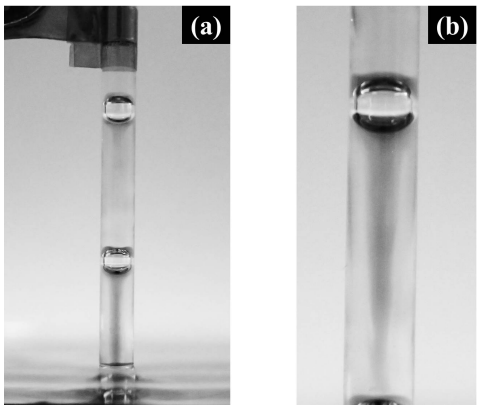

Figure 3.9 The images of KI solution in slug flow during plasma irradiation

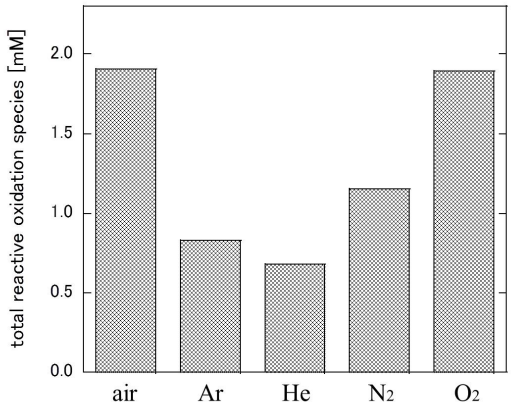

Figure 3.10 The total amounts of reactive oxidation species after the treatments of bipolar pulsed discharges in slug flow by using copper cathode

solution after the discharge by sodium thiosulfate. Figure 3.10 shows the total amounts of reactive oxidation species after the treatment at a time by bipolar pulsed discharges in slug flow by using copper cathode. OH radical was supposed to be the main species of reactive oxygen species according to optical emission spectra. The discharge in air bubbles was the most efficient for production of reactive oxidation species. The amount of reactive oxidation species by the discharge with O_2 gas is almost same as that with air. O atom observed by Fig.3.8 has high oxidation potential at 2.42 V, which is nearly equivalent to OH radical (2.80 V) [31]. It also contributed to generation of active oxidation species. The species derived from N_2 gas hardly contributed to reactive oxidation species production compared with that derived from O_2 gas. The discharges with inert gases were generated about half the amount of reactive oxidation species.

3.2.4 Oxidation reactions

CBB solution at 10 mg/L, whose conductivity was controlled 500 μS/cm by NaCl, was introduced in the capillary, and the discharge plasmas were generated in the slug flow at $\pm$10 kV by using copper cathode. CBB decompositions after treatments of the discharge at a time by using air, Ar, He, N_2,and O_2 gases were shown in Figure 3.11. The order of decompositions was same as that of total amount of reactive oxidation species as shown in Fig.3.10. When the discharge plasmas were generated over water surface in *Chapter 2*, atmospheric gases hardly affected decomposition of CBB (see section 2.7). In case of the discharge in gas-liquid slug flow, the discharge plasmas were considered to be generated between water electrodes. It enhanced generation of OH radical, leading to decomposition of CBB. Therefore, the gas dependence in Figs.3.10 and 3.11 assumed to be caused by the difference of amounts of OH radical generated by the discharge, although this work did

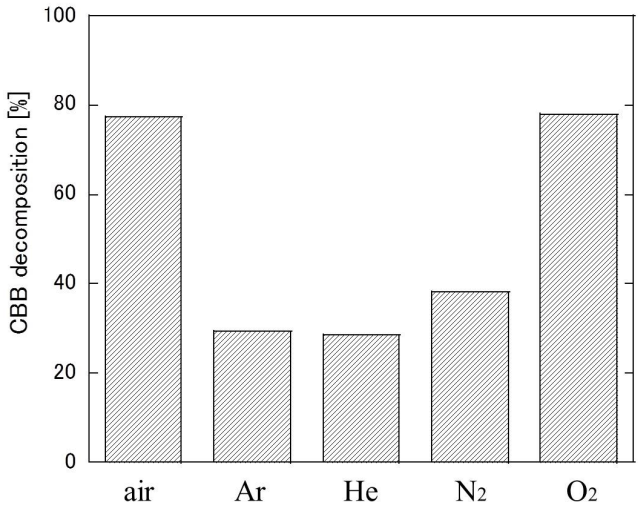

Figure 3.11 CBB decompositions after the treatments of bipolar pulsed discharges in slug flow by using copper cathode

not examine the amount of OH radical.

In case of air and O_2 gases, CBB in the solution decomposed more than 70%. It corresponded to CBB decomposition after 60 minutes of the discharges over the solution in *Chapter 2*. It takes 30 minutes for the treatment of 45 mL of CBB solution at 10 mg/L, considering the flow rate of the slug flow. Compared to CBB decomposition by using reactor 1-3 in section 2.8, the decomposition of the discharge in slug flow and that in reactor 3 (thin reactor) were almost the same. Therefore, high efficiency could be achieved in a continuous process of the discharge by controlling a convection flow.

3.3 Creeping discharge on wet wall

3.3.1 Experimental setup

The creeping discharge on wet wall was generated under atmospheric air by using an apparatus as shown in Figure 3.12. The bipolar pulsed voltages were applied to a cylinder copper electrode covered with glass, whose thickness was 0.25 mm. Aqueous solution flowed at 1.5 mL/min from the upper of the electrode and created thin layer less than 1 mm over the electrode. A copper ring, whose diameter was 3.2 mm, was set in the middle of the electrode, and connected to grounding. Aqueous solution was pooled at the copper ring temporarily while flowing. The creeping discharge propagated along the aqueous solution layer near the copper ring.

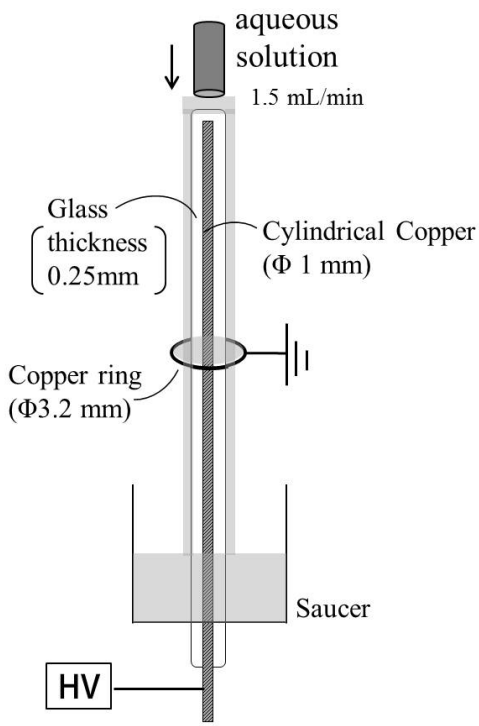

Figure 3.12 The schematic of experimental setup

3.3.2 Characteristics of discharge plasma

The photographs of discharge plasmas on wet wall under atmospheric air were shown in Figure 3.13. The creeping discharges were generated along the solution surface at the upper and lower of the copper ring. The plasma emissions were observed continuously. Optical emission spectrum of the discharge were shown in Fig.3.14. The spectrum was similar to that of the discharge over the solution at atmospheric air (see Fig.2.8 in section 2.4). The emissions of N_2 were dominant in the spectrum. However, the emission of O atom was not observed. According to section 2.4, it is believed that Hα and OH were

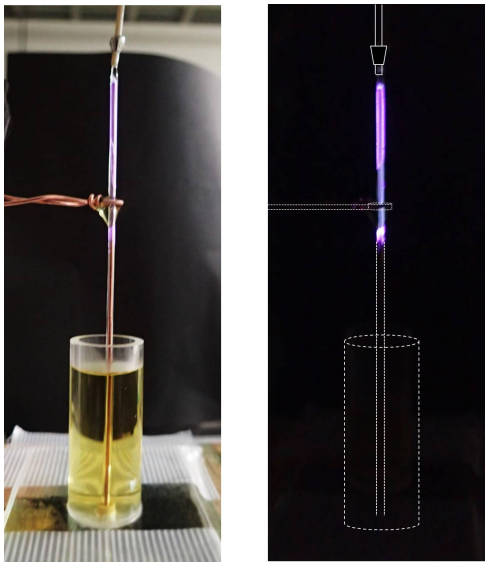

Figure 3.13 The images of creeping discharges on wet wall

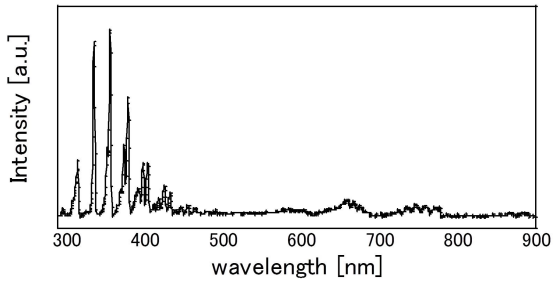

Figure 3.14 Optical emission spectrum of the discharge plasma on wet wall

generated at gas-aqueous solution interface. The emission lines of Hα (656 nm) and OH (310 nm) were supposed to overlap with N_2 first and second positive bands.

3.3.3 Oxidation reactions

The amount of total reactive oxidation species were determined by a titration of KI solution after the discharge at $\pm$6.8 kV. The amount of total reactive oxidation species was 1.75 mM, which was nearly equal to that of the discharge in the slug flow by using air. When the discharges were generated at $\pm$10 kV on 10 mg/L CBB solution, the decomposition of CBB after the discharge on the solution wall was 81.8%. It was also approximately the

same as that by the discharge in slug flow using air. Consequently, the discharge on wet wall, of which solution layer was less than 2 mm, realized high efficiency of oxidation reaction. The reactivity of the discharge by using wet wall was equivalent to that by using thin batch-reactor and that in gas-liquid slug flow.

3.4 Conclusions

New plasma processes using gas-liquid slug flow and wet wall were developed based on the results of *Chapter 2* in order to realize high efficiency of discharge plasma at gas-liquid interface. The discharge method by using gas-liquid slug flow aimed the convection flow of the solution in slug flow. The reacted solution circulated by a convection flow, leading to high reactive efficiency. On the other hand, thin layer of the aqueous solution, which is the entire region to reach reactive species by the discharge directly, was formed and discharge along the wet wall. High efficiencies could be achieved in continuous processes by using both discharge processes. The decompositions of CBB solution by these methods were equivalent to that by thin reactor (reactor 3 in section 2.8). Thus, an efficient process of discharge plasmas at gas-liquid interface can provide by managing a convection flow and a layer of aqueous solution.

Reference

[1] P Vanraes, A Nikiforov and C Leys (2012) Electrical and spectroscopic characterization of underwater plasma discharge inside rising gas bubbles *J. Phys. D: Appl. Phys.* **45** 245206-1-10.

[2] O Sakai, T Morita, N Sano, T Shirafuji, T Nozaki and K Tachibana (2009) Reduction of CO_2 solute by hydrogen microplasmas in an electrolyte *J. Phys. D: Appl. Phys.* **42** 202004-1-4.

[3] Y Hayashi, N Takada, H Kanda and M Goto (2015) Effect of fine bubbles on electric discharge in water *Plasma Sources Sci. Technol.* **24** 055023-1-6.

[4] P Vanraes, A Nikiforov and C Leys (2012) Plasma generation inside externally *J. Phys. D: Appl. Phys.* **45** 245206-1-6.

[5] P Bruggeman and C Leys (2009) Non-thermal plasmas in and in contact with liquid *J. Phys. D: Appl. Phys.* **42** 053001-1-28.

[6] T Shirafuji and Y Himeno (2013) Generation of three-dimensionally integrated micro-solution plasma and its application to decomposition of methylene blue molecules in water *Jpn. J. Appl. Phys.* **52** 11NE03-1-5.

[7] Y Matsui, N Takeuchi, K Sasaki, R Hayashi and K Yasuoka (2011) Experimental and theoretical study of acetic-acid decomposition by a pulsed dielectric-barrier plasma in a gas-liquid two-phase flow *Plasma Source Sci. Technol.* **20** 034015-1-11.

[8] S Muradia and M Nagatsu (2013) Low-voltage pulsed plasma discharges inside water using a bubble self-generating parallel plate electrode with a porous ceramic *Appl. Phys. Lett.* **102** 144105-1-4.

[9] S Ihara, T Miichi, S Satoh, C Yamabe and E Sakai (1999) Ozone generation by a discharge in bubbled water *Jpn. J. Appl. Phys.* **38** 4601-4604

[10] K Y Shih and B R Locke (2010) Chemical and physical characteristics of pulsed electrical discharge within gas bubbles in aqueous solutions *Plasma Chem. Plasma Process.* **30** 1-20.

[11] P M K Reddy, B R Raju, J Karuppiah, E L Reddy and C Subrahmanyam (2013) Degradation and mineralization of methylene blue by dielectric barrier discharge non-thermal plasma reactor *Chem. Eng. J.* **217** 41-47.

[12] P Baroch, V Anita, N Sauti and O Takai (2008) Bipolar pulsed electrical discharge for decomposition of organic compounds in water *J. Electrostatics* **66** 294-299.

[13] Y Zhao, G Chen, C Ye and Q Yuan (2013) Gas-liquid two-phase flow in microchannel at elevated pressure *Chem. Eng. Sci.* **87** 122-132.

[14] T Fukano and A Kariyasaki (1993) Characteristics of gas-liquid two-phase flow in a capillary tube *Nuclear Eng. Design* **141** 59-68.

[15] K A Triplett, S M Ghiaasiaan, S I Abdel-Khalik and D L Sadowski (1999) Gas-liquid two-phase flow in microchannels Part I: two-phase flow patterns *Inter. J Multiphase Flow* **25** 377-394.

[16] A Gunther and K F Jensen (2006) Multiphase microfluidics: from flow characteristics to chemical and materials synthesis *Lab Chip* **6** 1487-1503.

[17] M W Losey, R J Jackman, S L Firebaugh, M A Schmidt and K F Jensen (2002) Design and fabrication of microfluidic devices for multiphase mixing and reaction *J. Microelectrochem. System* **11** 6: 709-717.

[18] S A Khan, A Gunther, M A Schmidt and K F Jensen (2004) Microfluidic synthesis of colloidal silica *Langmuir* **20** 8604-8611.

[19] B K H Yen, A Gunther, M A Schnidt, K F Jensen and M G Bawendi (2005) A microfabricated gas-liquid segmented flow reactor for high temperature synthesis: the case of CdSe quantum dots *Angew. Chem.* **117** 5583-5587.

[20] B Zheng, J D Tice and R F Ismagilov (2004) Formation of arrayed droplets by soft lithography and two-phase fluid flow, and application in protein crystallization *Adv. Mater.* **16** 15: 1365-1368.

[21] M A Burns, B N Johnson, S N Brahmasandra, K Handique, J R Webster, M Krishnan, T S Sammarco, P M Man, D Jones, D Heldsiger, C H Mastrangelo, and D T Burke (1998) An integrated nanoliter DNA analysis device *Science* **282** 484-487.

[22] R E Thiers, A H Reed, and K Delander (1971) Origin of the lag phase of continuous-flow analysis curves *Clin. Chem.* **17** 1: 42-48.

[23] P A Walsh, E J Walsh and Y S Muzychka (2010) Heat transfer model for gas-liquid slug flows under constant flux *Int. J. Heat Mass Trans.* **53** 3193-3201.

[24] A Gunther, S A Khan, M Thalmann, F Trachsel and K F Jensen (2015) Transport and reaction in microscale segmented gas-liquid flow *J. Phys. D: Appl. Phys.* **48** 278-286.

[25] W Tian, K Tachibana M J Kushner (2014) Plasmas sustained in bubbles in water: optical emission and excitation mechanisms *J. Phys. D: Appl. Phys.* **47** 055202-1-13.

[26] P Bruggeman, C Leys and J Vierendeels (2007) Experimental investigation of dc electrical breakdown of long vapour bubbles in capillaries *J. Phys. D: Appl. Phys.* **40** 1937-1943.

[27] P Bruggeman, J Degroote, J Vierendeels and C Leys (2008) DC-excited discharges in vapour bubbles in capillaries *Plasma Source Sci. Technol.* **17** 025008-1-7.

[28] P Bruggeman, J Degroote, C Leys and J Vierendeels (2008) Electrical discharges in the vapour phase in liquid-filled capillaries *J. Phys. D: Appl. Phys.* **41** 194007-1-4.

[29] P Lukes, M Clupek, V Babicky, E Spetikova, I Sisrova, E Marsakova and B Marsalek (2013) High power DC Diaphragm Discharge excited in a vapor bubble for the treatment of water *Plasma Chem. Plasma Process* **33** 83-95.

[30] K Tachibana, Y Takekata, Y Mizumoto, H Motomura and M Jinno (2011) Analysis of a pulsed discharge within single bubbles in water under synchronized conditions *Plasma Sources Sci. Technol.* **20** 034005-1-12.

[31] M A Malik, A Ghaffar and S A Malik (2001) Water purification by electrical discharges *Plasma Sources Sci. Technol.* **10** 82-91.

Chapter 4

Electric discharge in water in the presence of fine bubbles

4.1 Introduction

Bubbles introduction in water enhance chemical reactivity of discharge plasmas at gas-water interface [1–3]. Almost all of previous discharge methods with bubbles introduced bubbles on the order of a millimeter from a nozzle set in water [4–6]. In these methods, bubbles rose one after another owing to the high rising speed of the millibubbles, and the discharge plasma is not stable if not discharge under controlled bubbles like the method in section 3.2.

In this chapter, fine bubbles were introduced to electric discharge area in water. A fine bubble is a bubble whose diameter is <100 μm, namely a microbubble or nanobubble. There are differences in behavior in water between millibubbles and fine bubbles. For example, fine bubbles of 50 μm in diameter exhibit extremely slow rising speeds of 1 mm/s and decrease in size and finally collapse in water during bubble rising [7,8]. Some reactive

species produced by the discharge plasma were supposed to exist inside the bubbles when discharge plasma generated inside bubbles. Although millibubbles including reactive species escape from the water immediately, fine bubbles are expected to retain for a long time in water with chemical active species owing to their slow rising speed. It leads to enhanced reactivity of discharge plasma presumably.

In present work, a pulsed discharge plasmas were generated in water with argon (Ar) and oxygen (O_2) fine bubbles. The effects of fine bubbles on the characteristics of the electric discharge and reactive species generated by discharge plasma with fine bubbles were examined.

4.2 Experimental setup

The experimental setup is schematically shown in Figure 4.1. Two cylindrical 1.0 mm-diameter copper electrodes were set at a distance of 0.7 mm apart in a reactor vessel. In case of production of active chlorine species, the experiments were conducted by using stainless steel electrodes, whose gap length was 1.0 mm, because available chlorine reacted with copper. The 67 mm-diameter vessel was filled with 250 mL of distilled water or NaCl solution. Fine bubbles were generated by a micro-nano bubble generator (MA3, Asupu Co., Ltd.) with water circulated at a flow rate of 150 mL/min. In case of the discharge in water without bubbles, water was circulated at the same rate. Feed gas (argon (Ar) or oxygen (O_2) gas) was introduced into micro-nano bubble generator at a flow rate of 30 mL/min and mixed with the water. The diameter of the bubbles was less than 80 μm and the bubble density was about 9.5×10^{10} m^{-3} according to shadowgraph measurement by ICCD camera. In other words, about 50 fine bubbles existed between the two electrodes

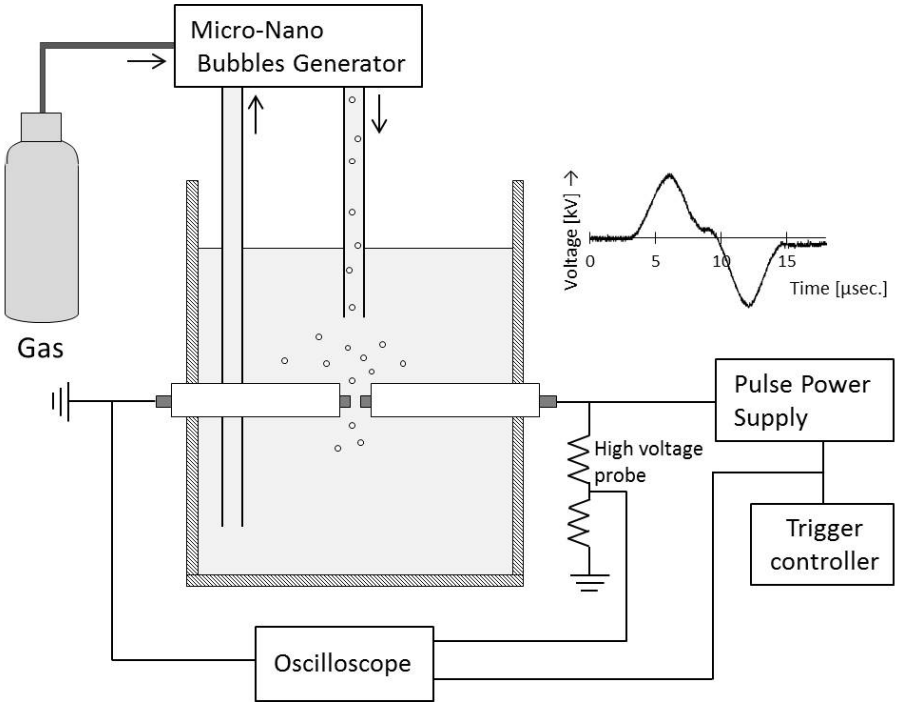

Figure 4.1 Schematic of the experimental setup

in ϕ 1 $\times$ 0.7 mm. The injection nozzle for water with fine bubbles was located 5 cm above the discharge region to prevent millibubbles from existing between electrodes. A bipolar pulsed voltage of $\pm$5–12 kV shown in the right side of Fig.4.1 was applied to one electrode by a pulse power supply (TE-HVP1510K300-NP, Tamaoki Electronics Co., Ltd.); the other was grounded. The frequency of the wave pulse was 10 kHz. Pulse power was operated by a trigger control (AFG-2005, Good Will Instrument Co., Ltd.), whose frequency and duty ratio were 20 Hz and 10%, respectively, to avoid erosion of the electrodes. The power was applied 30 seconds after beginning of fine bubble generation. Discharge voltage and current were monitored using an oscilloscope (TDS2024C, Tektronix Inc.) with a high-voltage probe (EP-50K, Nissin Pulse Electronics Co. Ltd.).

4.3 Effects of fine bubbles on discharge plasma in water

The pulsed discharge plasma was generated in distilled water with and without fine bubbles. Figure 4.2 shows the discharge inception voltage obtained by using bipolar pulsed power with and without Ar or O_2 fine bubbles. Discharge inception voltages decreased by 50% with argon bubbling and by 25% with oxygen bubbling compared with the no-bubbling case. Thus, the addition of fine bubbles made it easier to generate an electric discharge.

Water temperatures after the discharge were monitored by a digital temperature indicator at a distance of 20 mm from the discharge area. The water temperature after treatments of pulsed discharges at ± 9.5 kV is shown in Figure 4.3. The water temperature before the discharge was controlled to be at 20 ± 2°C. After treatment of the discharge without bubbles for 30 minutes, the water temperature increased steadily. In contrast, the discharge in water with fine bubbles restrained the rise in temperature.

Differences between no bubbling and fine bubbling were probably caused by the discharge ignition. Given the breakdown initiation in water without bubbles, thermal bubbles were created on the tips of the electrodes by Joule heating when the voltage was applied to the electrodes in water. The electric field was enhanced inside the bubbles, and initiates breakdown because the gas phase requires smaller electric fields than the liquid phase [43, 45]. In the case of discharge in water with fine bubbles, the fine bubbles that attached to the electrodes were assumed to lead the breakdown. Because thermal bubbles created by Joule heating are thus not needed when the discharge plasma was generated with fine bubbles, this led to the low discharge inception voltage and suppression of water temperature increase. In addition, the discharge inception voltage depended on the introduced gas because the discharge ignition probably occurred by the trigger bubbles,

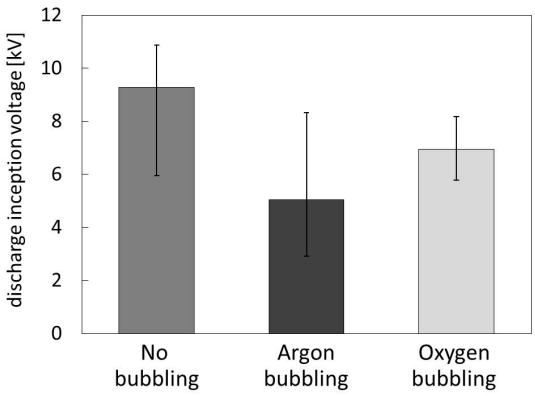

Figure 4.2 Discharge inception voltages with and without fine bubbles

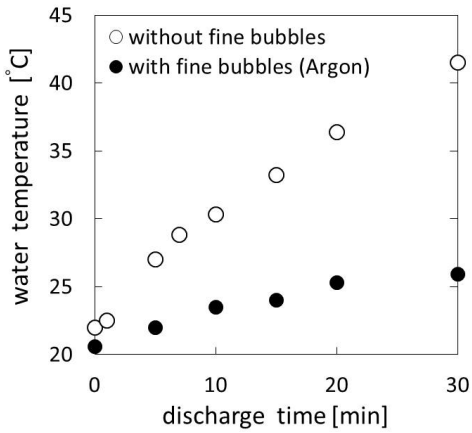

Figure 4.3 Temperature changes of water after treatments of pulsed discharges at ±9.5 kV

which attached to the electrodes. The degree of ionization was different from introduction gases, resulted in the differences in discharge inception voltages.

Optical emission spectra were observed to investigate the characteristics of plasma emission by using a high-resolution spectrometer (HR4000, Ocean Optics Inc.). Figure 4.4 shows the optical emission spectra for the discharge plasma generated in distilled water with and without fine bubbles when the discharge was applied at ±9.5 kV. Hydrogen and oxygen atomic lines from dissociation of H_2O molecules were dominant in the spectra. Fine bubbles significantly enhanced plasma emission. Hβ (486 nm), Hγ (434 nm), and Hδ (410 nm) lines, which are high energy levels of hydrogen atoms, were observed, but emissions due to OH radicals (309 nm) were not found. Based on the Stark effect, the discharge plasma with fine bubbles had high electron density. Under such conditions, almost all of the water molecules were dissociated into hydrogen and oxygen atoms due

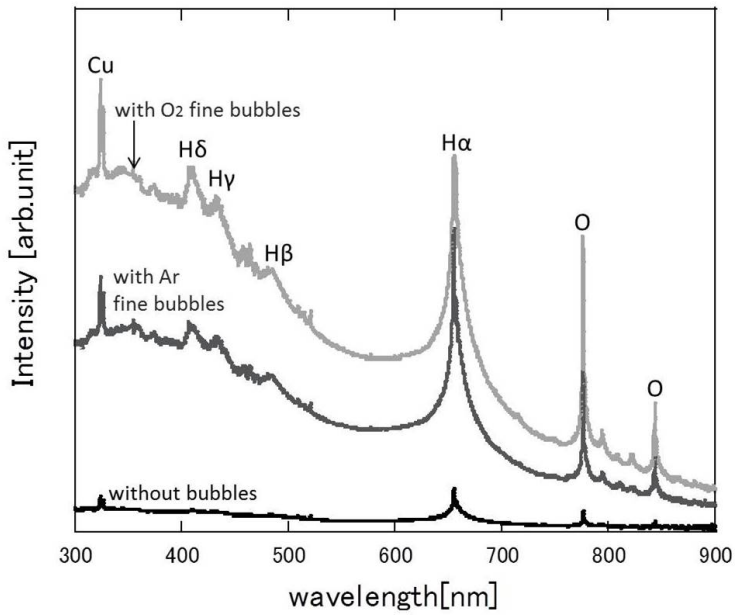

Figure 4.4 Optical emission spectra with and without fine bubbles when the discharge was applied at ±9.5 kV

to the high energy applied to the discharge region [13, 14]. These observations could likely be attributed to the lower breakdown voltage by the fine bubbles [15]. Intensive broad emissions were mainly attributed to the dynamic Stark effects of Hβ, Hγ and Hδ lines [16]. Recombination of water molecules [17], dissociation of hydrogen [18], and bremsstrahlung [19, 20] also will be considered as the cause of broad emissions in the shorter wavelength region. However, emissions from argon atoms were not observed even in the discharge plasma with Ar bubbles. This implies that the discharge plasma was not generated inside the bubbles. Instead, the introduction of bubbles enhances the dissociation of H_2O. An emission line due to atomic Cu (324 nm) was also observed in the spectra.

To evaluate water properties after the discharge, the copper concentration of water after

Table 4.1 Energy consumption calculated by voltage and current waveforms, electron density and intensity ratio of O (777 nm) and Hα (656 nm) estimated from optical emission in Figure 4.4

	Energy consumption [mJ/pulse]	Electron density [cm^{-3}]	Intensity ratio of O (777 nm)/Hα (656 nm)
no bubbling	21.9	3.8×10^{16}	0.47
Ar bubbling	105.2	2.0×10^{17}	0.52
O_2 bubbling	250.4	8.4×10^{17}	0.90

discharge at $\pm$9.5 kV were analyzed by an inductively coupled plasma optical emission spectrometry (ICP-OES; IRIS-AP Thermo Fisher Scientific). The copper concentration in water before the discharge was <0.05 ppm. After the discharge with no bubbling for 30 min, the copper concentration rose to 2.5 ppm. In contrast, water properties after the discharge with Ar bubbling in 30 min did not change, remaining at <0.05 ppm. These results considerably affect the electric field on the electrode surfaces, and strong electric fields contribute to electrodes erosion [21,22]. The electric field of the discharge in water with no bubbling is of the order of 10^9 V/m, compared to 10^6 V/m in the gas phase [23]. When fine bubbles assisted discharge ignition, electric field was supposed to be lower than no bubbling and Joule heating of electrodes were suppressed. Thus, water after the discharge with fine bubbles was contaminated slightly with copper.

The electron density was estimated from the Stark effect of the Hα (656 nm) line from optical emission spectra [24, 25]. Table 4.1 lists energy consumption, electron density and the intensity ratio of O (777 nm) and Hα (656 nm) lines from the optical emission

spectra in Figure 4.4. The values of energy consumption were calculated by voltage and current waveforms during the discharge, namely they express the energy consumed by plasma generation. The energy consumption per pulse of the discharge without bubbles was lower than that with fine bubbles because the energy was consumed by generation of Joule heating. The electron density of the discharge plasma with fine bubbling is about an order of magnitude higher than in the case with no bubbling. Meanwhile, the intensity ratio of O/Hα of Ar bubbling was almost the same as in the no bubbling case.

The electron density in the case of O_2 bubbling was a factor of 4 higher than that with Ar bubbling. Additionally, the intensity ratio of O/Hα with O_2 bubbling was higher than that with Ar bubbling. This difference could be attributed to the amount of dissolved oxygen in water; when O_2 gas was bubbling in the water, there was a high concentration of oxygen dissolved in the water [26]. Our experiment also indicated that dissolved oxygen in water increased to 23 mg/L with O_2 fine bubbling from 4 mg/L with no bubbling. At this time, the conductivity of water after O_2 fine bubbling rose to 1.7 μS/cm from 1.5 μS/cm of no-bubbling case in spite of no change of Ar fine bubbling. These values were measured after removing fine bubbles in water. Therefore, the rising of the conductivity was supposed to be caused by dissolved oxygen in water. Although the conductivity cannot measure in a state of including bubbles in water, the conductivity of water during O_2 fine bubbling is expected to be higher than Ar fine bubbling. It leaded to high electron density in the case of O_2 fine bubbling because high conductivity induced broad optical emission [16, 27]. Moreover, high concentration of dissolved oxygen in water presumably created more oxygen species which promoted dissociation of H_2O molecules [28, 29], and the discharge with O_2 fine bubbling indicated intense plasma emission compared to Ar fine bubbling.

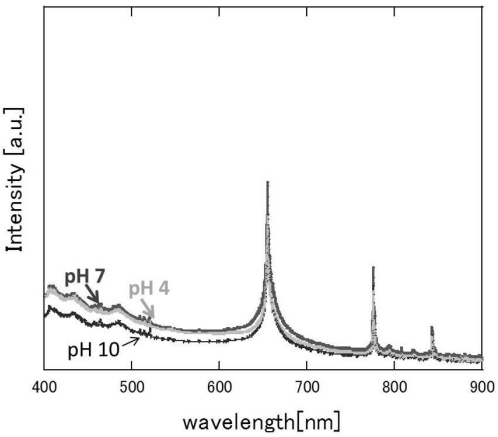

Figure 4.5 pH dependence of optical emission spectra of discharge with no bubbling

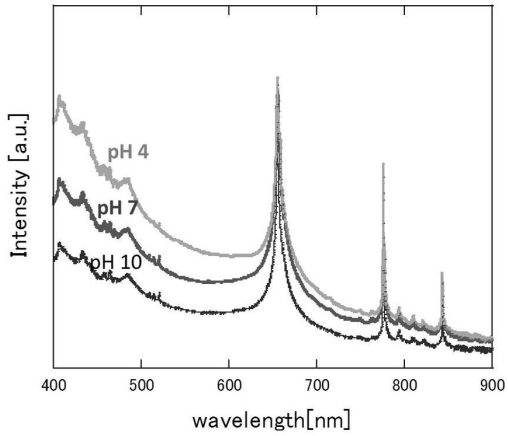

Figure 4.6 pH dependence of optical emission spectra of discharge with Ar bubbling

The electric charge on the fine bubble surface varied widely depending on the pH value of the aqueous solution [7]. To examine the effects on electric charge on the fine bubbles, discharge plasmas were generated in aqueous solutions at several pH values. The pH of the aqueous solution was adjusted by the addition of HCl, NaCl, and NaOH to distilled water. The conductivity of the aqueous solution was controlled at 90 μS/cm. The pH dependence of plasma emission with and without fine bubbles is shown in Figures 4.5 and 4.6. Emission peaks of sodium and chlorine from the solute are not found in either figure. The optical emission spectra of the electric discharge without bubbles were barely influenced by the pH value of the aqueous solution, as shown in Figure 4.5. Table 4.2 lists the intensity ratio of the O (777 nm) and Hα (656 nm) lines on Figs.4.5 and 4.6. The electron density at pH 10 was slightly higher than at pH 7 and pH 4. In contrast, the intensity ratio of O/Hα was approximately the same value at any pH condition for discharge without bubbles.

Table 4.2 Intensity ratio of O (777 nm) and Hα (656 nm) from optical emission in Figures 4.5 and 4.6

	pH value	Electron density [cm^{-3}]	Intensity ratio of O (777 nm)/Hα (656 nm)
no bubbling	pH 10	6.5×10^{16}	0.54
	pH 7	4.8×10^{16}	0.53
	pH 4	4.8×10^{16}	0.49
Ar bubbling	pH 10	1.5×10^{17}	0.64
	pH 7	6.6×10^{16}	0.54
	pH 4	2.1×10^{17}	0.70

In contrast, pH values did influence the emission spectra when the discharge plasmas were generated with Ar fine bubbles. The aqueous solution with fine bubbles at low pH induced strong emission, especially in the shorter wavelength region. Inspection of the intensity ratio of O/Hα in Table 4.2 indicates that the intensity ratio for the discharge with Ar fine bubbling at pH 7 was the same as that with no bubbling, but intensities of oxygen in Ar bubbling were stronger relatively at pH 4 and pH 10. In strong acid and basic conditions, high electron density was achieved by discharge in water. In our experiments discharge plasmas were more easily generated under high-pH conditions. This caused high electron density by electric discharge regardless of the presence of fine bubbles at pH 10, as indicated in Table 4.2. When the discharge plasma was generated at pH 4 with Ar fine bubbles, the electric charge on fine bubble surface probably affected plasma generation

because the electric charge of the solute generally influenced plasma emission [61]. Fine bubbles also have an electric charge on the interface between the bubble surfaces and the aqueous solution. ζ potential, which is electric potential in the interfacial double layer, of a fine bubble in aqueous solution at neutral and basic conditions is negative. However, ζ potential of fine bubbles is positive in acidic condition below pH 4.5 [11, 12]. In other words, there are many negative ions around the bubble surface at pH 4. Considering an early stage of plasma generation inside the bubble, which attached the electrode, an initial discharge was generated from the electrode toward bubble surface. At this time, the surface water layer inside the bubble was evaporated, and the plasma was propagated toward the other electrode. When the bubble with surface charge became a trigger of plasma generation, vapor including a lot of H^+ and OH^- ions was filled inside the bubble after the initial discharge. Since H^+ and OH^- ions give extremely high conductivity [31], it is supposed to be easy to form plasma inside the bubble when bubbles have surface charge. I speculate that it caused the difference of electron densities in the case of Ar fine bubbling shown in Table 4.2.

Moreover, the higher electron density resulted in the larger intensity ratio of O/Hα obtained. Although we have no results on the energy distribution of electrons, the O atom with its lower excitation energy compared with the H atom should be more easily emitted. Namely, the increase of the O/Hα ratio with increasing electron density would be caused by the increase in the intensity of the O line.

4.4 Hydrogen peroxide production

Hydrogen peroxide (H_2O_2) is utilized in various fields such as sterilization [32], bleaching [33], and degradation of pollutants [34] because it eventually decomposes into H_2O and O_2, which are environmentally friendly substances. Generally, catalysts and chemical agents are needed to produce H_2O_2 [35]. In contrast, methods based on electrical discharge have produced H_2O_2 *in situ* without a catalyst or chemical agent [36–38]. It dispenses with purification process of H_2O_2. Therefore, H_2O_2 produced by electric discharge is suitable to be utilized on the spot at a relatively low concentration, although it cannot realize high H_2O_2 concentration. The introduction of bubbles into the discharge region enhances H_2O_2 formation compared with discharge in water without bubbles reportedly [39, 40]. I found that discharge plasmas in water with fine bubbles promotes the dissociation of water molecules and produces a high electron density (see preceding section). Therefore, multiplier effects are expected to occur in the process of H_2O_2 formation with low gas consumption when a discharge plasma is generated in water with fine bubbles. I examine the formation of H_2O_2 and discuss the mechanism for H_2O_2 generation by discharge in distilled water with and without bubbles.

Hydrogen peroxide in water was evaluated by a colorimetric method using a titanyl reagent (Wako Chemical Co., Titanium Standard Solution) [41] and titration with potassium permanganate (Wako Chemical Co.). Hydrogen peroxide generation by the discharge plasma was analyzed after removal of the bubbles by stirring for 5 minutes. The concentration of H_2O_2 as a function of treatment time by pulsed discharge is shown in Figure 4.7. The formation of H_2O_2 was enhanced by the presence of bubbles. The H_2O_2 concentration increased immediately when the discharge plasma was generated with Ar bubbles, but reached saturation after 5 minutes, as shown in Fig.4.7. In the case of bubbling

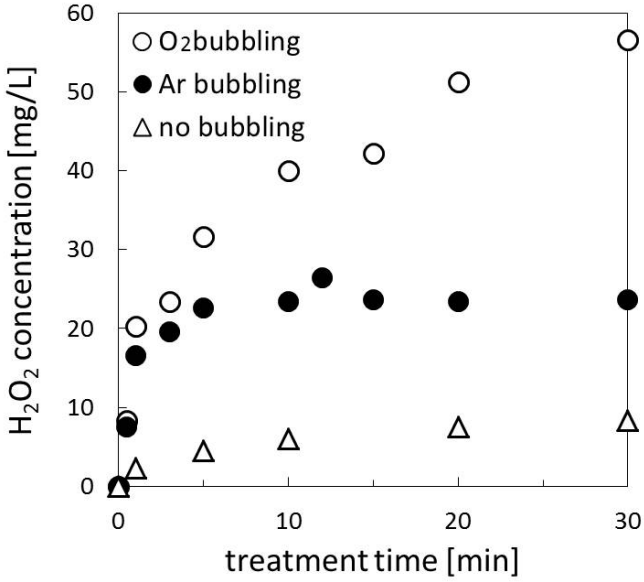

Figure 4.7 Concentration of H_2O_2 as a function of treatment time by electric discharge with O_2 bubbling (○), Ar bubbling (●), and no bubbling (△)

with O_2, the H_2O_2 concentration increased monotonically without saturation. Table 4.3 indicates powers of the discharge, energy yields, and generation rates of H_2O_2 when H_2O_2 was generated by the discharge with and without bubbles. The generation rate of H_2O_2 by the discharge with Ar bubbling was higher, but energy yield was lower than that of no bubbling. The power of discharge with Ar bubbles was high because of low breakdown voltage. It led to high energy yield in the case of Ar bubbling. The introduction of bubbles of O_2 resulted in the formation of more H_2O_2 and higher energy yield than the introduction of bubbles of Ar, although power of the discharge with O_2 bubbling was low compared with Ar bubbling.

Meanwhile, the concentration of dissolved oxygen (DO) in the water was measured after discharge plasma treatments by using a digital dissolved oxygen meter (Fuso Co. Ltd.,

Table 4.3 Powers, energy yields, and generation rates of H_2O_2 by the discharge with and without bubbles

	no bubbling	Ar bubbling	O_2 bubbling
Power [W]	21.9	105.2	43.3
Energy yield [g/kWh]	0.76	0.45	2.61
Generation rate [g/h]	16.6	47.3	113.2

PDO-520). Figure 4.8 shows the effect of plasma treatment on the DO concentration in water with or without Ar bubbles. The broken line shows the DO values when Ar bubbles were introduced in water (no discharge). The DO in distilled water before the treatment was 4 mg/L. The DO value did not change upon the introduction of Ar bubbles without the plasma. The concentration of DO in water treated with an electrical discharge in the presence of bubbles of Ar was about 1 mg/L after 5 minutes. The DO was not reduced any further when the discharge plasma was irradiated for more than 5 minutes. This behavior coincides with H_2O_2 formation, as shown in Fig.4.7. Namely, H_2O_2 formation by discharge in the presence of bubbles of Ar related to DO loss in the water. Because the DO of distilled water was supposed to be exhausted, the H_2O_2 concentration upon discharge with Ar bubbles was saturated, as shown in Fig.4.8. In the case of O_2 bubbles, discharge in the presence of bubbles of O_2 also consumed DO constantly, as shown in Fig.4.4. Therefore, it is conceivable that DO in the water affects H_2O_2 formation by discharge in the presence of bubbles of either Ar or O_2. An electrical discharge without bubbles did not consume DO. This implies that the formation mechanism of H_2O_2 by

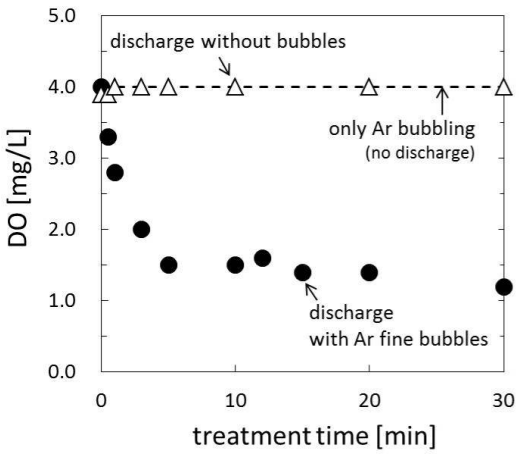

Figure 4.8 Dissolved oxygen (DO) concentration after plasma treatment with Ar fine bubbles (•) compared with no bubbling (△)

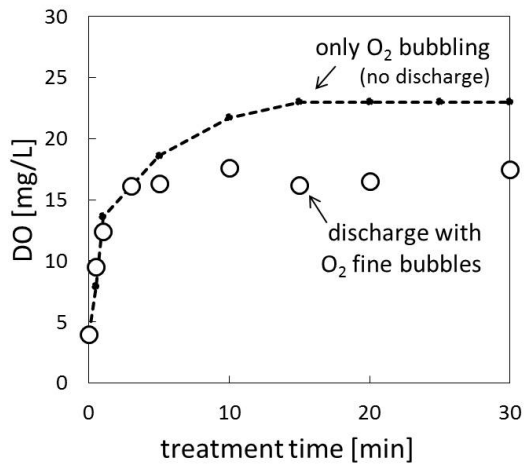

Figure 4.9 Comparison of DO in water by only O_2 fine bubbling (no discharge) and the discharge with O_2 fine bubbling

discharge plasma without bubbles is different from that with bubbles.

To examine the effect of DO on H_2O_2 formation, a discharge plasma was generated in water containing a high concentration of DO, which was obtained by bubbling O_2 for 10 minutes and then removing bubbles by stirring. The DO concentration of the high-DO solution was 23.3 mg/L. Figure 4.10 shows the concentration of H_2O_2 after treatments by electrical discharges in high-DO solution compared with discharges in distilled water. H_2O_2 formation by electrical discharge in a high-DO solution was greater than the formation of H_2O_2 by discharge in distilled water. These results implied that dissolved oxygen in the water was related to H_2O_2 formation even by discharge when the water contained high concentration of DO. In case of the discharge in distilled water, DO was scant for the reaction, resulted in no change in DO after the discharge. On the other hand, the discharge with fine bubbles enhanced dissociation of water molecules

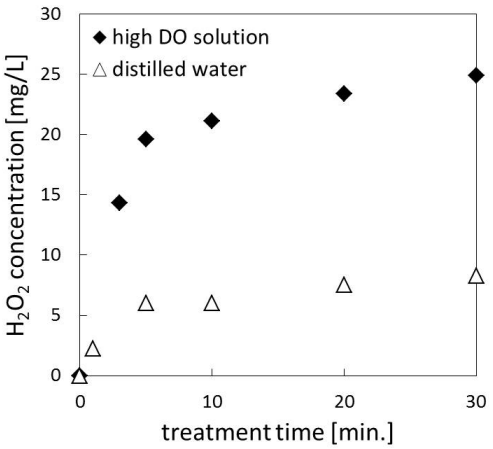

Figure 4.10 Concentration of H_2O_2 by discharge plasma in a high DO solution (♦) compared with distilled water (△)

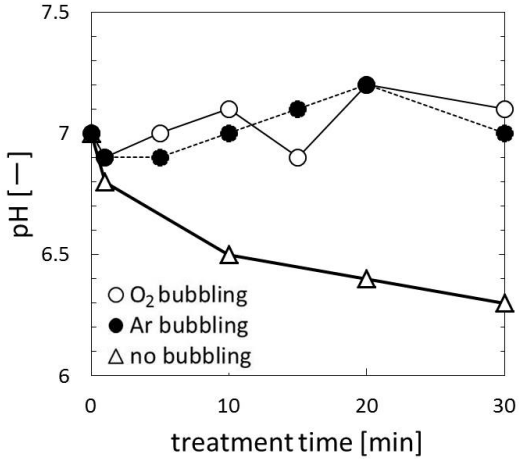

Figure 4.11 Changes in pH values during electric discharge with O_2 bubbling (○), Ar bubbling (●), and no bubbling (△)

accompanied by that of DO.

The changes in pH values during the electrical discharge is shown in Figure 4.4. The pH values of the water after treatments by discharge plasma with bubbles were maintained at around pH 7, although electrical discharge in water without bubbling decreased the pH value of water. These results also indicated that the formation mechanism of H_2O_2 by electrical discharge with bubbling was different from that without bubbling.

The formation mechanism for H_2O_2 by discharge in water with and without bubbles is discussed below. In the case of an electrical discharge in distilled water without bubbling, it was thought that H_2O_2 was formed by the dissociation of H_2O molecules as in Eq.(4.1), followed by the production of OH radicals as in Eqs.(4.2) and (4.3), resulting in H_2O_2 formation [14, 43]

$$H_2O \longrightarrow 2H + O \tag{4.1}$$

$$H + H_2O \longrightarrow OH + 2H \tag{4.2}$$

$$O + H_2O \longrightarrow 2OH \tag{4.3}$$

From the optical emission spectra shown in Fig.4.4 (see preceding section), our experiments did not produce OH radicals directly by electrical discharge, but H and O atoms were produced from water molecules. The energy thresholds for production of singlet $O(^1D)$ and triplet oxygen $O(^3P)$ by water dissociation are 7.0 and 9.5 eV respectively [42]. After dissociation by the discharge, almost all of these atoms recombined with each other, but some reacted with H_2O molecules, and generated OH radicals, as in Eqs.(4.2) and (4.3) [4,14,43,44]. It is assumed that these reactions occurred at the interface between plasma and water and OH radicals were produced in water, thus the emission of OH radical did not observed by emission spectra. Then, OH radicals created by Eqs.(4.2) and (4.3) recombined and formed H_2O_2 when the discharge plasma was generated in distilled water. At the same time, two H atoms were released by Eq.(4.2). They are supposed to be formed a H_2 molecule in most cases [39], but a small amount of H^+ ions expect to be created. This was what caused the decrease in the pH value in the case of the discharge without bubbles, as shown in Fig.4.4.

In contrast, dissolved oxygen in water was related to H_2O_2 formation when the discharge plasma was generated in water with bubbles. Oxygen molecules dissolved in

the water are ionized and dissociated by electrical discharges to produce superoxide anions (O_2^-) and oxygen atoms (O), based on Eqs.(4.4) and (4.5) [29, 45]. It is conceivable that Eqs.(4.4) and (4.5) are also induced by discharge in high-DO solution.

$$O_2 + e^- \longrightarrow O_2^- \tag{4.4}$$

$$O_2 + e^- \longrightarrow 2O + e^- \tag{4.5}$$

O_2^- ions in water are in equilibrium with the perhydroxyl radical (HO_2), as in Eq.(4.6) [43]. The lifetime of the O_2^- ion is about 5 seconds, while that of the OH radical is very short [44]. If hydrogen atoms are supplied to HO_2 by the discharge, H_2O_2 is formed via the OH radical, according to Eqs.(4.7) and (4.8). H_2O_2 formation by discharge with bubbles is thought to proceed by Eqs.(4.6)-(4.8).

$$O_2^- + H^+ \longrightarrow HO_2 \quad (in\ water) \tag{4.6}$$

$$HO_2 + H \longrightarrow 2OH \tag{4.7}$$

$$OH + OH \longrightarrow H_2O_2 \tag{4.8}$$

When bubbles were introduced in the discharge region, the O (777 nm)/ Hα (656 nm) intensity ratio in the optical emission spectra was larger than for the discharge without

bubbling (see preceding section). This means that DO in the water dissociated, producing O emissions in the spectra of the discharge with bubbles. Therefore, O atoms created by DO dissociation reacted by Eq.(4.3) to form H_2O_2 in the discharge with bubbles. In cases of H_2O_2 formation from dissolved oxygen, the reactions do not emit H^+ ions. Therefore, the pH values after treatment by discharge in the presence of bubbles did not change, as shown in Fig.4.4.

Table 4.4 indicates temperature range, reaction order, and rate expression of each reaction. All reaction expresses second-order reactions. Reactions Eqs.(4.2) and (4.3), which induce by the discharge in distilled water without bubbles, are difficult to occur according to rate expressions. When the plasma temperature is high enough over 2000 K, reaction Eq.(4.5) occurs easily. The plasma with fine bubbles assumed to have high temperatures from the results of optical emission spectra (Fig.4.4). It led to the reaction of dissolved oxygen and production of HO_2. After the production of HO_2, H_2O_2 can be easy to produce at low temperature as shown in Table 4.4. Consequently, the dissociation and recombination of H_2O molecules produced H_2O_2 by discharge without bubbling, but oxygen species derived from dissolved oxygen contributed to H_2O_2 formation by discharge with bubbles.

Table 4.4 List of reactions for H_2O_2 formation [42]

number	Reaction	Temperature range [K]	Reaction order	Reaction expression [cm^3 $molecule^{-1}$ s^{-1}]
discharge in distilled water (no bubble)				
4.2	$H + H_2O \rightarrow OH + 2H$	$2000 - 6000$	2	$5.8 \times 10^{-9}\, exp(-400/RT)$
4.3	$O + H_2O \rightarrow 2OH$	$300 - 2000$	2	$6.68 \times 10^{-13}\, (T/298)^{2.60}\, exp(-63.52/RT)$
discharge with fine bubbles				
4.5	$O_2 + M \rightarrow O + O + M$	$2000 - 10000$	2	$1.99 \times 10^{-10}\, exp(-9.5/RT)$
4.7	$HO_2 + H \rightarrow 2OH$	$300 - 2500$	2	$2.81 \times 10^{-10}\, exp(-3.66/RT)$
4.8	$OH + OH \rightarrow H_2O_2$	$200 - 1500$	2	$1.51 \times 10^{-11}\, (T/298)^{-0.37}$

4.5 Reaction of Cl^- ions

Active chlorine species demonstrate high sterilization performance [46–48]. Thus, water containing such species in solution is widely utilized in the agriculture and food industries as a sanitizer [49, 50]. Generally, active chlorine species are produced by electrolysis of a solution of NaCl [51–53]. During electrolysis, water molecules (H_2O) and Cl^- ions are converted to oxygen (O_2) and chlorine (Cl_2) molecules, respectively, at the anode due to the release of electrons, leading to the generation of active chlorine species. Meanwhile, hydrogen molecules (H_2) and hydroxide ions (OH^-) are produced from H_2O molecules at the cathode due to the supply of electrons. A discharge plasma in water is a mixture of various radicals, electrons, and excited species, and exhibits a high electron density [24]. The large electric current flows when discharge plasmas are generated in water. It presumably induces the reactions in a similar way to electrolysis [16,54]. Therefore, it was expected that Cl^- ions would react upon an electrical discharge in water to produce active chlorine species. In fact, the concentration of NaCl has been found to affect reactions when a discharge plasma is in contact with water [55,56]. Additionally, it has been reported that H_2 and O_2 molecules, which are also produced by electrolysis, are produced by discharge plasma in water [39].

The presence of fine bubbles into a discharge area resulted in a low inception voltage in the plasma, with intense plasma emissions and high electron densities compared with discharges in water (see section 4.3). If these factors contribute to the reaction of Cl^- ions upon discharge, more active chloride species should be produced by a discharge in the presence of fine bubbles. Therefore, I expected that the introduction of fine bubbles would have an effect on the reactions of Cl^- ions. Accordingly, fine bubbles were introduced to a NaCl solution in which discharge plasmas were generated, and the resulting reactions

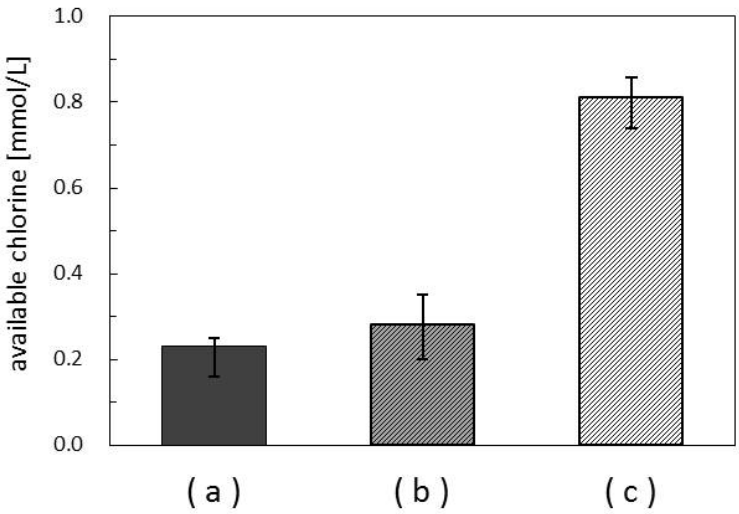

Figure 4.12 Concentrations of available chlorine after 60 minutes of (a) electrolysis, (b) electrical discharge in NaCl solution, and (c) electrical discharge in NaCl solution with Ar fine bubbles

were examined.

A pulsed discharge plasma was generated between stainless steel electrodes in NaCl solution when active chlorine species were generated by discharge plasmas, because copper reacts with active chlorine species. Ar gas, which is inert gas, was introduced as fine bubbles in NaCl solution. The experiment was also carried out electrolysis of the same NaCl solution using a DC power source (ZX-400L, Takasago Ltd.) as a comparative experiment. The NaCl solution (250 mL) was electrolyzed at 70 V/100 mA while the reactor temperature was maintained at 20°C by a cooling device (SCP-125, AS ONE Co.). Two electrodes (5 mm$\phi\times$50 mm, Kenis Ltd.), which made of titanium plated with platinum, were set at a distance of 25 mm.

Figure 4.12 shows the concentrations of available chlorine in the solution after 60 minutes of pulsed discharges in NaCl solution with and without fine bubbles. The

concentration of available chlorine after 60 minutes of electrolysis is also shown in Fig.4.12 (a). Some active chlorine species may be present in the solution, such as Cl_2 and hypochlorous acid (HClO), but it is difficult to assign each species because abundance ratios of them change depending on the water condition. Therefore, active chlorine species was measured altogether as available chlorine. The concentration of available chlorine was measurement by an iodometric method [57, 58]. The measurements were conducted at a solution temperature of 20-25°C. The discharge plasma in NaCl solution resulted in the production of slightly more available chlorine than electrolysis. However, the concentration of available chlorine after a discharge in the presence of Ar fine bubbles was more than twice that without bubbles. This implies that the special conditions created by a pulsed discharge plasma in NaCl solution in the presence of fine bubbles affected the reactions of Cl^- ions, resulting in a difference in the concentration of available chlorine after the discharge. In case of the discharge with O_2 bubbles, it was assumed that perchloric acid ($HClO_4$) was produced, and disturbed the measurement of available chlorine. Thus, an accurate quantification of available chlorine cannot be obtained.

The waveforms of the applied voltage and current for the discharge are shown in Figure 4.13. In NaCl solution, a voltage breakdown occurred after reaching the peak voltage at +10 kV, and the maximum discharge current was about 60 A, as shown in Fig.4.13 (a). In contrast, Fig.4.13 (b) indicates a low breakdown voltage due to the presence of fine bubbles. Consequently, a lower current was observed compared to the discharge in the solution without bubbles. The discharge plasma in NaCl solution exhibited a much larger current compared with that of electrolysis (100 mA). Thus, a large number of electrons were transferred in the solution area momentarily when the discharge plasma was generated in the NaCl solution. The current from the discharge plasma certainly

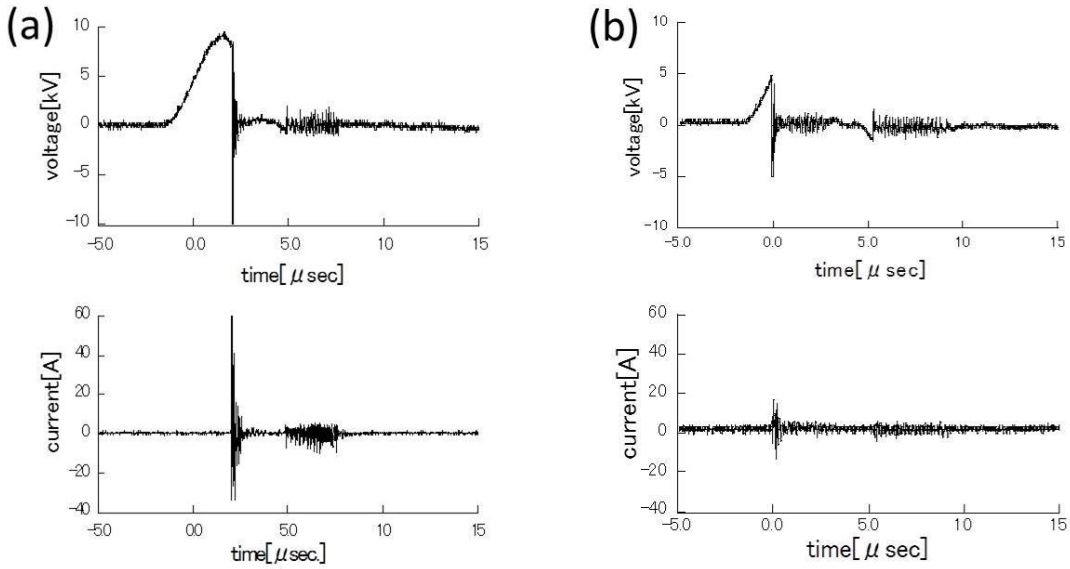

Figure 4.13 Waveforms of voltage and current for pulsed discharges (a) in NaCl solution and (b) in NaCl solution with fine bubbles of Ar

contributed to the production of available chlorine, similar to electrolysis. However, factors other than the current had an effect on production of available chlorine, because the discharge with fine bubbles, which had a lower measured current flow, produced more available chlorine than that without bubbles; that is, the amount of available chlorine by electric current of the discharge was limited. Therefore, there was a different mechanism of available chlorine production by discharge plasma.

The concentrations of Cl^- ions and available chlorine during discharge in NaCl solution in the absence and presence of fine bubbles of Ar are shown in Figure 4.14. The concentration of Cl^- ions in water was measured using an ion meter (F-53, 6560-10C, Horiba Ltd.) and an ion chromatograph (IA-300, PCI-205, TOA-DKK Co.). After beginning of the discharge, the amount of Cl^- ions in the solution decreased, and available

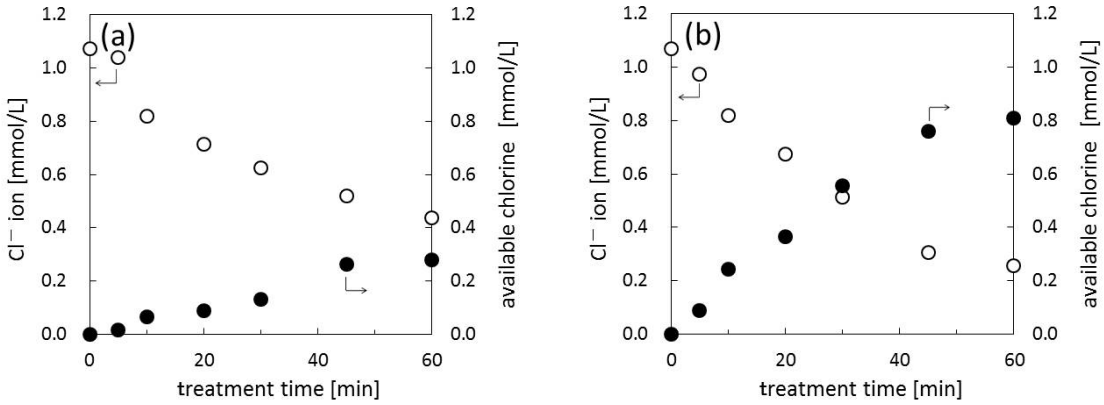

Figure 4.14 Concentration of Cl^- ions (○) and available chlorine (●) as a function of treatment time upon pulsed discharge (a) in NaCl solution and (b) in NaCl solution with Ar fine bubbles.

chlorine was produced gradually in either case. However, the amount of available chlorine produced by the discharge in the NaCl solution without fine bubbles was small when compared to the decrease in Cl^- ions, as shown in Fig.4.14 (a). In contrast, in the presence of fine bubbles, the decrease in the amount of Cl^- ions was nearly the same as the amount of available chlorine, as shown in Fig.4.14 (b). Based on the chlorine mass balance, 0.36 mmol/L of chlorine was lost after 60 minutes of discharge in the NaCl solution without bubbles, but only 0.01 mmol/L was lost after the discharge in the presence of fine bubbles. Therefore, some chlorine was released outside the solution during the production of available chlorine in the NaCl solution without fine bubbles, while almost all of the Cl^- ions were converted to available chlorine in the NaCl solution with fine bubbles.

The reactions in the production of available chlorine by electrolysis of the NaCl solution are shown in Eqs.(4.9) and (4.10). An electron is released at an anode, which results in the creation of a Cl_2 molecule from Cl^- ions (Eq.(4.9)). The Cl_2 molecule

then reacts with H_2O molecules to produce hypochlorous acid (HClO) with Cl^- and H^+ ions, as shown in Eq.(4.10) [57, 59, 60]. If the solution has a high pH value (more than pH 5), some of the HClO molecules are converted to hypochlorite ions (ClO^-), as shown in Eq.(4.11) [59]. Generally, the abundance ratio of Cl_2, HClO, and ClO^- in water depends on the solution condition. Based on my experimental conditions, the majority of available chlorine in the solution consisted of HClO, with a small amount of ClO^- ions, but almost no Cl_2 molecules.

$$2Cl^- \longrightarrow Cl_2 + 2e^- \tag{4.9}$$

$$Cl_2 + 2H_2O \rightleftharpoons HClO + Cl^- + H^+ \tag{4.10}$$

$$HClO + 2H_2O \rightleftharpoons ClO^- + H^+ \tag{4.11}$$

With regard to the loss of some chlorine upon discharge in the NaCl solution, it was presumed that some of the Cl_2 were produced by Eq.(4.9) in the bubbles, and released into the air with bubbles rising. Figure 4.15 shows the changes in pH as a function of treatment time after the discharge in NaCl solution in the presence and absence of fine bubbles. As shown in the figure, the pH of the solution decreased after discharge in the NaCl solution without fine bubbles. In general, electrolysis of a NaCl solution results in a decrease in the pH value of the solution due to the production of H^+ ions by the reaction shown in Eq.(4.10) [51, 61]. This means that the discharge in NaCl solution resulted in

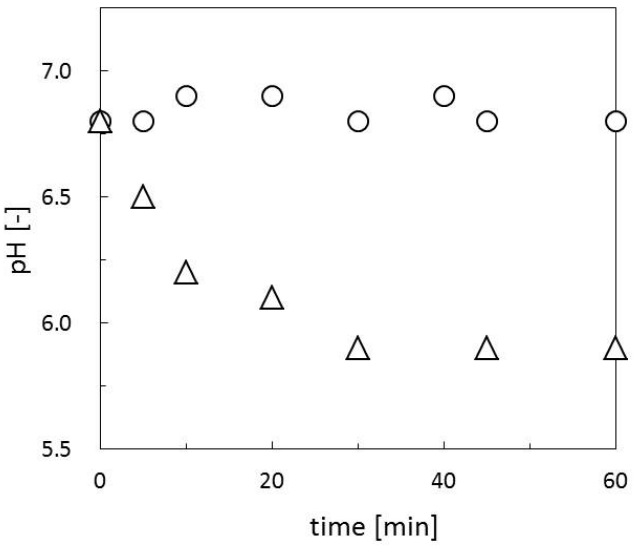

Figure 4.15 Changes in pH after pulsed discharges in NaCl solution (△) and pulsed discharges in NaCl solution with fine bubbles (◯).

the same reactions as electrolysis, producing available chlorine by the reactions shown in Eqs.(4.9)-(4.11). In this case, it was presumed that the large current from the discharge in NaCl solution activated the reaction of Cl^- ions, which is similar to electrolysis. In contrast, the discharge in NaCl solution in the presence of fine bubbles of Ar did not result in a loss of chlorine and a change in the pH of the solution, as shown in Figs.4.14(b) and 4.15. This means that the production of available chlorine was not via Cl_2 molecules. The introduction of fine bubbles in the discharge area promotes the dissociation of H_2O molecules and results in a high electron density with intense emissions. This is thought to induce other reaction pathways for the production of available chlorine.

A proposed pathway for the reaction of Cl^- ions upon discharge in the presence of Ar fine bubbles is as follows. When the discharge plasma was generated in the NaCl

solution in the presence of fine bubbles, H_2O molecules dissociated to hydrogen (H) and oxygen (O) atoms (Eq.(4.12)). At the same time, an electron was released from a Cl^- ion, producing a chloride radical ($Cl^\bullet$), as shown in Eq.(4.13). When $Cl^\bullet$ coexists with reactive oxygen species such as ozone and hydroxyl radicals, chlorine monoxide ($ClO^\bullet$) is produced [62–64]. The O atom also has high reactivity. Therefore, O atoms produced by the discharge reacted with $Cl^\bullet$ to produce $ClO^\bullet$ based on Eq.(4.14). This was then ionized to ClO^- (Eq.(4.15)), which entered an equilibrium with HClO as shown in Eq.(4.11). In this reaction pathway, two H atoms produced by Eq.(4.12) are released during the production of one HClO molecule. It is assumed that these were converted to H_2 molecules, rather than H^+ ions, and released into the air, because the ionization energy of hydrogen is comparatively high. This resulted in a constant pH, as shown in Fig.4.15.

$$H_2O \rightarrow 2H + O \tag{4.12}$$

$$Cl^- \rightarrow Cl^\bullet + e^- \tag{4.13}$$

$$Cl^\bullet + O \rightarrow ClO^\bullet \tag{4.14}$$

$$ClO^\bullet + e^- \rightarrow ClO^- \tag{4.15}$$

The pulsed discharges in NaCl solution in the presence of Ar fine bubbles also leads to electrolysis due to the current flow, which produces available chlorine by the reactions

shown in Eqs.(4.9)-(4.11). Moreover, the reactions shown in Eqs.(4.12)-(4.15) proceeded upon discharge even in the absence of fine bubbles. However, the dominant reactions for the production of available chlorine were thought to be different depending on the amount of O atoms created by the discharge. The promotion of H_2O dissociation by the fine bubbles resulted in the production of more O atoms, facilitating the production of $ClO^{\bullet}$, as shown in Eq.(4.14). Enhanced production of O atoms upon discharge in the presence of fine bubbles has been reported in section 4.3. This leads to the difference in the reactions of Cl^- ions upon discharge in NaCl solution in the presence and absence of fine bubbles.

Meanwhile, hydrogen peroxide (H_2O_2) were also generated by the discharge, and might react with available chlorine. However, the amount of H_2O_2 produced by the discharge was sufficient small compared to that of available chlorine. Therefore, effects of H_2O_2 on production of available chlorine was negligibly minimal.

4.6 Conclusions

Pulsed discharge plasmas in water with fine bubbles were generated by bipolar pulsed power. The effects of fine bubbles on the discharge plasmas and the generation of active species in water were examined in this chapter. Fine bubbles played a role in discharge initiation as an aid to breakdown, lowering the discharge inception voltage and avoiding Joule heating. Moreover, fine bubbles enhanced plasma emission of hydrogen and oxygen atoms, which derived from dissociation of water molecules, but optical emission from feed gas was not observed. Discharge plasmas with fine bubbles especially with high

electron density emitted hydrogen atoms with high energy levels. Dissolved oxygen in water strengthened the emission of oxygen atoms and produced discharge plasma with high electron density. The electric charge of fine bubbles also affected plasma emission. Plasma emission became strong and high electron density was observed for the discharge in low-pH solutions with fine bubbles because initial electrons could easily be supplied from the fine bubble surfaces, which were negatively charged.

H_2O_2 formation was successfully enhanced by introducing fine bubbles into the discharge region. Larger amounts of H_2O_2 were produced in water after treatments with bubbles, especially O_2 bubbles. The formation mechanism for H_2O_2 by electrical discharge in the presence of bubbles was thought to be different from that without bubbling. The amount of dissolved oxygen in water is a key parameter in the formation of H_2O_2 by electrical discharge in the presence of bubbles, although the dissociation of water molecules contributed to H_2O_2 formation by discharge in water without bubbling.

When pulsed discharge plasmas were generated in a NaCl solution, available chlorine species were produced from Cl^- ions. In the NaCl solution in the absence of bubbles, the reaction pathway is thought to be same as that for electrolysis, due to the large electric current. In contrast, in the presence of fine bubbles in the NaCl solution, the reaction pathway of Cl^- ions upon the generation of a discharge plasma was different. In this case, more O atoms were produced due to the dissociation of H_2O molecules. They reacted with $Cl^\bullet$ to produce available chlorine. The dominant reaction pathway of the Cl^- ions was different depending on amount of O atoms produced by the discharge.

Reference

[1] G R Stratton, C L Bellona, F Dai, T M Holsen and S M Thagard (2015) Plasma-based water treatment: conception and application of a new general principle of reactor design *Chem. Eng. J.* **273** 543-550.

[2] T Miichi, N Hayashi, S Ihara, S Satoh and C Yamabe (2002) Generation of radicals using discharge inside bubbles in water for water treatment *Ozone Sci. Eng.* **24** 471-477.

[3] H Nishiyama, K Niimuma, S Shinoki, and H Tanaka (2015) Decomposition of acetic acid using multiple bubble jets witn pulsed electrical discharge *Plasma Chem. Plasma Proc.* **35** 339–354.

[4] S Ihara, T Miichi, S Satoh, C Yamabe and E Sakai (1999) Ozone generation by a discharge in bubbled water *Jpn. J. Appl. Phys.* **38** 4601-4604.

[5] P Baroch, V Anita, N. Saito and O Takai (2008) Bipolar pulsed electrical discharge for decomposition of organic compounds in water *J. Electrost.* **66** 294-299.

[6] P Bruggeman, T Verreycken, M A Gonzalez, J L Walsh, M G Kong, C Leys and D C Schram (2010) Optical emission spectroscopy as a diagnostic for plasmas in liquids: opportunities and pitfalls *J. Phys. D: Appl. Phys.* **43** 124005-1-8.

[7] A Agarwal, W J Ng and Y Liu (2011) Principle and applications of microbubble and nanobubble technology for water treatment *Chemosphere* **84** 1175-1180.

[8] M Takahashi, K Chiba and P Li (2007) Free-radical generation from collapsing microbubbles in the absence of a dynamic stimulus *J. Phys. Chem. B* **111** 1343-1347.

[9] J Qian, R P Joshi, J Kolb and K H Schoenbach (2005) Microbubble-based model analysis of liquid breakdown initiation by a submicrosecond *J. Appl. Phys.* **97** 113304-1-10.

[10] S M Korobeinikov, A V Melekhov and A S Besov (2002) Breakdown initiation in water with the aid of bubbles *High Temp.* **40** 5 706-711.

[11] M Takahashi (2005) ζ potential of microbubbles in aqueous solutions: electrical properties of gas-water interface *J. Phys. Chem. B* **109** 21858-21864.

[12] Y Ueda, Y Tokuda and T Zushi (2014) Electrochemical performance of ultrafine bubble water *ECS Trans.* **58** 19: 11-19.

[13] O L Li, N Takeuchi, Z He, Y Guo, K Yasuoka, J S Chang and N Saito (2012) Active species generated by a pulsed arc electrohydraulic discharge plasma channel in contaminated water treatment *Plasma Chem. Plasma Process.* **32** 343-358.

[14] S M Thagard, K Takashima, A Mizuno (2009) Chemistry of the positive and negative electrical discharges formed in liquid water and above a gas-liquid surface *Plasma Chem. Plasma Process.* **29** 455-473.

[15] K Tachibana, Y Takekawa, Y Mizumoto, H Motomura and M Jinno (2011) Analysis of a pulsed discharge within single bubbles in water under synchronized conditions *Plasma Sources Sci. Technol.* **20** 034005-1-12.

[16] P Sunka, V Babicky, M Clupek, P Lukes, M Simek, J Schmidt and M Cernak (1999) Generation of chemically active species by electrical discharges in water *Plasma Sources Sci. Technol.* **8** 258-265.

[17] C Sehgai, R G Sutherland and R E Verrall (1980) Optical spectra of sonoluminescence from transient and stable cavitation in water saturated with various gases *J. Phys. Chem.* **84** 4: 388-395.

[18] B P Lavrov and A S Melnikov (1999) uv continuum emission and diagnostics of hydrogen-containing nonequilibrium plasmas *Phys. Rev. E* **59** 3: 3526-3543.

[19] S Park, W Choe, S Y Moon and J Park (2014) Electron density and temperature measurement by continuum radiation emitted from weakly ionized atmospheric pressure plasma *Appl. Phys. Lett.* **104** 084103-1-5.

[20] S Park, W Choe, H Kim and J Y Park (2015) Continuum emission-based electron diagnostics for atmospheric pressure plasmas and characteristics of nanosecond -pulsed argon plasma jets *Plasma Sources Sci. Technol.* **24** 034003-1-9.

[21] F Holzer and B R Locke (2008) Influence of high voltage needle electrode material on hydrogen peroxide formation and electrode erosion in a hybrid gas-liquid series electrical discharge reactor *Plasma Chem. Plasma Proc.* **28** 1-13.

[22] P Lukes, M Clupek, V Babicky and P Sunka (2006) Erosion of needle electrodes in pulsed corona discharge in water *J. Phys.* **56** B916-924.

[23] K Y Shih and B R Locke (2010) Chemical and physical characteristics of pulsed electrical discharge within gas bubbles in aqueous solutions *Plasma Chem. Plasma Proc.* **30** 1-20.

[24] T Namihira, S Sakai, T Yamaguchi, K Yamamoto, C Yamada, T Kiyan, T Sakugawa, S Katsuki and H Akiyama (1999) Electron temperature and electron density of underwater pulsed discharge plasma produced by solid-state pulsed-power generator *IEEE Trans. Plasma Sci.* **35** 3: 614-618.

[25] J Ashkenazy, R Kipper and M Caner (1991) Spectroscopic measurement of electron density of capillary plasma based on Stark broadening of hydrogen lines *Am. Phys. Soc.* **43** 5568-5574.

[26] T Tasaki, T Wada, K Fujimoto, S Kai, K Ohe, T Oshima, Y Baba and M Kukizaki (2009) Degradation of methyl orange using short-wavelength UV irradiation with oxygen microbubbles *J. Hazard. Mater.* **162** 1103-1110.

[27] M Simek, M Clupek, V Babicky, P Lukes and P Sunka (2012) Emission spectra of a pulse needle-to-plane corona-like discharge in conductive aqueous solutions *Plasma Sources Sci. Technol.* **21** 055031-1-12.

[28] M A Malik, A Ghaffar, and S A Malik (2001) Water purification by electrical discharges *Plasma Sources Sci. Technol.* **10** 82-91.

[29] T Takamatsu, K Uehara, Y Sasaki, H Miyahara, Y Matsumura, A Iwasawa, N Ito, T Azuma, M Kohno and A Okino (2014) Investigation of reactive species using various gas plasma *RSC Adv.* **4** 39901-39905.

[30] Q Chen, J Li, K Saito and H Shirai (2008) The characterization of radio-frequency discharge using electrolyte solution as one electrode at atmospheric pressure *J. Phys. D: Appl. Phys.* **41** 175212-1-6.

[31] P Atkins and J Paula (2012) *Elements of physical chemistry Oxford university press* 6th edition.

[32] P Swartling and B Lindgren (1968) The sterilizing effect against *Bacillus subtilis* spores of hydrogen peroxide at different temperatures and concentrations, *J. Dairy Res.* **35** 423-428.

[33] K Kawamoto and Y Tsujimoto (2004) Effects of the hydroxyl radical and hydrogen peroxide on tooth bleaching *J. Endodon.* **30** 1: 45-50.

[34] B Meunier and A Sorokin (1997) Oxidation of pollutants catalyzed by metallophthalocyanines *Acc. Chem. Res.* **30** 470-476.

[35] C W Jones (1999) Application of hydrogen peroxide and derivatives *RSC publishing*.

[36] B R Locke and S M Thagard (2012) Analysis and review of chemical reactions and transport process in pulsed electrical discharge plasma formed directly in liquid water *Plasma Chem. Plasma Process.* **32** 875-917.

[37] A A Joshi, B R Locke, P Arce and W C Finney (1995) Formation of hydroxyl radicals, hydrogen peroxide and aqueous electrons by pulsed streamer corona discharge in aqueous solution *J. Hazard. Mater.* **41** 3-30.

[38] P M K Reddy, B R Raju, J Karuppiah, E L Reddy and C Subrahmanyam (2013) Degradation and mineralization of methylene blue by dielectric barrier discharge non-thermal plasma reactor *Chem. Eng. J.* 217: 41-47.

[39] K Y Shih and B R Locke (2009) Effects of electrode protraction length, pre-existing bubbles, solution conductivity and temperature, on liquid phase pulsed electric discharge *Plasma Process. Polym.* **6** 729-740.

[40] B Sun, M Sato and J S Clements (1999) Use of a pulsed high-voltage discharge for removal of organic compounds in aqueous solution *J. Phys. D: Appl. Phys.* **32** 1908-1915.

[41] G M Eisenberg (1943) Colormetric determination of hydrogen peroxide *Ind. Eng. Chem.* **15** 5: 327-328.

[42] S Mededovic and B R Locke (2007) Primary chemical reactions in pulsed electrical discarge channels in water *J. Phys. D: Appl. Phys.* **40** 7734-7746.

[43] B R Locke and K Y Shih (2011) Review of the methods to form hydrogen peroxide in electrical discharge plasma with liquid water *Plasma Sources Sci. Technol.* **20** 034006-1-15.

[44] C A Vasko, D X Liu, E M Veldhuizen, F Iza and P J Bruggeman (2014) Hydrogen peroxide production in an atmospheric pressure RF glow discharge: comparison of models and experiment *Plasma Chem. Plasma Process.* **34** 1081-1099.

[45] D Moller (2009) Atmospheric hydrogen peroxide: evidence for aqueous-phase formation a historic perspective and one-year measurement campaign *Atmos. Environ.* **43** 5923-5936.

[46] S Nakagawa, T Goto, M Nara,Y Ozawa,K Hotta,Y Arita (1998) Spectroscopic Characterization and the pH Dependence of Bacterial Activity of the Aqueous Choline Solution *Anal. Sci.* **14** 691-698.

[47] M Saran, I B Speier (1999) Phagocytic killing of microorganisms by radical processes:Consequences of the reaction of hydroxyl radicals with chlorine atoms *Free Radic. Biol. Med.* **26** 482-490.

[48] K Hotta, K Kawaguchi,F Saitoh, N Saito, K Suzuki, K Ochi and T Nakayama (1994) Antimicrobial Activity of Electrolyzed NaCl Solutions: Effect on the Growth of *Streptomyces* spp *Actinomycetol.* **8** 2: 51-56.

[49] M Imaran, J Sugiyama, S Isobe (2005) Application of Electrized water in Agriculture & Food Industries *Food Sci. Technol. Res.* **11** 2: 135-150.

[50] T Suzuki, T Naro, Y Kawamura, K Fukunaga, M Watanabe, M Ohta, H Sugiue, Y Sato, M Kohno and K Hotta (2002) Decontamination of Aflatoxin-Forming Fungus and Elimination of Aflatoxin Mutagenicity with Electrolyzed NaCl Anode Solution *J. Agric. Food Chem.* **50** 633-641.

[51] L Szpyrkowicz, M Radaelli, S Daniele, A Baldacci and S Kaul (2007) Application of Electro-Catalytic Mediated Oxidation for the Treatment of a Spent Textile Bath in a Membrane Reactor *Ind. Eng. Chem. Res.* **46** 6732-6736.

[52] S V Len, Y C Hung, D Chung, J L Anderson, M C Erickson and K Morita (2002) Effects of Storage Conditions and pH on Chlorine Loss in Electrolyzed Oxidizing (EO) Water *J. Agric. Food Chem.* **50** 209-212.

[53] C C Sun and T C Chou (1999) Kinetics of Anodic Oxidation of Nitrite Ion Using in Situ Electrogenerated HClO in a NaCl Aqueous Solution *Ind. Eng. Chem. Res.* **38** 4545-4551.

[54] N K V Leitner, G Syoen, H Romat, K Urashima, J S Chang (2005) Generation of active entities by the pulsed arc electrohydraulic discharge system and application to removal of atrazine *Water Res.* **39** 4705-4714.

[55] S N Ramjaun, R Yuan, Z Wang and J Liu (2011) Degradation of reactive dyes by contact glow discharge electrolysis in the presence of Cl^- ions: Kinetics and AOX formation *Electrochimica Acta* **58** 364-371.

[56] M H Kang, Y J Hong, P Attri, G B Sin, G J Lee, K Panngon, G C Kwon, E H Choi, H S Uhm and G Park (2014) Analysis of the antimicrobial effects of nonthermal plasma on fungal spores in ionic solutions *Free Radic. Biol. Med.* **72** 191-199.

[57] S Neodo, D Rosetolato, S Ferro and A D Battisti (2012) On the electrolysis of dilute chloride solutions: Influence of the electrode material on Faradaic efficiency for active chlorine, chlorate and perchlorate *Electrochimica Acta* **80** 282-291.

[58] F Mogyorody (2006) Influence of chlorine-water equilibria on the electrochemical destruction of tiocarbamate herbicides in NaCl solution *J. Appl. Electrochem.* **36** 765-771.

[59] Y M Zheng, R F Yunus, K G N Nanayakkara and J P Chen (2012) Electrochimical decoloration of synthetic wastewater containing rhodamine 6G:Behavior and mechanism *Ind. Eng. Chem. Res.* **51** 5953-5960.

[60] F Mogyorody (2006) Electrochemical degradation of thiocarbamates in NaCl solutions *J. Appl. Electrochem.* **36** 773-781.

[61] K Umimoto, S Nagata and J Yanagida (2013) Development of device producing electrolyzed water from home care *J. Phys.* **450** 012035-1-5.

[62] A G Maki and G Thompson (1987) Infrared measurements of the ClO radical *J. Molecular Spectroscopy* **124** 139-161.

[63] H Park, C D Vecitis and M R Hoffmann (2009) Electrochemical water splitting coupled with organic compound oxidation: the role of active chlorine species *J. Phys. Chem. C* **113** 7935-7945.

[64] R M Stimpfle, R A Perry and C J Howard (1979) Temperature dependence of the reaction of ClO and HO_2 radicals *J. Chem. Phys.* **71** 12: 5183-5190.

Chapter 5

Discharge plasma at pressurized gas/aqueous solution interface

5.1 Introduction

Discharge plasmas were widely used for material synthesis and modification over the past few decades [1–5]. Recently, many researchers reported that metal nanoparticles were synthesized by gas-liquid interfacial plasma at atmospheric pressure [6–8]. Meanwhile, high pressure condition is also utilized for material synthesis and modification. The unique materials can be produced by peculiar properties of high pressure condition over atmospheric pressure [9–13]. Discharge plasma at high pressure condition creates particular reaction field [14, 15], and few researchers confirmed that the discharge at pressurized gas produced some materials [16–19], which could not be synthesized by the discharge at low pressure and atmospheric conditions.

This work performed the pulsed discharge at pressurized gas/aqueous solution

interface. It has possibility of unique materials synthesis with high affinity to water, and synthesized water-dispersible carbon nanoparticles in one-step.

Arc discharge in a liquid medium is one of the simplest techniques for the synthesis of carbon materials. Two different approaches can be applied within this technique. The first method involves using two graphite electrodes; carbon vapors produced by arc discharge from these electrodes are rapidly quenched in a liquid, leading to the formation of carbon materials. Previous studies have reported the synthesis of carbon nanotubes (CNTs) [20, 21], carbon onion particles [22, 23], and porous carbon [24] based on this method. The other approach is arc discharge in organic solvents. In this case, the carbon precursor is not supplied by the electrodes, but by organic materials in a liquid phase. This approach was previously applied to synthesize CNTs or amorphous carbon [25, 26]. In the present work, organic compounds in aqueous solution were utilized as the carbon precursor. As the discharge with an aqueous solution containing organic compounds supplies a different source of carbon, these approaches can be used to control the structure and the doping density of specific elements in the carbon material. Unique properties can be achieved by doping various atoms in carbon. For example, nitrogen doping leads to enhanced catalytic activity of carbon materials [27], and boron doping can alter their electrical characteristics [28]. Achieving full control over the doping density of specific elements into the carbon materials would thus enable to target several desirable features.

Water-dispersible carbon is widely applied in medical and environmental applications [29–32]. Recently, it was reported that carbon nanostructures had positive effects on cell cultivation [33, 34], and moreover they had low toxicity for cells [35]. Generally, carbon materials do not disperse in water. When carbon materials are utilized for biomedical applications, they are required to disperse in water because their applications are conducted

in water mediums. In conventional methods to prepare water-dispersible carbon, the carbon surface is modified by chemical agents [36, 37] or by a physical treatment [38] after synthesis of carbon materials. The method of arc discharge in a liquid also induces modification of the carbon surface reportedly [39,40]. Here, I describe a method involving synthesis of carbon particles and surface modification in one-step, by arc discharge over an aqueous solution containing organic compounds, under a pressurized gas. It is expected that carbon nanocapsules produced by this method exhibit dispersibility in water, because the organic compounds as carbon precursors certainly have hydrophilic groups. In particular, amino acids dissolved in deionized water were converted into carbon materials in this work by pulsed arc discharge performed over a liquid surface under pressurized argon. Amino acids have two hydrophilic groups: an amino (-NH_2) and carboxyl groups (-COOH). If these groups are present on the surface of carbon materials after their synthesis, the carbon products will exhibit dispersibility in water. Moreover, amino acids are harmless and not affect to biomaterials. If amino acids stay in products even after separation of carbon products, it has no effect on applications; on the contrary it can be use without separation.

The characteristics of discharge plasma over amino acid solution at high pressure condition were investigated, and carbon materials from amino acids were synthesized. Effects of amino acid on carbon products were examined by using several amino acids as carbon precursors.

5.2 Experimental

5.2.1 Setup

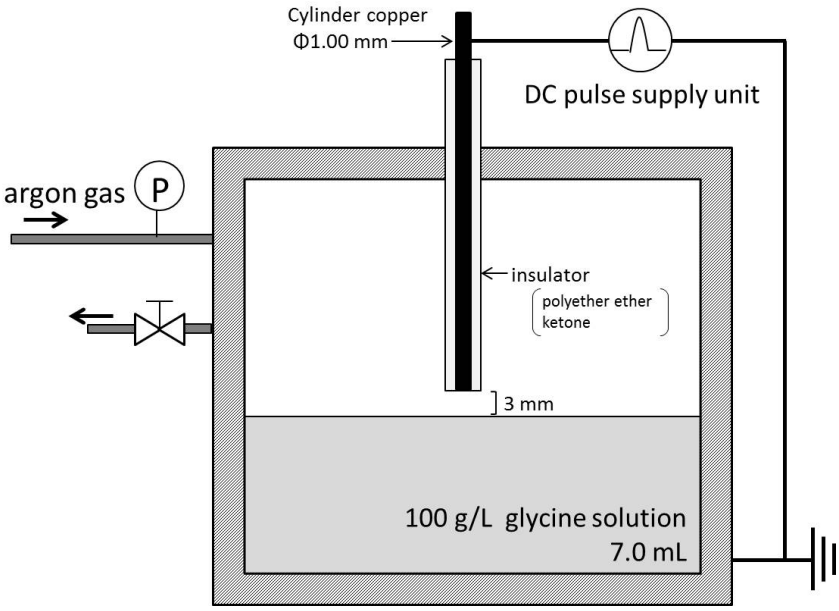

Figure 5.1 Schematic of the experimental setup

Figure 5.1 shows the schematic of the experimental setup. An aqueous solution of 7.0 mL containing amino acid was filled into the reactor. The atmosphere in the reactor was replaced and pressurized using argon (purity $>$ 99.999%, Taiyo Nissan Co.) at a pressure of 4.0 MPa. Pulsed arc discharge was repeatedly generated from a cylindrical electrode to an aqueous solution surface in a batch reactor. A copper cylindrical electrode with a diameter of 1.00 mm was placed at a distance of 3 mm from the solution surface. Except the end surface, the outside of the electrode was covered with polyether ether ketone,

which exhibits good insulation. A pulsed voltage of 18.6 kV was repeatedly applied to the electrode using a high-voltage pulse generator (MPC2000S, Suematsu Electronics Co. Ltd.). The reactor, made of stainless steel (Akico Co. Ltd.), was grounded.

5.2.2 Materials

In this study, several amino acids as carbon precursors were selected, which is easily soluble in water; glycine (>99.0%, Wako Chemical Co.), DL-α-alanine (>98.0%, Wako Chemical Co.), L-threonine (>99.0%, Nacarai Tesque Ltd.), L-Ornithine Monohydrochloride (>98.0%, Nacarai Tesque Ltd.), L-lysine monohydrochloride (>99.0%, Wako Chemical Co.), L-valine (>99.0%, Wako Chemical Co.), L-isoleucine (>99.0%, Nacarai Tesque Ltd.), L-proline (>99.9%, Peptide Instiument INC.), DL-phenylalanine (>99.0%, Wako Chemical Co.), and L-histidine (>98.0%, Nacarai Tesque Ltd.). To investigate effects of amino acid structure on carbon products, L-isomer of amino acids as possible was utilized for carbon materials synthesis. They were dissolved in distilled water, and then the solution filled with the reactor. Additionally, the discharge plasmas were also generated over the solution including acetic acid and ammonium acetate (>99.0%, Wako Chemical Co.) as conventional experiments.

5.2.3 Analysis

The discharge voltage and current were monitored by an oscilloscope (TDS 2024C, Techtronix Inc.) via a high voltage probe (EP-50K, Nissin Pulse Electronics Co. Ltd.) and a current probe (5046, Pearson Electronics Inc.). In order to examine reaction mechanism,

optical emission spectra of the discharge were observed by using a high-resolution spectrometer (HR4000, Ocean Optics Co.).

The products in liquid state were dialyzed by dialysis membrane (Spectra/Por3, Spectrumlabs) in order to remove the raw material (amino acid) before the analysis. Structure of carbon products were determined by field-emission scanning electron microscopy (FE-SEM, JSM-6330, JEOL Ltd.) and high-resolution transmission electron microscopy (HRTEM, JEM2010, JEOL Ltd.). Raman spectroscopy (NRS-1000, JASCO Co.) was performed in order to determine carbons properties. The functional groups on the carbon surface were characterized by X-ray photoelectron spectroscopy (XPS, ESCA-3300, Shimadzu Co.) and Fourier transform infrared spectroscopy (FTIR, Spectrrum two, Perkin Elmer Co. Ltd.).

5.3 Characteristics of discharge plasma over glycine solution at pressurized argon

The discharge plasma was generated over glycine solution at pressure of 0.1 to 4.0 MPa. The conductivity of glycine solution at 100 g/L was 18.45 μS/cm. Figure 5.2 shows voltage waveforms when pulsed voltage applied at 18.6 kV to the copper electrode under atmospheric and pressurized argon. The time until voltage drop was different depending on the pressure. Generally, breakdown mechanism can be expressed as follow when breakdown takes place in a plane gap d under certain pressure p by DC voltage V [41,42].

$$\alpha d = ln\left(\frac{1}{\gamma} + 1\right) \tag{5.1}$$

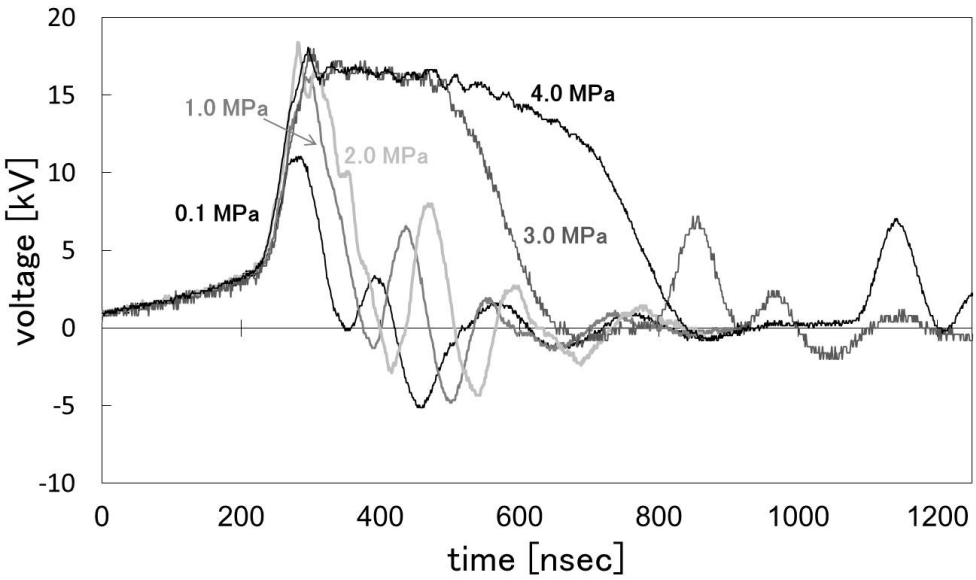

Figure 5.2 The voltage waveforms by pulsed discharge over glycine solution at 18.6 kV under atmospheric and pressurized argon

Equation (5.1) is called Townsend formula. Ionization coefficient α is indicated electron production per unit length. Secondary electron coefficient γ depends on cathode materials. In addition, ionization coefficient α related the pressure p and the parameters A and B as follow, which are determined by gas species.

$$\frac{\alpha}{p} = Aexp\left(-\frac{B}{E/p}\right) \tag{5.2}$$

Because electric field indicates $E = V/d$, the breakdown voltage depends on gap length d and pressure p. In my experiments, the gap length was the same, thus the voltage breakdown was difficult to occur at high pressure condition. It led to wide pulse width

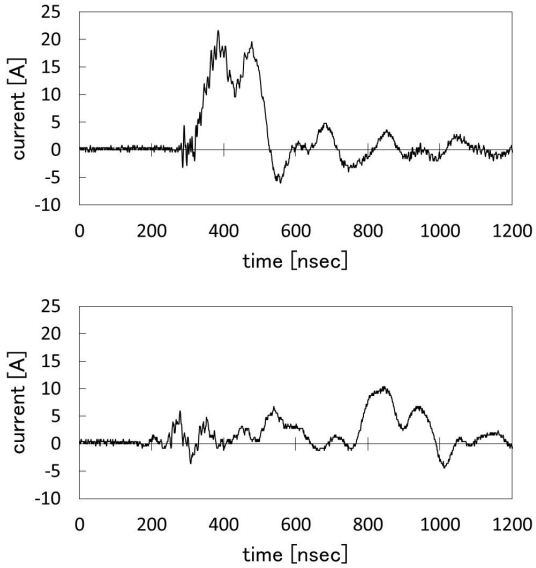

Figure 5.3 The current waveforms of the discharge at 0.1 MPa and 4.0 MPa

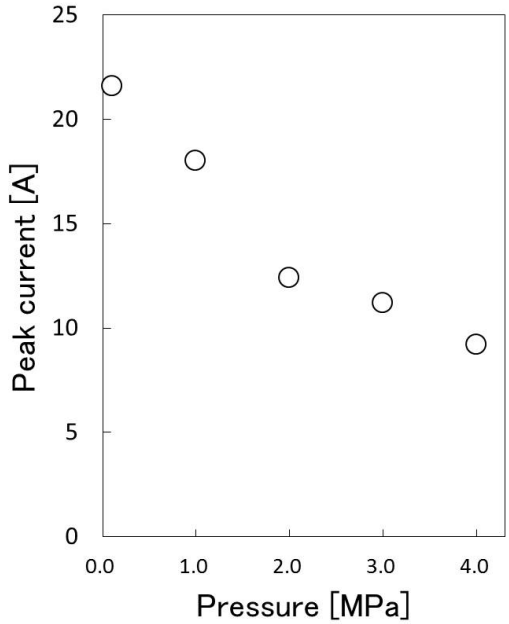

Figure 5.4 The current peaks of the discharge as a function of pressure

of voltage at high pressure condition in Fig.5.2.

In contrast, the current waveforms of the discharge at 0.1 MPa and 4.0 MPa were indicated in Figure 5.3. The current peaks of the discharge become small with increasing pressure as shown in Fig.5.4. In either case, the current flowed immediately after the breakdown, but the peak current of the discharge at 4.0 MPa was lower than that at 0.1 MPa. When electric field is sufficiently high, accelerated electrons move with colliding against neutral species. In the case of high pressure condition, mean free path is short, namely electrons and ions collide frequently. Therefore, energy loss was large when the discharge plasma was generated at high pressure condition due to inelastic collision between ions and electrons. It resulted in low current peak of the discharge at high pressure.

Optical emission spectra of pulsed discharge at 0.1 to 4.0 MPa of argon atmosphere

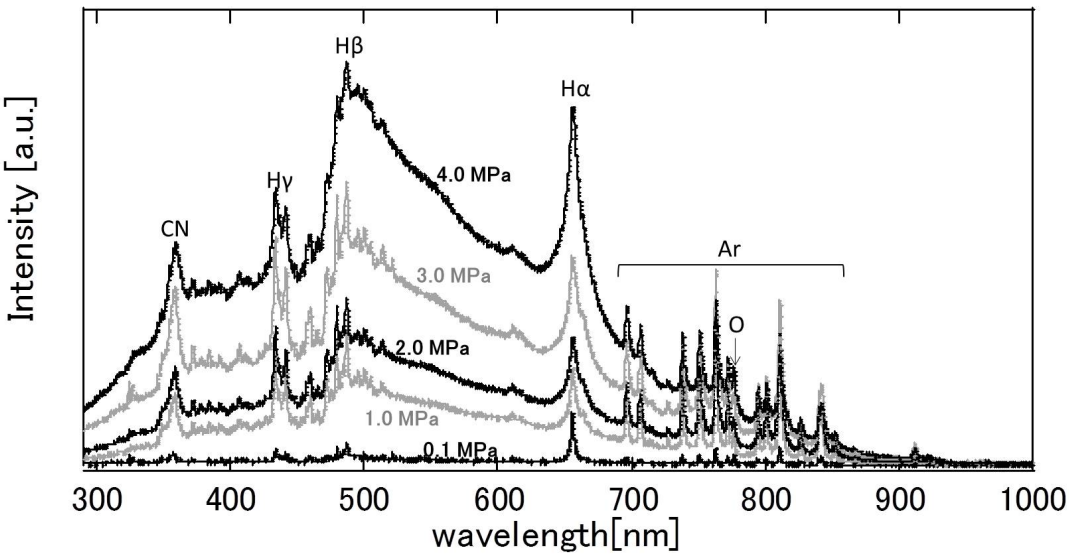

Figure 5.5 Optical emission spectra of pulsed discharge over glycine solution at 0.1 to 4.0 MPa of argon

were shown in Figure 5.5. The emissions were observed not only argon lines but hydrogen and oxygen line from water molecules. Additionally, the line at 359 nm was assigned to CN molecule [43–45]. It derived from glycine in water. The intense emissions were observed when high pressures were operated during the discharge. Dynamic broad emissions were mainly attributed to Stark effects, which caused by high density of charged particles. Considering quasistatic ion and impact-electron density, electron density can be calculated from Stark broadening by determining the reduced wavelength $\alpha_{1/2}$ corresponding to electron density N_e experimentally and in theory. The electron density in terms of hydrogen line is expressed in Eq.(5.3) [46].

$$N_e = 8.02 \times 10^{12} \left(\frac{\Delta\lambda_{1/2}}{\alpha_{1/2}} \right) \tag{5.3}$$

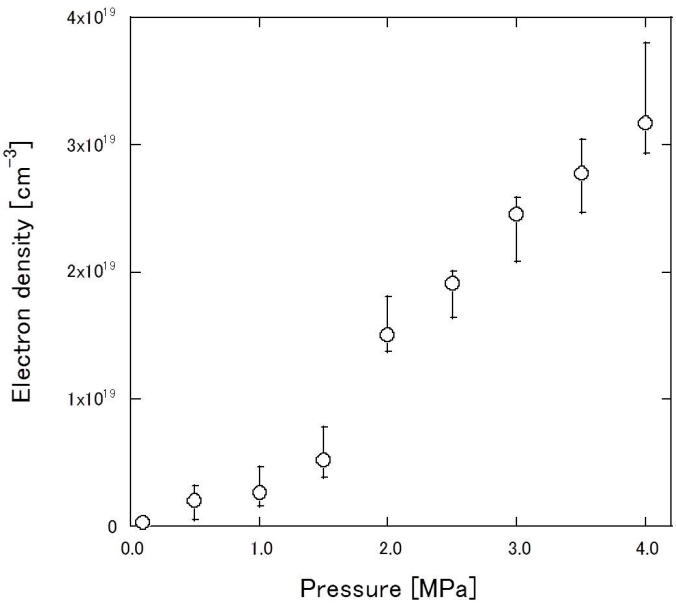

Figure 5.6 Electron densities calculated by Stark effects of H_α emission

where $\Delta\lambda_{1/2}$ is half-value width of hydrogen lines in angstrom. The Hα line was performed fitting based on profile [47] and calculated electron densities by Stark broadening of Hα line in Fig.5.5. The electron densities of discharge plasma as a function of pressure condition are shown in Fig.5.6. When the discharge plasma was generated at pressurized argon, more atoms were ionized because of frequent collision, resulted in high electron density.

When total atomic density of ionization state n_p is in proportion to ion density n_i, atoms density distribution corresponds to a classical Maxwell-Boltzmann distribution, Saha-Eggert equation as shown in Eq.(5.4) is established [48].

$$\frac{n_{(g)}n_e}{n_{(p)}} = 2\frac{g_{(g)}}{g_{(p)}}\left(\frac{m_e k_b T}{2\pi h^2}\right)^{3/2} exp\left(-\frac{E_p}{k_b T}\right) \tag{5.4}$$

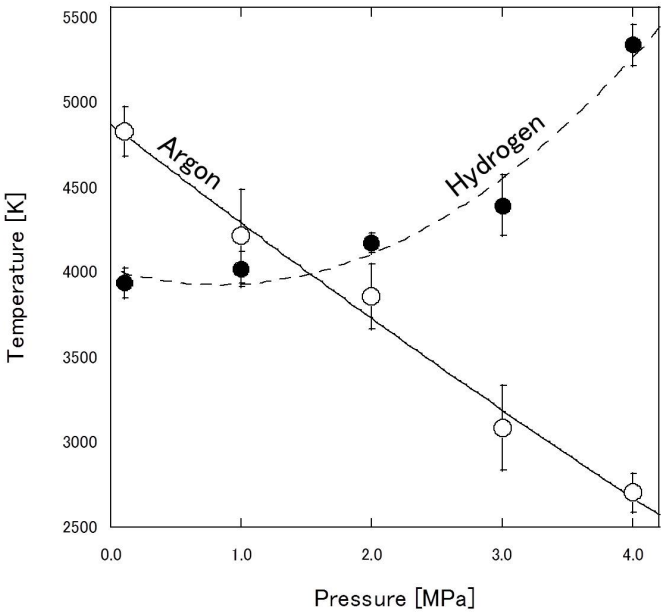

Figure 5.7 Excitation temperatures of argon and hydrogen as a function of pressure

where $n_{(q)}$ is total atomic density of ground state (q); n_e is electron density; g is the statistical weight; m_e is the mass of electron; h is Plank constant; k_b is Boltsmann constant; T is temperature and E_p is the ionization energy of the level p. When the local emission line λ_p and intensity I_p is measured experimentally, the density $n_{(p)}$ can be obtained in Eq.(5.5).

$$n_{(p)} = \frac{4\pi I_p \lambda_p}{A_z} \tag{5.5}$$

where A_z is the state transition probability. According to Eqs.(5.4) and (5.5), temperature was determined uniquely by emission intensity as Eq.(5.6).

$$ln\left(\frac{I_p\lambda_p}{g_{(p)}A_z}\right) = -\frac{E_p}{k_bT} + const. \tag{5.6}$$

There were some emission lines of argon in the range 690-850 nm in Fig.5.5. Therefore, Boltzmann plot ($ln(I\lambda/gA)\ vs.\ -E/k_b$) was drawn by intensity of argon emission in the spectra as shown in Fig.5.5 and excitation temperatures of argon were determined by the inclination of approximate straight line given by Boltzmann plot. Additionally, excitation temperatures of hydrogen were also determined by spectra of Hβ (486 nm) and Hγ (434 nm). Fig.5.7 shows excitation temperature of argon and hydrogen as a function of gas pressure during the discharge. The excitation temperature of argon was different from that of hydrogen. It meant that pulsed discharge plasmas by the present method were non-equilibrium plasmas. The discharge current and change of solution properties by pressure condition were unlikely to affect excitation temperature [49]. At atmospheric and over 0.1 MPa argon, exciting temperatures of argon were higher than that of hydrogen. However, the temperatures of argon decreased against that of high pressure condition. Although electron density of the plasma became high at pressurized condition, energy of each electron was probably low. The energy of argon required for excitation is slightly high compared with that of hydrogen [50]. It led to the increase in emission of hydrogen relatively with increasing atmospheric pressure, resulted in the increase in excitation temperature of hydrogen by the discharge under pressurized argon.

5.4 One-step synthesis of water-dispersible carbon nanocapsules from glycine solution

5.4.1 Synthesis of water dispersible carbon materials

Pulsed arc discharges were repeatedly generated over an aqueous solution containing 100 g/L glycine (H_2NCH_2COOH) under argon gas at pressures between 0.1 and 4.0 MPa. Figure 5.8 shows a photograph of the liquid products after 10000 discharge pulses at several different pressures. Carbon materials were produced by the discharge from glycine in deionized water only at high argon pressures according to colors of the liquid products in Fig.5.8 (d), (e), and (f). Additionally, the liquid product obtained at 1.5 MPa, shown in Fig.5.8 (c), also had a small carbon content analyzed by FE-SEM and Raman spectroscopy. However, no carbon materials were produced by the discharge at atmospheric pressure and at 1.0 MPa. It has been reported that the operating pressure influences the structure of multi-walled CNTs prepared by arc discharge in water with graphite electrodes by affecting the quenching rate of the carbon vapor bubbles and the thermal conductivity of the plasma [51]. As shown in Fig.5.5 (see section 5.3), the intensity of CN molecules became intense at higher pressure condition. Meanwhile, carbon nanoparticle was not produced when the discharge was generated over aqueous solution including acetic acid and ammonium acetate, which did not have C-N bond, at pressurized argon. Therefore, CN molecules probably contributed to formation of carbon products. Additionally, the ease of carbon materials synthesis by this method did not depend on glycine concentration in water.

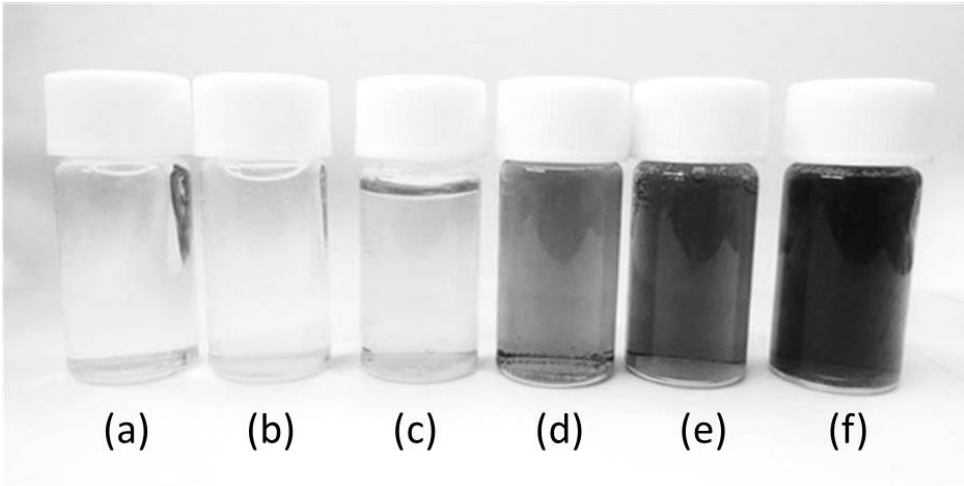

Figure 5.8 Liquid products after treatments by pulsed arc discharge under argon at a pressure of (a) 0.1, (b) 1.0, (c) 1.5, (d) 2.0, (e) 3.0, and (f) 4.0 MPa

The carbon materials produced by the present method exhibited dispersibility in water, which implied the presence of hydrophilic groups on their surface. Since glycine possesses amino and carboxylic groups, the surfaces of the synthesized products were most likely modified by either or both groups.

5.4.2 Structures and functional groups

The structure of carbon products after 10000 discharge pulses at 4.0 MPa was examined by HRTEM. The corresponding images in Figure 5.9 highlight multi-walled carbon nanoparticles with walls comprising two to six graphene layers. The spacing between atomic layers estimated from Fig.5.9 is 0.34±0.02 nm, which corresponds to the lattice spacing of graphene. Similar carbon nanoparticles were synthesized by heating under high vacuum and high temperature [52, 53] or by an acetylene flame method [54]. It

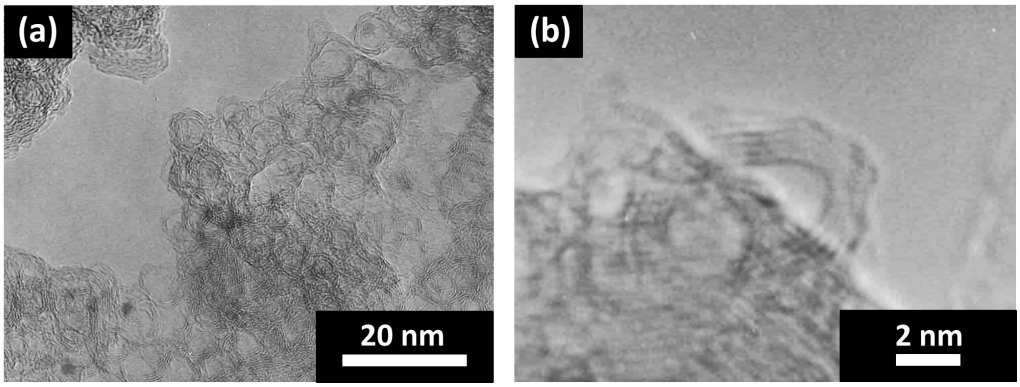

Figure 5.9 TEM images of carbon products generated by pulsed arc discharge at 4.0 MPa: (a) an aggregate of carbon nanoparticles; (b) enlargement of a carbon nanoparticle

was reported that an instantaneous temperature increase led to the formation of carbon nanoparticles consisted of graphene layers. Pulsed arc discharge at a gas/liquid interface was also found to induce an increase in the temperature at the solution surface in a moment [55]. It led to the production of carbon nanoparticles. The atomic layers of the carbon nanoparticles are not well defined in Fig.5.9 (b) partially due to nitrogen and oxygen doping. Nitrogen and oxygen atoms were easily mixed into the graphene layer during the formation of carbon nanoparticles by our method, because both elements are contained in the glycine carbon source.

The Raman spectrum of the carbon nanocapsules is shown in Figure 5.10. The Raman spectrum of the products exhibited the D-band (1340 cm^{-1}), G-band (1582 cm^{-1}), and 2D-band (2670 cm^{-1}), attributed to important bands in carbon materials. These bands were not detected in the amino acid sources, implying that discharge forms several C-C bonds from amino acid sources. The G-band provides information about ordered carbon

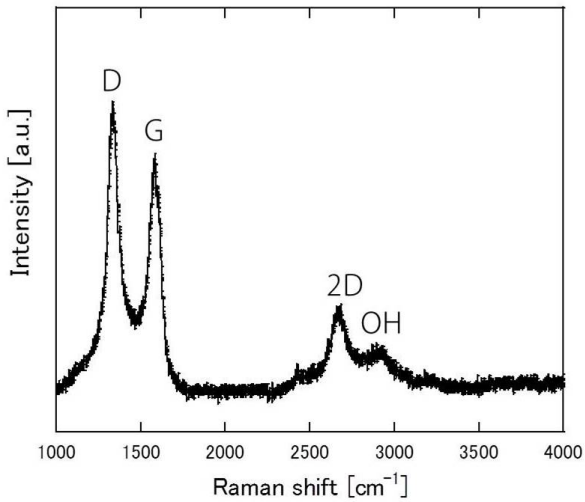

Figure 5.10 Raman spectrum of carbon nanocapsules produced by pulsed arc discharge at 4.0 MPa argon pressure

(sp2 carbon), while the D-band provides information about disordered carbon (sp3 carbon) [56, 57]. When carbon materials are doped with other atoms or carbon surfaces are modified, the intensity of the D-band increases in comparison with that of the G-band [40, 58]. Additionally, the 2D-band peak is attributed to the electron-hole scattering rate; that is, it indicates the long-range order of carbon in the sample [20, 59]. Hence, the spectrum indicates that a graphene layer exists in the carbon nanoparticles produced by this method. The intensity ratio between D- and G-bands was 1.32. However, the defection, doping, and surface modification ratio of carbon could not be determined simply, because the curves of carbon nanoparticles also exhibit the D-band [60]. Moreover, the peak at 2920 cm^{-1} was assigned to the OH group [61]. It can thus be inferred that OH or COOH groups modified the external surface of the carbon nanocapsules, imparting hydrophilic properties to these products.

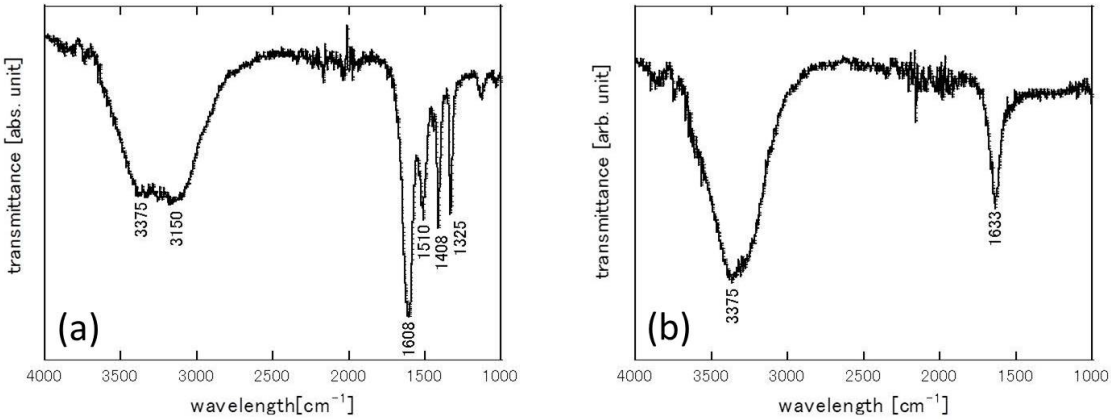

Figure 5.11 FTIR spectra of (a) pure glycine and (b) carbon products obtained by pulsed discharge at 4.0 MPa

In order to identify the functional groups present on the carbon nanocapsules surface more precisely, the carbon products in liquid state were analyzed by FTIR. The FTIR spectrum of deionized water was subtracted from that of the liquid carbon products and from that of the pure glycine solution. Figure 5.11 shows the FTIR spectra of pure glycine and of the carbon nanocapsules produced by pulsed discharge at 4.0 MPa. A broad band at 3375 cm^{-1} corresponds to the carboxylic OH group. The ionic amino group (-NH_3^+) band was observed at 3150 cm^{-1}, partially overlapping with the weak-intensity signal of the C-H vibration at $\sim$3000 cm^{-1}. The four peaks between 1300 and 1650 cm^{-1} are characteristic of amino acids [63, 64]. In particular, the peaks at 1608 and 1325 cm^{-1} were assigned to the C=O stretch, and the peak at 1510 cm^{-1} to the C-N-H vibration. The C-H vibration is associated to the peak at 1408 cm^{-1}. Turning to the FTIR spectrum of carbon nanoparticles in Fig.5.11 (b), the OH and C=O peaks were observed at 3375 and 1633 cm^{-1}, respectively. The shift of the C=O band from 1608 to 1633 cm^{-1} was

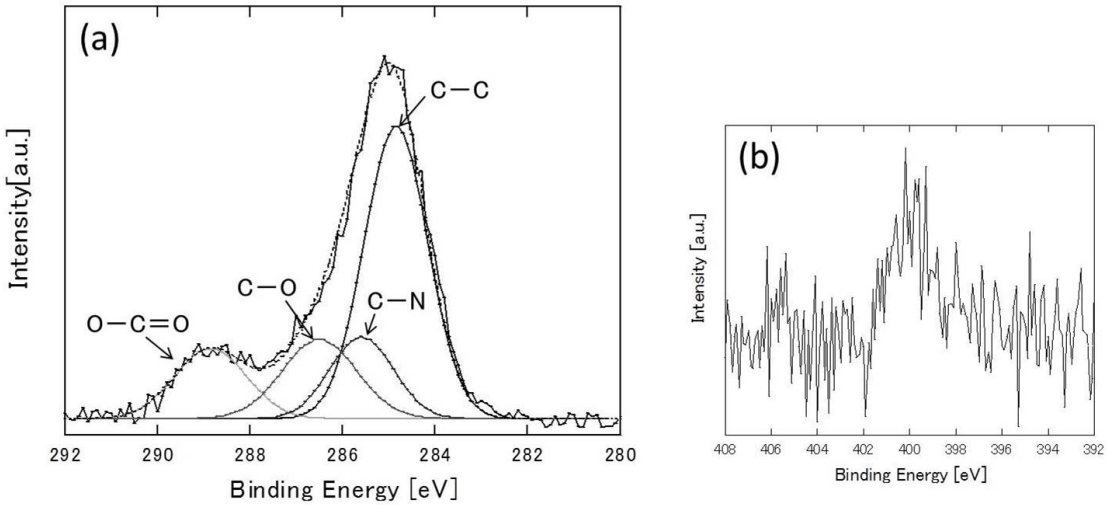

Figure 5.12 XPS spectra of carbon nanocapsules produced by pulsed discharge under 4.0 MPa argon pressure: (a) C1s and (b) N1s spectra

due to the disappearance of C-N and C-H bands [65]. The intensity of the C-H band was reduced as a result of the formation of the graphene layer. The disappearance of the NH_3^+ and C-N-H bands implied that only a small amount of amino groups was present on the carbon surfaces. Therefore, carboxylic group (-COOH) was the main functional group on the carbon nanoparticle surface, and such feature enabled the particles to be dispersed in water.

The XPS analysis was performed to determine amounts of nitrogen and oxygen atoms in and on carbon nanoparticles. Fig.5.12 shows the XPS spectra of the carbon nanocapsules produced by pulsed discharge at 4.0 MPa. The C1s spectrum shown in Fig.5.12 (a) included not only the C-C peak at 284.8 eV, but also peaks with higher binding energy assigned to C-N (285.6 eV), C-O (286.5 eV) and O-C=O (288.8 eV) [64]. It can be conjectured that the C-O and O-C=O peaks are mostly associated to surface modification

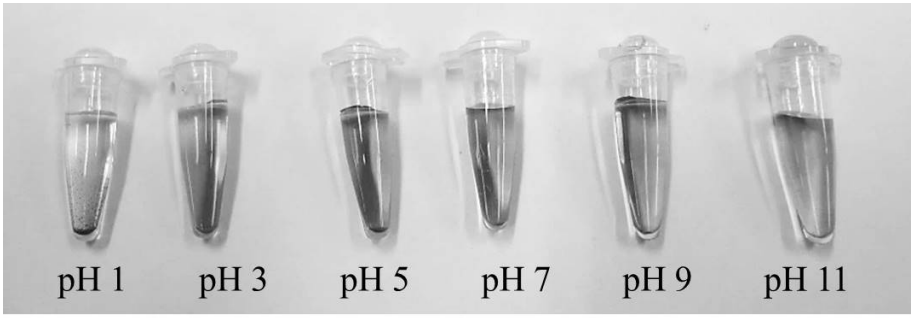

Figure 5.13 Effect of solution pH on dispersibility of carbon products

by carboxylic groups. The presence of nitrogen was also confirmed by the N1s spectrum shown in Fig.5.12 (b). The C-N peak is due to nitrogen doping in the graphene layer. In summary, the carbon products obtained by pulsed discharge from glycine were carbon nanoparticles composed of few graphene layers doped with nitrogen, and whose surfaces were modified by carboxylic groups.

Fig.5.13 shows effect of solution pH on dispersibility of carbon products. The pH values of the solution were controlled by HCl and NaOH after synthesis of carbon nanoparticles. The carbon products in water at the pH over pH 3 kept dispersibility, but they were deposited the solution at pH 1. It was due to COOH group on carbon surface. Generally, COOH group exists as anion, but it does not keep ion state in water at strong acidity. On the other hand, if NH_3 group is exist on carbon surface, carbon products would disperse in water even at strong acidity. Therefore, Fig.5.13 implied that NH_3 group hardly existed on carbon surface.

5.4.3 Pressure effects

The carbon products were easy to form at higher pressure condition, as indicated by the color of the products shown in Fig.5.8. Carbon products synthesized by the discharge were observed by FE-SEM. Figure 5.14 shows SEM images of carbon products by the discharge at 1.5, 2.0, 3.0, and 4.0 MPa. In case glycine remained in the sample even after a dialysis, crystal was observed like Fig.5.14 (d). Small nanoparticles were produced with increasing pressure. Characteristics of discharge plasma changed drastically between the discharge at 2.0 and 4.0 MPa, for example, high excitation temperature of hydrogen exhibited at pressurized condition (see section 5.3). These properties changing by pressure

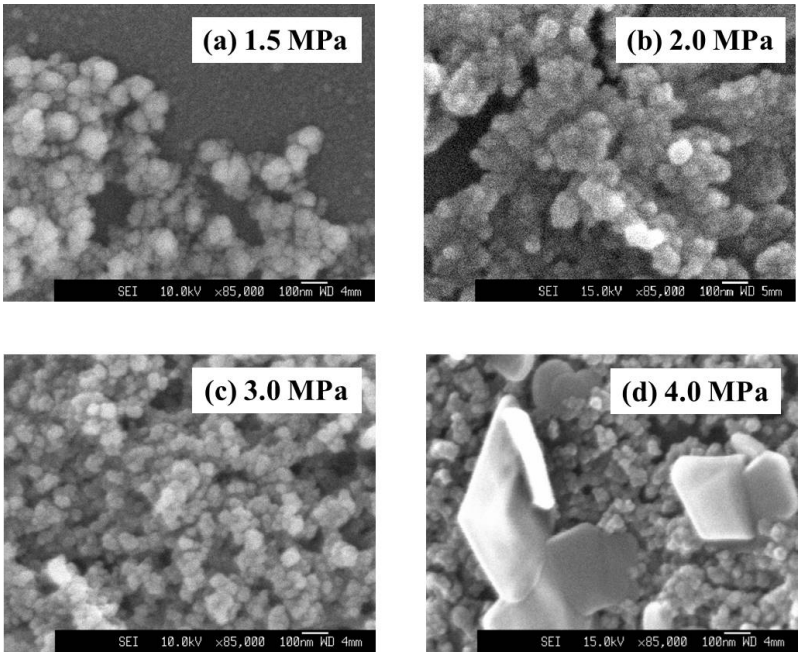

Figure 5.14 SEM images of carbon products by the discharge at (a) 1.5, (b) 2.0, (c) 3.0, (d) 4.0 MPa

Table 5.1 Pressure effects on carbon products obtained by pulsed discharge under pressurized argon

	Raman		XPS	
Pressure	I_D/I_G	I_{2D}/I_G	N/C	O/C
2.0 MPa	1.22	0.30	0.04	0.37
3.0 MPa	1.25	0.43	0.10	0.37
4.0 MPa	1.32	0.48	0.15	0.38

were supposed to be affected on synthesis of carbon nanoparticles, resulted in difference in particle diameter of carbon products.

The effects of pressure on the carbon nanoparticles produced by pulsed discharge were examined by comparing the Raman and XPS data obtained under 2.0, 3.0, and 4.0 MPa argon pressure (Table 5.1). The intensity ratio between the D- and G-bands (I_D/I_G) in the Raman spectra provides information on the density of defects in the graphene layer and the modification ratio. Carbon nanoparticles produced by the discharge under higher argon pressure had a high I_D/I_G ratio, showing that defects density or modification ratio in the carbon nanoparticles increased when carbon nanoparticles synthesized at higher pressure condition. Based on nitrogen to carbon ratio determined by XPS, higher nitrogen contents were incorporated in the carbon nanoparticles at higher pressure, leading to high I_D/I_G. The intensity of CN molecules in Fig.5.5 became intense at higher pressure condition. It was considered that it related to synthesis of carbon nanoparticles. It was believed that more production of CN molecules by the discharge at higher pressure condition led to high

nitrogen doping level as indicated in Table 5.1. On the other hand, the amount of oxygen in carbon nanoparticles was hardly affected by the argon pressure.

The intensity ratio of 2D- and G-bands (I_{2D}/I_G) in the Raman spectra denotes that a higher I_{2D}/I_G for carbon products generated by the discharge at higher pressure. In the case of nitrogen-doped graphene, it has been reported that I_{2D}/I_G tends to decrease, while I_D/I_G increases [64]. Additionally, large amounts of nitrogen doping in graphene layers determined a reduction in the intensity of the 2D-band [63]. By contrast, the I_{2D}/I_G ratio of the carbon nanoparticles with graphite layer produced by our method increased with increasing pressure, although higher amounts of nitrogen atoms were doped in the graphene layers upon the high-pressure treatment. Moreover, the intensity of the 2D-band diminishes relatively to that of the G-band when the number of graphene multi-layers increases [65]. This same trend is also shown by carbon onions, which are carbon nanoparticles with graphene layers [66]. Therefore, the I_{2D}/I_G ratio in the carbon nanoparticles produced by our method was probably affected by the number of graphene layers. The number of graphene layers in the carbon nanoparticles will decrease at higher pressure condition, taking into account the pressure effect on the I_{2D}/I_G ratio.

5.5 Synthesis of water-dispersible carbon materials from various amino acid

5.5.1 Effects of carbon straight chains of source amino acids on carbon structures

Pulsed discharges were generated over 50 g/L amino acid solution surface under 4.0 MPa argon and synthesized carbon materials. In order to examine the effects of straight carbon chain of amino acid on carbon structures and properties, glycine, alanine, threonine, ornithine, and lysine were utilized for carbon sources. Figure 5.15 shows photographs of the products after the discharge of 20000 and 40000 pulses, which correspond to the structure of the carbon source (amino acids). Carbon materials produced from each amino acid corresponded to different colors of liquid products; moreover, their generation

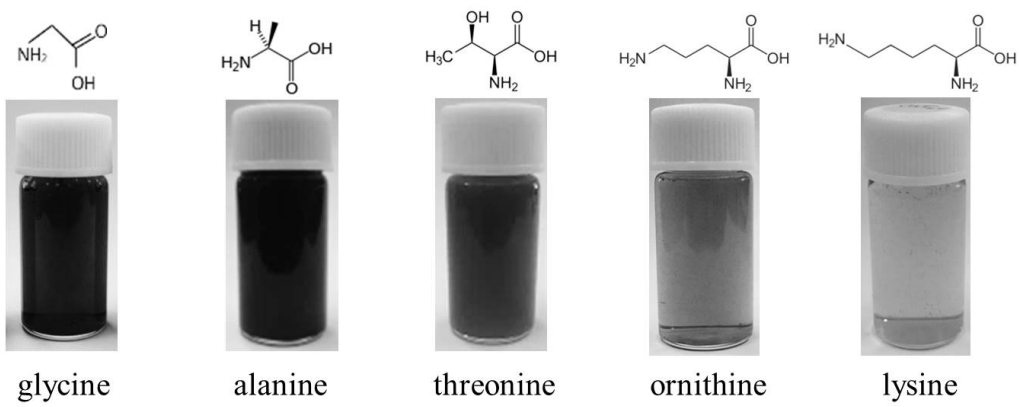

Figure 5.15 Photographs of the carbon products obtained after discharge of 20000 (glycine, alanine, threonine) and 40000 (ornithine, lysine) pulses, corresponding to the structure of the carbon sources

speeds were different depending on the carbon sources. As shown in Fig.5.15, a discharge of 20000 pulses resulted in a change of the color of the solution containing glycine, alanine, and threonine to black, indicative of the formation of carbon products. On the other hand, when a discharge of 20000 pulses was applied to the solution containing ornithine and lysine, carbon products were not visually discriminated. Moreover, with increasing discharge of 40000 pulses, carbon products from ornithine and lysine were clearly observed. As compared to those obtained from lysine, carbon products were easily formed when ornithine was used as the carbon source. Thus, it was more difficult to produce carbon products from amino acids containing a longer straight chain as compared to those with a shorter straight chain. When carbon materials are synthesized from amino acids, they react with each other and create C-C, C-N, or C-O bonds. In my study, carbon materials synthesized from amino acids such as ornithine and lysine consisted of long straight chains. It was difficult for these amino acids to react with each other because of steric effects, which probably led to a slower generation of carbon products. Additionally, all carbon materials produced from each amino acid exhibited dispersibility in water. According to preceding section, surface of carbon materials were mainly modified by COOH group, leading to dispersibility in water. It is thought that all carbon products produced from amino acid had COOH group as functional group on the surfaces.

Figure 5.16 shows the SEM images of the products obtained from the amino acids by a discharge of 20000 pulses; their structures were observed by FE-SEM. Nanoparticles were formed by the discharge. Every sample produced from amino acids exhibited the same shape; however, the particle sizes of the products were different depending on carbon sources. Figure 5.17 shows the number-average particle diameters of the carbon products as a function of the carbon chain of amino acid sources. When nanoparticles were

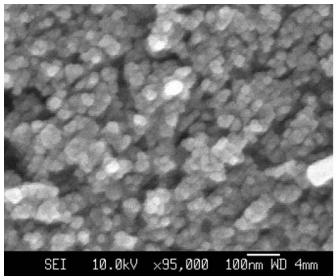

(a) glycine

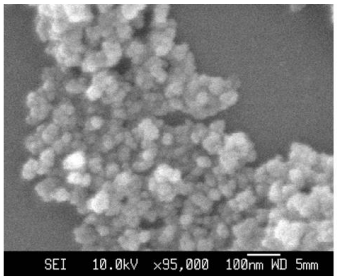

(b) alanine

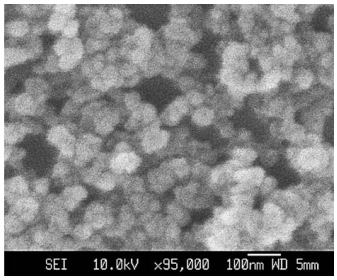

(c) threonine

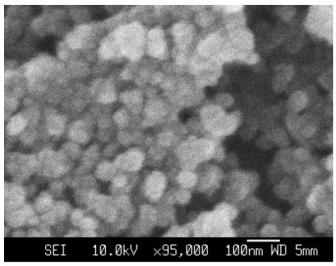

(d) ornithine

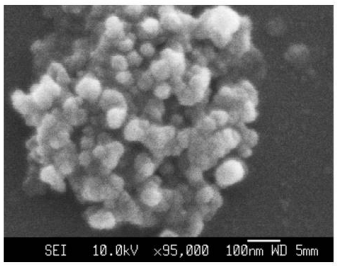

(e) lysine

Figure 5.16 SEM images of the carbon products obtained from amino acids by a discharge of 20000 pulses

produced from amino acids with a long carbon chain, large nanoparticles were obtained, probably attributed to steric effects of amino acids. The long straight chain of amino acids prevented the formation of curved surfaces of carbon nanoparticles, leading to large particle formation. In addition, the low generation speed of carbon products led to the production of large carbon nanoparticles when they were produced from amino acids with a long carbon chain.

Table 5.2 lists the atomic ratios of nitrogen (N) to carbon (C) and oxygen (O) to carbon (C) in the carbon products as analyzed by XPS and those in the amino acid sources. According to the O/C ratios in the carbon products, some amount of oxygen was present and exhibited no dependence on carbon sources. Although threonine had an OH group

Table 5.2 Atomic ratios of nitrogen to carbon and oxygen to carbon in the carbon products analyzed by XPS and those in amino acid sources

Carbon source	Atomic ratio (carbon products) N/C	O/C	(source amino acids) N/C	O/C
glycine	0.15	0.38	0.50	1.00
alanine	0.08	0.37	0.33	0.67
threonine	0.07	0.38	0.25	0.75
ornithine	0.13	0.38	0.40	0.40
lysine	0.11	0.39	0.33	0.33

in its structure, as shown in Fig.5.15, the amount of oxygen in the product obtained from threonine was the same as that in the other samples. Hence, oxygen atoms derived from the OH group did not remain in the carbon products. In contrast, the nitrogen amount in the carbon products exhibited dependence on the amino acid source. The N/C ratios of the carbon products were in approximate agreement with the atomic ratios of nitrogen in amino acid sources. Particularly, as compared with the products obtained from alanine, those obtained from lysine exhibited a higher N/C ratio, although the atomic ratios of alanine and lysine were the same. Considering the structures of amino acids shown in Fig.5.15, a terminal NH_3 group, examples of which are glycine, ornithine, and lysine, tended to contain more nitrogen in the products as compared to the other amino acids. In this method, CN molecules produced from amino acid contributed to carbon nanoparticles synthesis. It is thought that amino acids, which has terminal NH_3, were easy to produce CN molecules

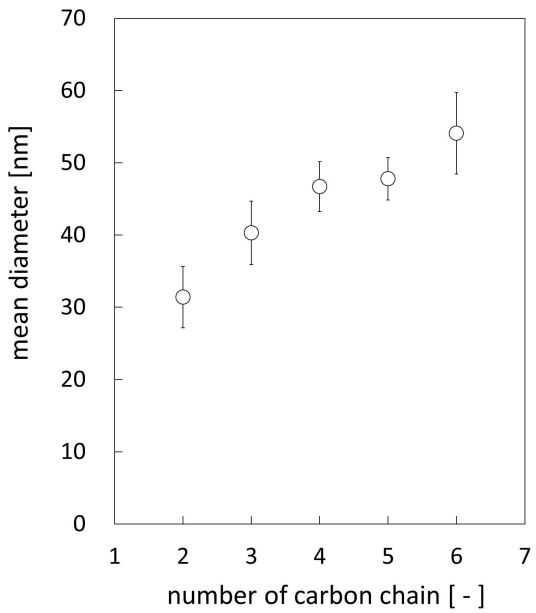

Figure 5.17 Number-average particle diameters of the carbon products as a function of the carbon chain in the amino acid source

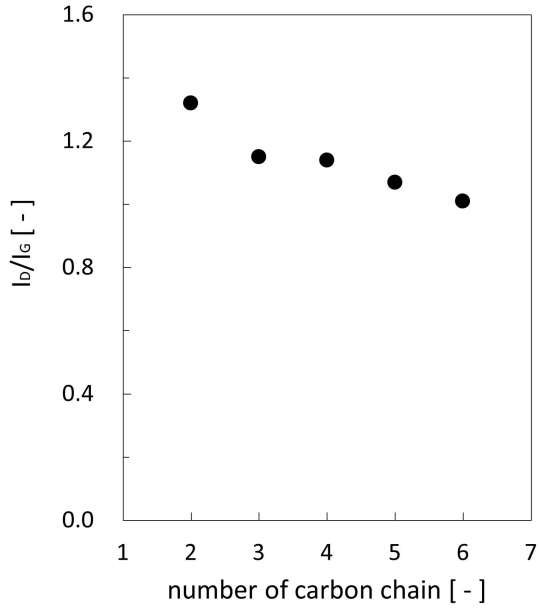

Figure 5.18 Intensity ratios between the D- and G-bands (I_D/I_G) as a function of the carbon chain of amino acid source

by the discharge, and more CN molecules impacted on synthesis of carbon nanoparticle. It led to high N/C ratios of carbon products from amino acid with terminal NH_3. In any case, the percentages of nitrogen and oxygen in the carbon products were even less than those in the amino acid sources. Some amount of NH_3 and COOH groups remained in the carbon products as doping atoms or modifying groups on the carbon surfaces. However, a majority of NH_3 and COOH groups in the amino acids is released while generating carbon nanoparticles.

Figure 5.18 shows the intensity ratio between the D- and G-bands (I_D/I_G) as a function of the carbon chain of amino acids. The I_D/I_G ratios of carbon products decreased for the

amino acid sources with a large number of carbon chains. In other words, ordered carbons were easily formed from amino acids with a long carbon chain. However, the atomic ratios of nitrogen and oxygen in the carbon products did not correlate with the I_D/I_G ratios. Thus, the surface modification and doping of in carbon products with nitrogen and oxygen atoms did not significantly contribute to the decrease in the I_D/I_G ratios. Accordingly, the change of the I_D/I_G ratios represents the amount of ordered and disordered carbon in the products. Carbon nanoparticles produced from amino acids with a long carbon chain exhibited more ordered carbon as compared with those produced from amino acids with a short carbon chain. Small carbon nanoparticles exhibited a large number of curved surfaces, resulting in a high I_D/I_G ratio [60] for the carbon nanoparticles produced from the amino acids with a short carbon chain.

5.5.2 Effects of side chains and cyclic structures of amino acid on carbon structures

In order to examine the effects of side chain and cyclic structures of amino acid, on carbon structure and properties, carbon materials were synthesized from valine, isoleucine, proline, histidine, and phenylalanine by the discharge at pressurized argon. Figure 5.19 shows photographs of the products obtained after discharge of 20000 pulses corresponding to the structure of the carbon source. Carbon materials were also produced from amino acids consisted of side carbon chain and cyclic structure. Carbon materials were hard to produce from valine compared with threonine (Fig.5.15) according to the colors of the products, although structure between valine and threonine were different only one

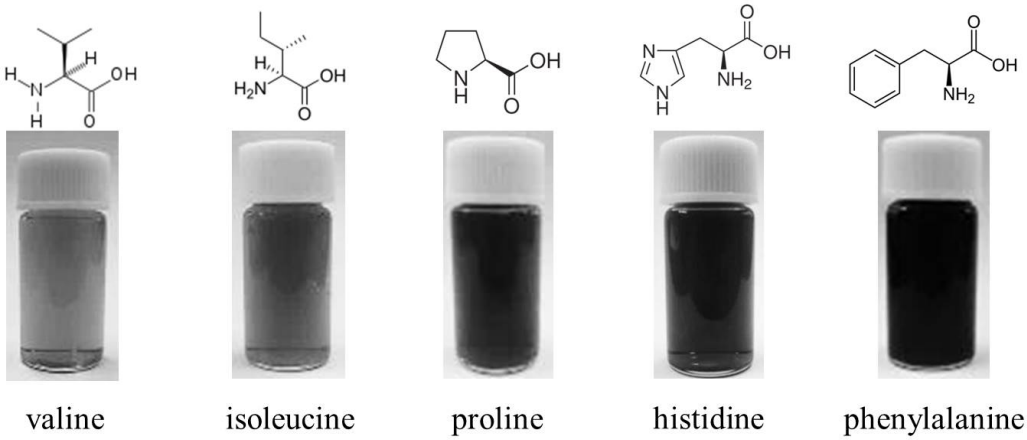

Figure 5.19 Photographs of the carbon products obtained after discharge of 20000 pulses corresponding to the structure of the carbon sources

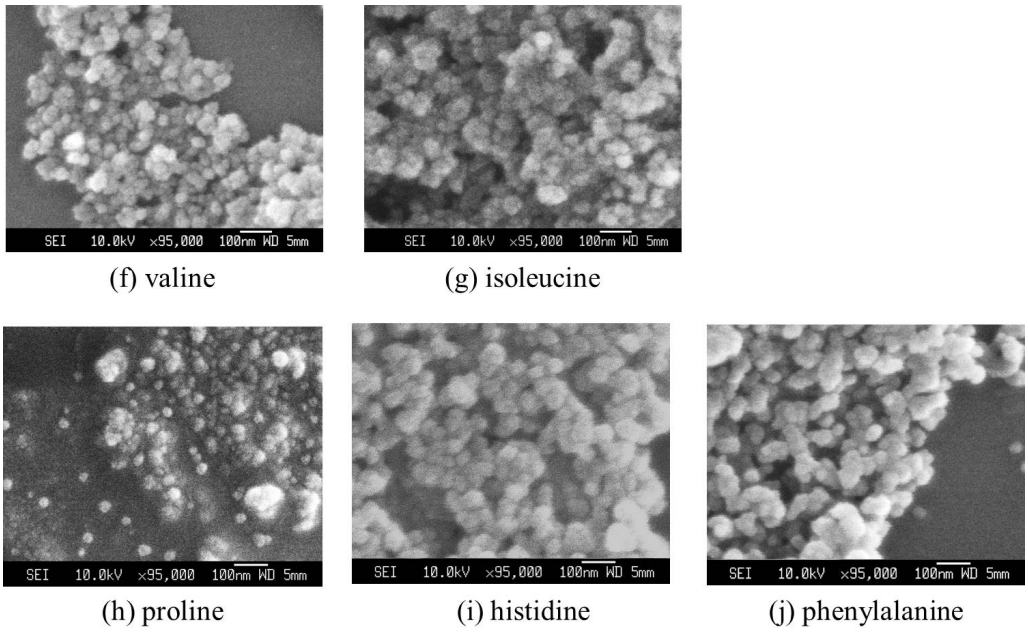

Figure 5.20 SEM images of the carbon products obtained form amino acids with side carbon chain or cyclic structure by a discharge of 20000 pulses

Table 5.3 I_D/I_G ratio and atomic ratios of nitrogen to carbon and oxygen to carbon in the carbon products analyzed by Raman spectroscopy and XPS

Carbon source	Raman I_D/I_G	XPS N/C	XPS O/C
valine	1.11	0.10	0.58
isoleucine	1.16	0.18	0.57
proline	1.00	0.10	0.40
histidine	0.99	0.14	0.39
phenylalanine	0.95	0.09	0.38

functional group (side chain). In addition, isoleucine has longer straight carbon chain than valine, but carbon products were easy to form from isoleucine slightly. Isoleucine has side chain in the third place from CH_3 terminal group as shown in Fig.5.19. Thus, structure of isoleucine is easy to make six-membered ring, leading to production of more carbon materials. Meanwhile, amino acids with cyclic structure were easy to be synthesized carbon materials. Fig.5.20 shows the SEM images of the products obtained from the amino acids, which have side chain or cyclic structure. All carbon products were nanoparticles, whose diameter depended on carbon sources.

Table 5.3 indicates I_D/I_G, N/C, and O/C ratios of carbon products from each amino acid analyzed by Raman spectroscopy and XPS. The carbon products from amino acids with cyclic structures had low I_D/I_G ratios relatively. These amino acids have some sp2 carbon in the structures as shown in Fig.5.19. Thus, more graphene layer contained in the products

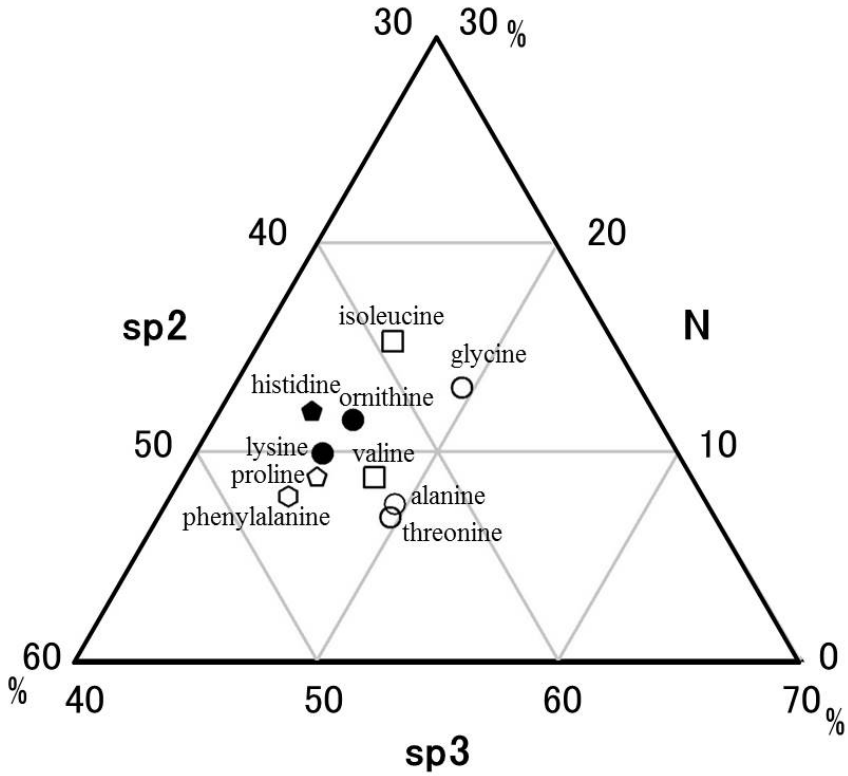

Figure 5.21 Component ratios of sp2 carbon, sp3 carbon, and nitrogen in the carbon products from each amino acid

presumably, leading to high I_D/I_G. The percentages of nitrogen in the products from amino acids with side chain or cyclic structures were low in both cases. As mentioned, a terminal NH_3 of amino acid was resulted in high N/C ratio. Because they did not have a terminal NH_3, nitrogen atoms were difficult to contain in carbon products. Focused on oxygen atoms in the carbon products, O/C ratios of the products from cyclic amino acids was almost the same as that from straight amino acids. However, in the case of the products from amino acid including side chain, the amounts of oxygen in the products

were relatively high. According to the structures of valine and isoleucine, it was easy to form six-membered rings including oxygen atoms because of side chains. Therefore, it is believed that oxygen existed not only on the carbon surface as COOH group but also in graphene layers when the carbon products were created by amino acids including side chain.

Figure 5.21 shows component ratios of sp2 carbon, sp3 carbon, and nitrogen in the carbon products from each amino acid determined by Raman spectra and XPS analysis. The amounts of sp3 carbon in the products from glycine, alanine, and threonine were almost the same, moreover that from ornithine and lysine were also the same. In case of amino acids, which had only carbon straight chain, the amounts of sp3 carbon determined uniquely by the number of NH_3 groups, and that of sp2 carbon increased by forming the products from longer carbon straight chain. Side chain of amino acids made the products include more oxygen atoms, thus the ratios of nitrogen to carbon were estimated to be higher than actual. There were supposed to be a lot of defects of carbon order in the products from isoleucine because of oxygen doping, resulted in low sp2 carbon component. The carbon products from cyclic amino acids tended to consist of more sp2 carbon because cyclic amino acids had six-membered rings. The amounts of nitrogen in the products from cyclic amino acids depended on the number of nitrogen in source amino acids.

5.6 Conclusions

The discharge plasmas were generated over amino acid solution at high pressure condition, and investigated the characteristics of discharge plasma and synthesized carbon materials. The electron density of the plasmas and excitation temperature of hydrogen were increased with increasing pressure, although excitation temperature of argon decreased against pressure increase. Intense emissions of CN molecules, derived from glycine molecules in aqueous solution, were observed by the discharge at pressurized argon.

The pulsed discharge over water at pressurized argon enabled one-step synthesis of hydrophilic carbon nanoparticles from amino acids. Carbon materials were obtained only at high pressure condition, over 1.5 MPa. The carbon products kept dispersing in water because hydrophilic groups derived from amino acids modified the carbon surfaces. The products had a capsule structure consisting of several graphene layers. The graphene layers of the carbon nanoparticles were doped with nitrogen atoms, and their surfaces were modified by COOH groups. The CN molecules from glycine produced by the discharge related to formation of carbon particles. The discharge under higher pressures produced carbon nanoparticles rapidly with high nitrogen doping levels, because production of CN molecules was promoted by the discharge with increasing argon pressure.

The structures of source amino acids were great impact on component of carbon products. The amino acids consisted of long straight chain were difficult to generate the carbon nanoparticles due to steric effect of source amino acids. The large carbon nanoparticles were produced from amino acids with long straight chain, leading to decrease in I_D/I_G ratios of the products. The content percentages of oxygen in the carbon products did not depended on source amino acid except that consisted of side carbon chain, but those of nitrogen were affected by atomic ratio of nitrogen and binding site of NH_3

group of source amino acid. Cyclic amino acids were easy to form carbon products with more sp2 carbon.

Reference

[1] M A Lieberman and A J Lichtenberg (2005) Principles of plasma discharges and materials processing, 2nd edition *Wiley*.

[2] S Iijima (1991) Helical microtubules of graphitic carbon *Nature* **354** 7: 56-58.

[3] L Mangolini, E Thimsen and U Kortshagen (2005) High-yeild plasma synthesis of luminescent silicon nanocrystals *Nano Lett.* **5** 4: 655-659.

[4] Y Sawada, S Ogawa and M Kogoma (1995) Synthesis of plasma-polymerized tetraethoxysilane and hexamethyldisiloxane films prepared by atmospheric pressure glow discharge *J. Phys. D:Appl. Phys.* **28** 1661-1669.

[5] W Jiang and K Yatsui (1998) Pulsed wire discharge for nanosize powder synthesis *IEEE Trans. Plasma Sci.* **26** 5: 1498-1501.

[6] T Kaneko, K Baba, T Harada and R Hatakeyama (2009) Novel gas-liquid interfacial plasmas for synthesis of metal nanoparticles *Plasma Process. Polym.* **6** 713-718.

[7] N Shirai, S Uchida and (2009) Novel gas-liquid interfacial plasmas for synthesis of metal nanoparticles *Plasma Process. Polym.* **6** 713-718.

[8] C Richmonds and R M Sankaran (2008) Plasma-liquid electrochemistry: Rapid synthesis of colloidal metal nanoparticles by microplasma reduction of aqueous cations *Appl. Phys. Lett.* **93** 131501.

[9] J Sun, S Fujita, F Zhao and M Arai (2004) Synthesis of styrene carbonate from styrene oxide and carbon dioxide in the presence of zinc bromide and ionic liquid under mild condition *Green Chem.* **6** 613-616.

[10] T Adschiri (2007) Supercritical hydrothermal synthesis of organic-inorganic hybrid nanoparticles *Chem. Lett.* **36** 10: 1188-1193.

[11] Y S Rim, W H Jeong, D L Kim, H S Lim, K M Kim and H J Kim (2012) Simultaneous modification of pyrolysis and densification for low-temperature solution-processed flexible oxide thin-film transistors *J. Mater. Chem.* **22** 12491-12497.

[12] Wahyudiono, K Murakami, S Machmudah, M Sasaki and M Goto (2012) A Dry process for polymer nano-microfibers prepared by electrospining under pressurized CO_2 *Jpn. J. Appl. Phys.* **6** 613-616.

[13] S Machmudah, Wahyudiono, N Takada, H Kanda, K Sasaki and M Goto (2013) Fabrication of gold and silver nanoparticles with pulsed laser ablation under pressurized CO_2 *Adv. Nat. Sci.: Nanosci. Nanotechnol.* **4** 045011.

[14] T Kiyan, M Sasaki, T Ihara, T Namihira, M Hara, M Goto and H Akiyama (2009) Pulsed breakdown and plasma aided phenol polymerization in supercritical carbon dioxide and sub-critical water *Plasma Process. Polym.* **6** 778-785.

[15] K Sasaki, S Soma, H Akashi, M Elsabbagh and Y Ikeda (2015) Electron temperature and electron densities in microwave helium discharges with pressures higher than 0.1 MPa *Contrib. Plasma Phys.* **55** 8: 563-569.

[16] Z A Munir, U A Tamburini (2006) The effect of electric field and pressure on the synthesis and consolidation of materials: A review of the spark plasma sintering method *J. Mater. Sci.* **41** 763-777.

[17] Wahyudiono, H Watanabe, S Machmudah, T Kiyan, M Sasaki, H Akiyama and M Goto (2012) Pyrrole conversion induced pulse discharge plasma over a water surface under high-pressure argon *Chem. Eng. Process: Process. Intensification* **61** 51-57.

[18] S Stauss, D Z Pai, T Shizuno and K Terashima (2014) Nanosecond pulsed electric discharge synthesis of carbon nanomaterials in helium at atmospheric pressure from adamantane *IEEE Trans, Plasma Sci.* **42** 6: 1594-1601.

[19] F Oshima, S Stauss, Y Inose and K Terashima (2014) Synthesis and investigation of reaction mechanism of diamondoids produced using plasmas generated inside microcapillaries in supercritical xenon *Jpn. J. Appl. Phys.* **53** 010214.

[20] S Scalese, V Scuderi, S Bagiante, F Simone, P Russo, L D Urso, G Compagnini and V Privitera (2010) Controlled synthesis of carbon nanotubes and liner C chains by arc discharge in liquid nitrogen *J. Appl. Phys.* **107** 1-6.

[21] M Ishigami, J Cumings, A Zettl and S Chen (2000) A simple method for the continuous production of carbon nanotubes *Chem. Phys. Lett.* **309** 457-459.

[22] N Sano, H Wang, I Alexandrou, M Chhowalla, K B K Teo and G A J Amaratunga (2002) Properties of carbon onions produced by an arc discharge in water *J. Appl. Phys.* **92** 2783-2788.

[23] J Suehiro, K Imasaka, Y Ohshiro, G Zhou, M Hara and N Sano (2003) Production of carbon nanoparticles using pulsed arc discharge triggered by dialectic breakdown in water *Jpn. J. Appl. Phys.* **42** 1483-1485.

[24] S D Wang, M H Chang, J J Cheng, H K Chang and K M D Lan (2005) Unusual morphologies of carbon nanoparticles obtained by arc discharge in deionized water *Carbon* **43** 1317-1339

[25] T Okada, T Kaneko and R Hatakeyama (2007) Conversion of toluene into carbon nanotubes using arc discharge plasma in solution *Thin Solid Films* **515** 4262-4265

[26] J Kang, O L Li and N Saito (2013) Synthesis of structure-controlled carbon nano spheres by solution plasma process *Carbon* **60** 292-298

[27] P H Matter, L Zhang and U S Ozkan (2006) The role of nanostructure in nitrogen-containing carbon catalysts for the oxygen reduction reaction *J. Catal.* **239** 83-96

[28] B Wei, R Spolenak, P K Redlich, M Ruhle and E Arzt (1999) Electrical transport in pure and boron-doped carbon nanotubes *Appl. Phys. Lett.* **74** 3149-3151

[29] Y Sheng, J Wei, J Pan, P Huang, S Guo, J Zhang, X Zhang and B Feng (2015) The up-converted photoluminescence and cell imaging of water-soluble carbon dot *Chem. Phys. Lett.* **638** 196-200

[30] A Sakudo, H Chou, K Ikuta and M Nagatsu (2015) Integration of antibody by surface functionalization of graphite-encapsulated magnetic beads using ammonia gas plasma technology for capturing influenza A virus *Bioorg. Med. Chem.* **25** 1876-1879

[31] V Chandra, J Park, Y Chun, J W Lee, I C Hwang and K S Kim (2010) Water-dispersible magnetite-reduced graphene oxide composites for arsenic removal *ACS Nano* **4** 3979-3986

[32] L Zhu, Y Lu, Y Wang, L Zhang and W Wang (2012) Preparation and characterization of dopamine-decorated hydrophilic carbon black *Appl. Surf. Sci.* **258** 5387-5393

[33] O M Yakymchuk, Perepelytsina, A D Rud, I M Kirian and M V Sydorenko (2014) Impact of carbon nanomaterials on the formation of multicellular spheroids by tumor cells *Phys Status Solidi A* **211** 12: 2778-2784

[34] V Marchesano, A Ambrosone, J Bartelmess, F Strisciante, A Tino, L Echegoyen, C Tortiglione and S Giordani (2015) Impact of carbon nano-onions on Hydra vulgaris as a model organism for nanoecotoxicology *Nanomaterials* **5** 1331-1350

[35] S Kang, J E Kim, D Kim, C G Woo and P V Pikhitsa (2015) Comparison of cellular toxicity between multi-walled carbon nanotubes and onion-like shell-shaped carbon nanoparticles *J. Nanopart. Res.* **17** 378

[36] G Vikovic, A Marinkovic, M Obradovic, V Radmilovic, M Colic, R Aleksic and P S Uskokovic (2009) Synthesis, characterization and cytotoxicity of surface amino-functionized water-dispersible multi-walled carbon nanotubes *Appl. Surface Sci.* **255** 8067-8075

[37] J N Wang, L Zhang, J J Niu, F Yu, Z M Sheng, Y Z Zhao, H Chang and C Pak (2007) Synthesis of high surface are, water-dispersible graphitic carbon nanocages by an in situ template approach *Chem. Mater.* **19** 453-459

[38] T E Saraswati, A Ogino and M Nagatsu (2012) Plasma-activated immobilization of biomolecules onto graphite-encapsulated magnetic nanoparticles *Carbon* **50** 1253-1261

[39] H Jiang, F Chen, M G Lagally and F S Denes (2010) New strategy and functionalization of carbon nanoparticles *Langmuir* **26** 1991-1995

[40] T Shirafuji, Y Noguchi, T Yamamoto, J Hieda, N Saito, O Takai, A Tsuchimoto, K Nojima and Y Okabe (2013) Functionalization of multiwalled carbon nanotubes by solution plasma processing in ammonia aqueous solution and preparation of composite material with polyamide 6 *Jpn J Appl Phys* **52** 1-6

[41] A Fridman and L A Kennedy (2004) Plasma physics and engineering *Taylor & Francis Books, Inc.*.

[42] A Fridman (2008) Plasma chemistry *Cambridge University Press.*.

[43] S Acquaviva, A P Caricato, M L De Giorgi, A Luches and A Perrone (1997) Spectroscopic studies during pulsed laser ablation deposition of C-N films *Appl. Surface Sci.* **109** 408-412.

[44] D Zhou, A R Krass, L C Qin, T G McCauley, D M Gruen, T D Corrigan, R P H Chang and H Gnaser (1997) Synthesis and electron field emission of nanocrystalline diamond thin films grown from N_2/CH_4 microwave plasma *J Appl. Phys.* **82** 9: 4546-4550.

[45] S Acquaviva and M L D Giorgi (2002) High-resolution investigation of C_2 and CN optical emissions in laser-induced plasmas during graphite ablation *J. Phys. B: At. Mol. Opt. Phys.* **35** 795-806.

[46] J Ashkenazy, R Kipper, and M Caner (1991) Spectroscopic measurements of electron density of capillary plasma based on Stark boadening of hydrogen lines *Phys. Rev. A* **43** 10: 5568-5574.

[47] H R Griem (1974) Spectral line broadening by plasmas *Academic Press*.

[48] H J Kunze (2009) Introduction to plasma spectroscopy *Springer-Verlag Berlin Heidelberg*.

[49] P Bruggeman, E Ribezl, A Maslani, J Degroote, A Malesevic, R Rego, J Vierendeelsand C Leys (2008) Characteristics of atmospheric pressure air discharges with a liquid cathode and a metal anode *Plasma Sources Sci. Technol.* **17** 1025012.

[50] A Sarani, A Y Nikiforov and C Leys (2010) Atmospheric pressure plasma jet in Ar and Ar/H_2O mixtures: optical emission spectroscopy and temperature measurements *Phys. Plasma* **17** 063504.

[51] N Sano, M Naito, M Chhowalla, T Kikuchi, S Matsuda, K Iimura, H Wang, T Kanki and G A J Amaratunga (2003) Pressure effects on nanotubes formation using the submerged arc in water method *Chem. Phys. Lett.* **378** 29-34

[52] K Asaka, R Kato, Y Maezono, R Yoshizaki, K Miyazawa and T Kizuka (2006) Light-emitting filament composed of nanometer-sized carbon hollow capsules *Appl. Phys. Lett.* **88** 1-3

[53] W A Heer and D Ugarte (1993) Carbon onions produced by heat treatment of carbon soot and their relation to the 217.5 nm interstellar absorption feature *Chem. Phys. Lett.* **207** 480-486

[54] T C Liu, Y Y Li (2006) Synthesis of carbon nanocapsules and carbon nanotubes by an acetylene flame method *Carbon* **44** 2045-2050

[55] J Janca, S Kuzmin, A Maximov, J Titova, A Czernichowski (1999) Investigation of chemical action of the gliding and “point” arcs between the metallic electrode and aqueous solution *Plasma Chem. Plasma Proc.* **19** 53-67

[56] N Li, Z Wang, K Zhao, Z Shi, Z Gu and S Xu (2010) Synthesis of single-wall carbon nanohorns by arc-discharge in air and their formation mechanism *Carbon* **48** 1580-1585

[57] H Yang, P Mercier, S C Wang and D L Akins (2005) High-pressure synthesis of carbon nanotubes with a variety of morphologies *Chem. Phys. Lett.* **416** 18-21

[58] D J Late, U Maitra, L S Panchakarla, U V Waghmare and C N R Rao (2011) Temperature effects on the Raman spectra of graphenes: dependence on the number of layers and doping *J. Phys: Condens. Matter* **23** 055303-1-5

[59] K Vasu, K Pramoda, K Moses, A Govindaraj and C N Rao (2014) Single-walled nanohorns and other nanocarbons generated by submerged arc discharge between carbon electrodes in liquid argon and other media *Mater. Res. Express* **1** 015001

[60] D Roy, M Chhowalla, H Wang, N Sano, I Alexamdrou, T W Clyne and G A J Amaratunga (2003) Characterization of carbon nano-onions using Raman spectroscopy *Chem. Phys. Lett.* **373** 52-56

[61] Parker F S (1983) Application of infrared, Raman, and resonance Raman spectroscopy in biochemistry *New York: Plenum Pub Corp*

[62] T Ramanathan, F T Fisher, R S Ruoff and L C Brinson (2013) Evolution of Raman spectra in nitrogen doped graphene *Carbon* **61** 57-62

[63] R M Silverstein, F X Webster and D Kiemle (2005) Spectrometric identification of organic compounds. 7th ed. *Wiley*

[64] T Ramanathan, F T Fisher, R S Ruoff and L C Brinson (2013) Evolution of Raman spectra in nitrogen doped graphene *Carbon* **61** 57-62

[65] M Ibrahim, A Nada, D E Kamal (2005) Density functional theory and FTIR spectroscopic study of carboxylic group *Indian. J. Pure Appl. Phys.* **43** 911-917

[66] K Bogdanov, A Fedorou, V Osipov, T Enoki, K Takaki, T Hayashi, V Ermakov, S Moshkalev, A Baranov (2014) Annealing-induced structural changes of carbon onions: High-resolution transmission electron microscopy and Raman studies *Carbon* **73** 78-86

Chapter 6

Summary of the works

The discharge plasmas over water surface can induce chemical reactions without catalyst and chemical agent in simple process. It has been actively researched for biomedical and environmental applications recently. This work focused on chemical reactions and transport mechanisms in aqueous solution irradiated pulsed discharge plasmas.

Chemical reactions by pulsed discharge plasmas

The effects of pulsed discharge plasmas on aqueous solution were investigated in order to realize high efficient process of discharge plasma over aqueous solution surface. When the discharge plasmas were generated at gas-aqueous solution interface, some active species were generated near aqueous solution surface, and affected on the solution. They induced oxidation reactions in aqueous solution mainly. Oxidation reactions were caused by not only specific species but various species, produced by plasma irradiation. Especially, reactive oxidation species from dissociation of water were effective in the reactions.

There were some differences between positive and negative pulsed discharges. Positive pulsed discharges were efficient for high speed processing, but some persistent compounds

in water were difficult to be oxidized. On the other hand, decomposing persistent compounds were effectively oxidized by negative pulsed discharges because of OH radical, although processing speed was slow.

Transport mechanisms of aqueous solution under plasma irradiation

In order to utilize discharge plasmas for chemical process, not only chemical reactions but transport mechanisms in aqueous solution are essential. Spatial distributions of active species and reacted solution during the discharges were observed by using chemical methods in this study. The discharge plasmas formed the layer of reacted solution in the depth of 10 mm from the solution surface. The thickness of this layer did not depend on reactor shape. In case of positive pulsed discharges, reactive oxidation species reached and reacted directly 2 mm in the depth from the solution surface in the deepest, in spite of 1 mm by negative pulsed discharges. Therefore, the depth of aqueous solution in a reactor and a flow of reacted solution are key factors for an efficient reactor design of discharge plasmas at gas-aqueous solution interface.

New processes of discharge plasma at gas-aqueous solution interface

Two plasma processes using gas-liquid slug flow and wet wall were developed as new plasma processes in this work. High efficiencies were achieved by using either process. Reactivity was approximately the same as the discharge by using thin batch-reactor, which is the most efficient of the batch reactors. It was found that an efficient discharge process could be realized by controlling a convection flow and a layer of reacted solution.

Discharge plasmas in water with fine bubbles

Almost all of previous discharge methods with bubbles, bubbles rose one after another owing to high rising speed of the bubbles. In this work, fine bubbles, which had extremely slow rising speeds, were introduced in discharge area. The effects of fine bubbles on characteristics of discharge plasma and generation of active species were examined. Fine bubbles in water affected discharge ignition, resulted in low inception voltage and suppression of rising temperature. In addition, fine bubbles enhanced plasma emission with high electron density. It led to the increase in H_2O_2 generation by the discharge. Dissolved oxygen in the water also contributed to H_2O_2 formation by the discharge with fine bubbles. Moreover, active chlorine species were produced when the discharges were generated in NaCl solution with fine bubbles. Oxygen atoms from dissociation of water reacted with chlorine radicals resulted in the production of available chlorine.

Discharge plasmas at pressurized gas/aqueous solution interface

The discharge plasmas were generated over amino acid solution at pressurized gas over 0.1 MPa, and the characteristics of discharge plasma and carbon materials synthesis were investigated. The high electron density of discharge plasma was generated at high pressure condition, and intense emissions of CN molecules, which derived from glycine in water, were observed in optical emission spectra. In addition, high excitation temperature of hydrogen exhibits by discharge plasmas under pressurized argon, but that of argon decreased monotonously.

Water-dispersible carbon nanoparticles were synthesized from amino acids in water by pulsed discharges at high pressure argon, over 1.5 MPa. The carbon products obtained

high dispersibility in water because of surface modification by carboxylic groups, derived from functional groups of amino acids. The amounts of CN molecules produced by the discharge related to synthesis of carbon nanoparticles. The structures of source amino acids were great impacts on component of carbon products. In particular, binding site of NH_3 group of source amino acids influenced on atomic ratio of nitrogen in carbon products.

Future prospects

Discharge plasmas in the presence of water are valid for chemical processing obviously. Availability of discharge plasmas may be researched actively, especially in biomedical field. Therefore, plasma processes with water will be much more important for practical use in industry.

This work gave you some information about chemical reactions and transport mechanisms in water by using simplify discharge methods, and proposed the efficient processes of discharge plasmas. However, there are still many questions regarding active species and chemical reactions in water induced by discharge plasmas. The plasma processing in the presence of water can lead more efficient by deepen understanding of detailed chemical reactions induced by discharge plasmas.

In addition, plasma processes are likely to enlarge possibilities by combination with external factors, such as fine bubbles and high pressure condition. Future studies will reveal utilities of their processes.

Acknowledgement

I would like to thank my supervisors *Prof. Motonobu Goto* and *Dr. Hideki Kanda* for their guideless and support not only in the successfulness of my research but many aspects.

I would especially like to express my special thanks to *Dr. Noriharu Takada* (Technical Center, Nagoya University), *Prof. Koichi Sasaki* (Division of Quantum Science and Engineering, Hokkaido University), and *Prof. Tatsuru Shirafuji* (Department of Physical Electronics and Informatics, Osaka City University) for their technical support, sagacious advice, and encouragement. I am grateful the members of *Plasma Electronics Division of JSAP* for discussion and advices. They gave me a lot of sagacious advices on my study.

My gratitude should be extended to *Dr. Wahyudiono*, *Mr. Kakeru Mano* and *Mr. Shigenori Takahashi* for their cooperation and assistance of my research. This work would not have been possible without their cooperation.

Finally, I would like to appreciate to all members of *Goto laboratory* and *Nagoya University JSAP Student Chapter* for their support and encouragement.

Yui Hayashi